BRUYèRE, CINDY LYNNETTE

NUMERICAL MODELLING OF SEVERE THUNDERSTORMS OVER

THE SOUTH AFRICAN HIGHVELD WITH THE AID OF THE

CLARK CLOUD MODEL

MSc   UP   1997

NUMERICAL MODELLING OF SEVERE THUNDERSTORMS OVER THE SOUTH AFRICAN HIGHVELD WITH THE AID OF THE CLARK CLOUD MODEL

by

Cindy Lynnette Bruyère

A dissertation submitted in part fulfilment of the requirements for the degree

MASTER OF SCIENCE

in the

Department of Civil Engineering

Faculty of Engineering

UNIVERSITY OF PRETORIA

January 1997

i

Summary

Numerical modelling of severe thunderstorms over the South African Highveld with the aid of the Clark cloud model

By:	C L Bruyère
Supervisor:	Prof J van Heerden
Co-Supervisor:	Mr D E Terblanche
Department:	Civil Engineering
University:	University of Pretoria
Degree:	Master of Science (Meteorology)

Precipitation research, with a view to rainfall augmentation, especially in a drought stricken country like South Africa, is an attractive option as a source of good quality water. Numerical models can be useful tools in these programmes to help investigate the dynamical and microphysical processes in clouds. They can also be of great benefit to better understand the outcome of cloud seeding and to assist in the formation of a seeding hypothesis. This dissertation serves as a first step in establishing if the Clark model could predict mesoscale conditions in South Africa accurately enough, in order to be used as a tool in the precipitation research programme.

The Clark model was used to simulate the mesoscale conditions of two selected days over the Bethlehem area. On both case days severe storms were responsible for extensive hail damage over the area. It was assumed that if the model could accurately predict severe conditions, it would also be able to predict general mesoscale conditions (this assumption was proved in the dissertation). The model also highlighted the fact that a single initializing sounding would not always be sufficient to accurately simulate severe convective activity.

The model was also used to study the effect that surface heating and topography have on the development of convective activity.

Samevatting

Numerical modelling of severe thunderstorms over the South African Highveld with the aid of the Clark cloud model

Deur: C L Bruyère

Studieleier: Prof J van Heerden

Mede-Studieleier: Mr D E Terblanche

Department: Siviele Ingenieurswese

Universiteit: Universiteit van Pretoria .

Graad: Magister Scientiae (Weerkunde)

Sleutel terme: Clark model, mesoscale, initialization, large scale data, ice parameterization, surface heating, topograpical effects, precipitation research, numerical simulation, severe storms

Neerslag navorsing, met die oog op reënval vermeerdering, veral in 'n droë land soos Suid-Afrika, is 'n aantreklike opsie vir 'n bron van goeie kwaliteit water. Numeriese modelle kan 'n belangrike rol speel in hierdie programme in di eondersoek van dinamiese en mikro-fisiese prosesse in wolke. Hulle kan ook baie waardevol wees om die uitkoms van wolk bestrooiing beter te verstaan en om te help met dir formuleering van 'n bestrooiings hipotese. Hierdie verhandeling dien ook as 'n eerste stap om te bewys dat die Clark model meso-skaal kondisies in Suid-Afrika akuraat genoeg kan voorspel, om gebruik te kan word in die neerslag navorsings program.

Die Clark model was gebruik om die meso-skaal kondisies van twee dae oor die Bethlehem area te simuleer. Swaar donderbuie was, op beide dae, verantwoordelik vir uitgebreide hael-skade oor die area. Daar was aangeneem dat indien die model uiterste toestande akuraat kan voorspel, dit ook algemene meso-skaal kondisies sal kan voorspel (hierdie aanname was bewys in die verhandeling). Die model het ook bewys dat 'n enkele opstyding om die model mee te inisialisee nie altyd voldoende sal wees om swaar konvektive toestande akuraat te simuleer nie.

Die model was ook gebruik om die effek wat oppervlak verhitting en topografie op die ontwikkeling van konveksie het te ondersoek.

Acknowledgement

I wish to express my appreciation to the following organisations and persons who made this dissertation possible:

This dissertation is dedicated with love to:
My father - Charles Howes
My husband - Marcel Bruyère

Contents

List of tables

List of figures

x

xi

Chapter 1

Introduction

South Africa is a country blessed with great mineral riches, spectacular scenery, a rich wild life and a very pleasant climate. Unfortunately, South Africa also experiences prolonged droughts and, from time to time, hazardous weather phenomena (like floods, tornadoes and hailstorms). With an average rainfall of only 600 mm (two-thirds of the world average), South Africa is currently classified by the World Bank as one of 25 crisis areas in the world (Van Niekerk, 1996).

South Africa's rapid population growth and economical activities, coupled with prolonged droughts, increasing pollution of water bodies and the over-exploitation of aquifers, have already resulted in seasonal water scarcity in some parts of the region. It has been estimated that the water demand in South Africa will exceed the total available supply around the year 2020 (Mather and Terblanche, 1993).

In the summer rainfall areas of South Africa, it has been recognized that the convective storms which are responsible for the majority of the rain are inefficient in terms of rainfall production. Only about 30 percent of the atmospheric water vapour that enters the storms reaches the ground as precipitation (Mather and Terblanche, 1993). Rainfall augmentation, if feasible, has therefore been identified as an attractive source of good quality water.

Since 1983, research at Bethlehem and Nelspruit has been focussed on finding a rainfall augmentation hypothesis. If such a hypothesis could be tested successfully, it could lead to the ability to augment South Africa's dwindling water resources. In order to achieve this goal, a consolidation of the South African rainfall augmentation

1

research projects was necessary. Therefore, early in 1990 an amalgamation of the Bethlehem and Nelspruit research projects, under the banner NPRP (National Precipitation Research Programme), took place.

The NPRP set as its primary objectives (Mather and Terblanche, 1993):

A. To investigate both the natural and artificially modified precipitation processes in multicellular convective clouds and to attain a better understanding of the physical mechanisms of precipitation development in the larger cloud systems.

B. To use the knowledge gained in (A) to identify those environmental (synoptic) conditions in which the precipitation efficiency of larger cloud systems may be increased by human intervention, should there be any reason to believe that the natural processes are inefficient at times.

To achieve these objectives the NPRP identified four main research avenues. The first two of these are:

1. Comprehensive field studies to document the fundamental cause and effect relationships during each step of the physical chain of events, in natural and artificially modified clouds, in order to quantify the physical processes and develop an adequate physical understanding of such processes.

2. Numerical cloud modelling to provide a framework for comparisons between observations and theory, and to test and/or refine an underlying hypothesis.

The other two objectives deal with the development of technology, instrumentation, data and local expertise, both not relevant to this study.

1.1 Objective of the dissertation

The objective of this dissertation is twofold; 1) To address the research needs, as set out in the second main research avenue above, and 2) To study the development of severe thunderstorms over the South Africa Highveld region.

2

1.1.1 Numerical cloud modelling as research tool

The first objective of this study is ultimately to be in a position to utilize a chosen numerical model as a support tool for the rainfall augmentation programme.

Numerical modelling of cumulus clouds is an important area of weather modification research. In order to formulate a rainfall augmentation hypothesis, a comprehensive study of the natural rainfall processes is needed. Numerical cloud models can be utilized successfully to help investigate the complicated interactions between the dynamical, microphysical and thermodynamical processes in clouds.

There is also a great need to better understand the outcome of cloud seeding activities. Detailed cloud models are well suited for such analysis. For any particular case, cloud models can depict the outcome of both seeded and unseeded activities. Since these studies are done in a controlled environment, cloud model simulations not only save money, but they are able to avoid the great natural variability of rainfall processes that provides problems for statistical methods (Grosh *et al*, 1990).

1.1.2 Severe thunderstorm studies

In the semi-arid, subtropical interior of South Africa, insufficient rainfall is the dominant limiting factor on agricultural production. In addition to this, hailstorms (amongst the most devastating weather manifestations of the mid-latitudes (Rakovec, 1989)) cause an economical drain on South Africa's agriculture. In South Africa hail damage is estimated at tens of millions of Rand each year. In the light of this Obasi (1995) said; "A high priority must be given to the monitoring of hydrological, meteorological and associated environmental elements which are also essential for the protection of people and property against water-related hazards and droughts".

The Free State is agriculturally a very sensitive region in South Africa (for more details, see sections 2.1.3 and 2.2.3). Understanding the complex physical and dynamical interactions within any severe hailstorm, and in particular hailstorms over

3

the Free State, is thus of fundamental importance. In the light of this, the need for a sophisticated numerical model to try to simulate, and understand, these destructive hailstorms becomes apparent. This study was therefore undertaken to try to bridge this gap in our understanding of the physical and dynamical elements at work in severe storms.

1.2   Methodology

Due to computer limitations, assumptions have to be made when running numerical models. This might cause a model to be suitable for one application and not another. The Clark cloud model has proven itself in other applications (see section 2.4), but only once before has it been utilized in a study over Bethlehem (Bruintjes, 1992). This study proved that the model has the potential to be used as a support tool in the rainfall augmentation program, but more research is needed to properly investigate the model's accuracy over the project area.

As a first step in analysing the Clark model's accuracy over the project area, it was decided to numerically simulate extreme events over the Bethlehem area. This approach will not only address the occurrence of severe hail storms over the area, but it will also investigate the model's capabilities to handle extreme events.

Two case studies were chosen to achieve the objectives of this dissertation. The first case is that of a severe multicell storm that brought hail and destruction to towns to the north of Bethlehem. The second case investigates a solitary supercell in an otherwise stable environment. This supercell caused severe damage to a farming community to the east of Bethlehem.

1.3   Structure of the dissertation

Chapter two contains the background material needed to understand the problems associated with severe hailstorms over the Free State. The chapter gives a brief

4

summary of South Africa's weather. The BPRP area and its associated weather are also discussed in more detail. Some time is also spent on the different storm types as well as on numerical models.

Chapter three describes the Clark three-dimensional numerical model mathematically. The dynamical and physical sections of the model are considered separately, the latter in greater detail.

Chapter four describes the first case study, 24 November 1992. On this day a severe multicell storm caused approximately two million Rands hail damage to the north of Bethlehem in the Reitz area. The synoptic and mesoscale conditions surrounding the development of this multicell storm are discussed in the first half of the chapter. The Clark cloud model was used to numerically simulate the storm and it succeeded in capturing its development and movement. The results obtained during the numerical simulations, as well as some sensitivity studies are presented in the latter half of chapter four.

Chapter five, where the second case study - 9 December 1991 - is presented, follows the same pattern as chapter four. On this day a severe supercell storm developed over a farming community to the east of Bethlehem. The storm produced hail and left a path of destruction, to the value of approximately one million Rand, in its wake. The first half of the chapter describes the synoptic and mesoscale conditions surrounding this destructive supercell. The Clark model was again utilized to numerically simulate this storm. Unlike the multicell storm, the Clark model failed to capture the development of the supercell storm. The latter half of chapter five describes the results obtained during the numerical simulations. At the end of the chapter some time is spent on trying to improve the model results.

Finally, in chapter six conclusions obtained during the course of the study are highlighted, as well as some views on what the future may hold.

5

Chapter 2

Background

This chapter covers the background material needed to understand the problems associated with severe hailstorms in the Free State.

Section 2.1 describes the South African climate in general and more specifically the precipitation experienced throughout the country and its effects on South African agriculture. This section also deals with the climatic regions of South Africa, with specific reference to the Highveld region.

The area of study in this dissertation is known as the BPRP (Bethlehem Precipitation Research Project) area. Section 2.2 deals with the atmospheric circulation over this area and its associated weather and precipitation patterns. This is mainly an agricultural area, but very few studies have been done concerning the hailfall and its effects. Section 2.2.3 deals with these aspects in more detail.

In order to study the hail producing storms of a specific area, one needs to look first at storms in general. Section 2.3 gives an overview of the three basic storm types (single cell, multicell and supercell).

A discussion on the ways in which numerical models can be of benefit to the BPRP follows in section 2.4, together with a short introduction to the Clark three-dimensional cloud model. Section 2.4.2 also supplies some background on various studies already undertaken with the aid of the Clark model.

2.1 South Africa

The Republic of South Africa, is bordered in the north by Namibia, Botswana, Zimbabwe and Mozambique; on the east and south by the Indian Ocean, and on the west by the Atlantic Ocean. Lesotho and Swaziland form enclaves in the eastern part of the country (figure 2.1). The topography of South Africa consists primarily of a great plateau that occupies about two-thirds of the country (figure 2.2). This plateau rises from about 1000 m in the centre to a general level of about 1200 m and terminates in the great escarpment (Lesotho), which rises to over 3000 m. Between the edge of the plateau and the eastern and southern coastline, the land descends seaward in a series of abrupt grades, or steps. On the southwestern coast the edge of the plateau is marked by a range of folded mountains, irregular in character and direction, which descends abruptly into a coastal plain.

2.1.1 Precipitation in South Africa

Precipitation in South Africa occurs most commonly as rain which, in both frequency and quantity, by far exceeds any other form of precipitation (Schulze, 1965). The rainfall generally decreases meridionally, from east to west. The interior plateau of South Africa has a marked orographic effect on the rainfall of the region. The summer rainfall areas, i.e., the eastern and interior parts of South Africa, receive the bulk of their rainfall as a result of showers and thundershowers. Thunderstorms are most frequent on the eastern high plateau and less frequent in the western and southwestern Cape, where this phenomenon occurs on only five days per year (figure 2.3). When comparing this figure with one showing the annual hail frequency (figure 2.4), the similarity of the lines of equal hail frequency to those of days with thunder is obvious. It can be seen that on the eastern high plateau, the average number of days with hail is roughly an order of magnitude lower than the number of days with thunder.

Looking at the occurrence of hail (figure 2.4), one notes the distinct way in which the isopleths of hail incidence conform with the general topography of southern Africa.

7

The greatest incidence of hail (eight days a year) occurs over the Free State and the Lesotho Highlands. In comparison to this other world wide highs are; Cheyenne (Wyoming, USA) eight to ten hail days per year, Paris approximately ten, and Württemberg, Germany, records about thirteen (Hughes and Wood, 1993). In the light of this, it is thus not surprising that hail damage is a hazard that has to be reckoned with in South Africa.

In contrast to the annual maxima of rainfall and thunderstorms - which mostly occur during the months December to February - hailstorms occur most frequently in the early summer (October to December), with a peak in November (Schulze, 1965). This is in direct contrast to results obtained in North America and Europe (Carte and Held, 1978). A possible explanation for the severity of hailstorms experienced in South Africa during the early summer, may lie in the atmospheric circulation that occurs over South Africa at this time. Two essential ingredients for the development of hailstorms, namely, instability and shear in upper air winds, reach their peak in early summer. At this time of the year the winter baroclinic processes start to give way to the summer barotropic conditions. After the winter the upper atmosphere warms up slowly due to a lag in the exchange of heat from the lower atmosphere. This leads to an increase in the vertical temperature lapse rate and consequently an increasingly unstable upper atmosphere. The strong wind shear is associated with the high level of baroclinicity of the atmosphere in the early summer. The atmospheric circulation patterns and their possible links to the formation of severe hailstorms in the early summer are discussed in detail by Held (1974), Olivier (1990), Poolman (1992) and Van Heerden *et al* (1988).

2.1.2 The South African Highveld

For practical purposes the South African Weather Bureau (SAWB) has divided South Africa into fifteen climatic regions (figure 2.5). This division was based on geographical considerations, like prominent mountain ranges and rivers, as well as other features such as political boundaries (Schulze, 1965). The climatic region of interest to this study (see next paragraph), is the so-called "Highveld" region.

8

The Highveld, which covers most of the interior plateau, is generally higher than 1500 m above sea level. The average annual precipitation over the Highveld region varies from about 900 mm in the east to about 650 mm in the west. Approximately 85 percent of the annual rainfall falls in the summer months (October to March, with a maximum in January), leaving the winter months mostly dry. The rainfall is almost exclusively due to showers and thunderstorms. Heavy falls of 125 to 150 mm occasionally occur in a single day. The annual average number of thunderstorms varies from about 75 in the north to 100 in the south. These storms are often violent with severe lightning, strong (but short-lived) gusty winds and sometimes hail. The region has the highest hail frequency in South Africa (four to seven occurrences may be expected annually at any one point). Occasionally these hailstorms produce hailstones the size of hen's eggs, or tennis balls, causing devastation.

Snow occurs approximately eight times annually (mainly in midwinter) over the high-lying areas. The frequency decreases rapidly northwards, with snow being reported at most once or twice a year on the northern border of the Highveld region.

Average daily maximum temperature for this region oscillates between 27°C in January and 17°C in July, but in extreme cases these may rise to 38°C and 26°C, respectively. On the other hand, average daily minima range between 13°C in January to 0°C in July, whereas extremes can sink as low as 1°C and -13°C, respectively.

2.1.3 The impact of hailstorms on South African agriculture

Limited rainfall and infertile soil restrict the areas in South Africa suitable for crop cultivation. As a result, approximately 85 percent of farmland is devoted to raising livestock, particularly sheep, goats, cattle, hogs, and poultry. The majority of farmland utilized for cultivating crops (figure 2.6) lies within the Highveld region. Unfortunately (as seen in the previous section), this area is also the area of highest hail frequency in South Africa. The major crops produced on the Highveld are maize and wheat. Incidently, these two crops are also economically the most important

9

crops in South Africa (see table 2.1). Combined, maize and wheat consist of approximately 55 percent of the total crop production of South Africa with maize making up more than 40 percent of the total (Abstract of Agricultural Statistics, 1996). It is thus understandable that South African maize production is very susceptible to hail damage, and studies aimed at the understanding of hailstorms in the critical areas are very important.

2.2   The BPRP area

The BPRP area is an area within which the SAWB and the Water Research Commission (WRC) conduct precipitation research with a view to rainfall stimulation (Harrison *et al,* 1978; Mather and Terblanche, 1993). This area is defined as the region within a circumscribe of 100 km radius around the town of Bethlehem in the Free State. The areas, within this 100 km radius, that lie in the province of KwaZulu/Natal or Lesotho are excluded from the BPRP area (figure 2.7). Generally speaking, the terrain throughout the BPRP area rises gradually from west to east and north to south, but towards Lesotho the land rises more sharply. Bethlehem itself, at 28°15' S and 28°20' E, is located on the eastern portion of the Highveld region, at an elevation of 1687 m above sea level. Geographical features outside the BPRP area that greatly affect the climate of the area, are the Drakensberg mountains to the east and southeast of the area and the Indian Ocean approximately 350 km from Bethlehem.

2.2.1 Atmospheric circulation patterns over the BPRP area

The atmospheric circulation over the BPRP area plays an important role in the developing and maintaining of severe convective storms over the area. Tyson (1984) identified the main atmospheric circulation patterns responsible for the rain producing systems over South Africa (figure 2.8). The Free State is an interesting meteorological region as it lies within a transition zone between three of these main atmospheric circulation patterns. To the north of the region the precipitation is

controlled by the tropical easterlies and easterly waves, while anticyclonic ridging is responsible for rainfall to the south and southeast. To the west and southwest the main factor controlling the rain is the Southern Indian Ocean blocking circulation (Hudak, 1988).

The BPRP area lies in the region where the annual migration of the subtropical high takes place. In winter the high is stationed north of the area, but in the summer it moves south to the approximate latitude of Bethlehem. In addition, the intensity of the high varies meridionally due to the land-sea temperature difference. In winter the strongest cell of high pressure tends to remain over the land (which is generally much cooler than the warm water of the Indian Ocean), while in summer the reverse is true. In conjunction with the annual migration of the subtropical high, the position and strength of the zone of westerlies aloft combine to govern the weather over the project area.

In summer the westerlies aloft generally skirt south of the project area. At the surface the subtropical high has now moved south to approximately Bethlehem's latitude, but with its strongest cell still situated to the east over the Indian Ocean. Over the interior of South Africa there is a tendency for low level thermal troughing. The meandering nature of the westerlies aloft, along with the steady march of the subtropical high, give rise to a great variety of climatic conditions. Two extreme cases occur when a surface high or a surface low extend into the upper atmosphere. When a surface low pressure system extends into the upper atmosphere, conditions become more favourable for convective activity. When a surface high pressure system extends into the upper atmosphere, the situation becomes less favourable for convective activity (Hudak and Steyn, 1980; Steyn, 1984).

Kelbe and De Jager (1986) examined, on a synoptic scale, dynamical and thermodynamical fields related to free convection processes, in order to find specific meteorological phenomena associated with hail and non-hail days. Their results indicated that the development of severe convective activity could be due to either

11

thermal instabilities, convergence, or moisture supply depending on the location of the migratory westerly waves.

2.2.2 Precipitation over the BPRP area

The climate of the area may be described as a continental climate with cold winters and warm summers and is typified by high summer rainfall. The BPRP area receives approximately 85 percent of its annual precipitation during the summer months (October to March), mainly due to convective activity, although occasional prolonged periods of rain do also occur. The annual precipitation is between 580 and 680 mm in the immediate vicinity of Bethlehem, with the highest monthly total recorded in January (Hudak and Smith, 1980).

Steyn and Bruintjes (1990) studied the characteristics of convective clouds over the Bethlehem area. In their study they considered radar echoes greater than 10 dBZ. They found that the two main local factors controlling the development of convective activity over the project area are surface heating and topography. They also found that the diurnal distribution of development in areas where the terrain is fairly flat, shows a single pronounced peak in the onset of first development. The higher terrain, to the south of Bethlehem, shows two or more such peaks (figure 2.9).

Mather and Terblanche (1993) conducted a similar study, but concentrated on 30+ dBZ radar echoes instead of 10 dBZ echoes. The aim of their study was to summarize the characteristics of the more significant clouds which are represented in the precipitation research programme. They found a rapid increase in the number of 30+ dBZ echo development after 12:00 SAST. The majority of storm development was found to occur between 15:00 and 16:00 SAST, where after a gradual decrease in echo development took place (figure 2.10), again emphasising the major influence that surface heating has in the onset of convection. This study agrees well with that of Steyn and Bruintjes (1990), although the latter found a more gradual increase between the early morning and maximum activity.

12

2.2.3 Severe hail studies

There are three major hail study areas in South Africa: the Free State, the Eastern Transvaal and Gauteng. The Free State and Gauteng are both situated on the Highveld, some 250 km apart. The Eastern Transvaal is located to the northeast of Gauteng in a climatic region known as the "Lowveld" (figure 2.5). Understandably, all three of these areas fall within the belt of highest hail occurrence in South Africa. The Free State receives between seven and eight hail days per year, in comparison to the five to six of Gauteng and the four to five of the Eastern Transvaal (Schulze, 1965).

In the Free State hail occurrence is common on many days when cumulus nimbus development takes place. The most widespread and severe hailstorms occur in the first half of the season, with a maximum of hail occurrence in November. Carte and Held (1978) found this to be also true in Gauteng. Court (1979b) found that the peak hours for hailfall in the Free State are between 15:00 and 18:00 SAST. This is slightly earlier than what Carte and Held (1978) found for Gauteng, namely, between 16:00 and 18:00 SAST. Not only do hailstorms in the Free State start earlier, but they also seem to last longer and produce bigger hailstones than the storms over Gauteng. Court (1979b) found that the mean duration for point hail fall in the Bethlehem area was around 9.2 minutes, while in Gauteng it was only about 7.8 minutes.

Few studies concerning the development of severe hail producing storms over the Free State have been done. Research in this area, specifically concerned with hail producing systems were by Court (1979b) and Kelbe and De Jager (1986). Other related studies over the Free State were by Court (1979a), Greenacre and Pearce (1979), Harrison (1983) and Steyn (1988), but these were concerned with convective storms and not specifically with hail producing storms.

Some studies concerning hail producing storms over the Eastern Transvaal were conducted by Garstang *et al* (1987) and Kelbe (1984). Research over this area,

13

specifically concerned with hail suppression, were by Mather (1977), Mather, Bigg and Renton (1990) and Mather, Treddenick and Parsons (1976).

More studies concerning the development of hail producing storms over Gauteng have been published thought the years, than has been the case for either the Free State or the Eastern Transvaal. Some of these studies include: Carte (1965, 1966a, 1966b, 1979, 1980, 1981), Carte and Basson (1970), Carte and Held (1972, 1978), Carte and Mader (1977), Held (1973, 1974, 1977, 1978), Held and Carte (1973, 1979), Mader (1979), Mader *et al* (1986), Olivier (1988, 1989, 1990) and Terblanche (1985).

On a more general note, Poolman (1992) developed a one-dimensional model to objectively analyse the upper-air, in order to recognize favourable conditions for the development of large hailstones. He showed that the model is capable of predicting probable hailstone sizes for the interior of South Africa.

2.3   Storms

In order to simulate storms numerically, it is necessary first to understand the development and structure of storms as they occur in nature. The WMO Meeting of Experts (1981) discussed certain kinds of storms that seemed to be more regular in their behaviour than others. They classified these storms into three main groups, single cell storms, multicell storms and supercell storms. This classification, as set out by the Meeting of Experts, will be followed in this dissertation.

This classification scheme is based on the concept of a "cell", defined as a local precipitation maximum produced by a convective updraft. On this basis, the three storm categories can be defined as follow:

Single cell: A short-lived storm having only one cell

Multicell: A compact storm made up of short-lived cells that regenerate in a regular manner

Supercell: A big, destructive storm having a single long-lived cell.

This simple classification does not describe all observed storms, but it does describe a significant number of them. The storms not falling within these categories are mainly combinations of storms, for example, squall lines.

2.3.1 Single cell storms

Single cell storms (figure 2.11) are, on the macroscale, the simplest type of storm that can produce hail. They are usually relatively weak and produce hail on a small scale. The radar echo from the cell, when viewed in the horizontal plane, normally appears round or slightly oval in shape. When viewed in the vertical plane, it usually appears axisymmetric.

These storms do not always produce hail, but the location of the first echo serves as a good indication whether a storm cell will produce hail. Normally, first echoes from hail producing single cell storms, appear high in the supercooled region of the cloud. When these first echoes of single cell storms appear near the zero degree isotherm, it is an indication that the storm will not produce hail. After the first appearance of the echo at high altitude (of a hail producing single cell), the echo grows rapidly and precipitation reaches the ground within 20 minutes. Due to the axisymmetry of cells, precipitation eventually begins to fall into the region of updrafts. The updrafts are thus suppressed, while the downdrafts are stimulated, leading to the dissipation of the single cell. The average lifetime of such a single cell ranges between 30 and 45 minutes. The structure of the observed radar echoes changes significantly with time, and can thus be used as a good indicator of the stage of development of the storm cell. These storms normally develop on days when the wind shear and pressure gradients are small.

15

It is thought that hail embryos form in the upper part of the cloud, by the freezing of large drops or by riming of ice crystals. It is suggested that the air motions within the cell resemble a spherical vortex. In such a model, the embryos will be carried downwards near the edges of the cloud, before being advected inwards into the updraft region. The final hailstone growth will then take place during one simple ascent and descent. The calculated time required for a hailstone to reach 10 to 15 mm in diameter, is between 10 and 15 minutes after the initial appearance of the radar echo.

2.3.2 Multicell storms

A multicell storm (figure 2.12) is composed of a number of short-lived cells that undergo a regular life cycle. Multicell storms typically consist of one dominant cell, with one or more younger cells originating on a preferred flank (normally left in South Africa). The younger cells grow with time and subsequently become the dominant cell, while the older cells dissipate. New cells typically form every 5 to 10 minutes and may last for 30 to 45 minutes each. Chisholm and Renick (1972) claim that a total of 30 or more cells may develop during a typical storm's lifetime. This more or less regular manner in which the new cells are generated, is the reason why these multicell storms may persist for several hours. The movement of these storms is strongly influenced by cellular propagation, and the storms tend to deviate from the mean wind towards the low-level inflow sector. It is thought that the degree of regularity and organization of the cells is dependent on the wind shear. Of the three storm types discussed here, the majority of storms tend to fall into the category of multicell storms.

Hail embryos are believed to begin growing in the weaker updrafts of the new cells. It is suggested that the new cells do not interact with the older cells. Hail embryos, formed in the new cells, are carried along with the cell and continue to grow into hail during the stage in which the new cells merge with the mature part of the storm. If there is an interchange of particles between older cells and younger cells, the hail growth mechanisms are likely to be more varied and complicated.

16

2.3.3 Supercell storms

The term "supercell" was first used by Browning (1962) to describe what then appeared to him to be a particular form of the mature stage of a multicell storm. The supercell is, in fact, far more than this, and in subsequent years the model has been modified several times. This modified model, as it stands today, appears to account for the most significant kinematical characteristics of very severe local storms.

The important characteristics of supercell storms are their long life, large size and severity. Supercell storms are not as common as multicell storms, but they can account for a substantial amount of the total seasonal hail damage over an area, because of the large amount of hail that they produce. Some common features of a supercell's radar echo are: a large echo-weak vault, a persistent forward overhang, and occasionally a hook pattern in plan view.

Supercell storms (figure 2.13), like multicell storms, tend to form in environments with moderate to high instability. In the case of supercell storms, the wind shear tends to be larger than is observed during the formation of multicell storms. Strong low-level winds and a higher than average stability in the lower atmosphere are also features that lead to large, long-lived cells and the suppression of smaller, weaker convection. The vault is characterized by strong updrafts, estimated at between 30 and 50 ms^{-1}. At the middle and upper levels this strong updraft acts as an obstacle to the ambient wind, causing the airflow to split, resulting in a cyclonic and an anticyclonic branch on opposite sides of the storm. In general, it is believed that the precipitation core is associated with a significant downdraft.

In supercell storms the dominant updraft is in a quasi-steady state, and the two stages of hail growth are thought to take place in different regions of the storm. According to Browning and Foote (1976), the hail embryos tend to originate on the upwind side of the storm. These embryos will grow either in the turrets alongside the major updraft, or as re-circulated particles that may have grown during a pass through the edge of the main updraft. In either case, the embryos are thought to be embedded in the cyclonic branch of the streaming flow and will thus be forced to

17

pass around the sides of the storm and so avoid the sloping updraft. Through sedimentation and mixing, some of the hail embryos will eventually enter the main updraft where they will grow into hail.

2.4 Numerical models

2.4.1 Numerical models and their place in the BPRP

Numerical models can be of great benefit in a field project like the BPRP. In 1978 Harrison *et al* stated that there are five main ways in which model simulations can be useful to the BPRP:

1. They can refine the existing seeding methods by helping to specify the timing and/or amount of treatment;

2. They can suggest new modification hypotheses;

3. They can be used in real time as a forecasting tool to screen out situations unfavourable for the planned modification from those with conditions suitable for launching the experimental procedures;

4. They can be employed to develop seeding climatologies leading to estimates concerning the potential for water resource augmentation;

5. They can be used in evaluation to provide covariates and predictors helping to mitigate the high natural variability.

During the early years of the project (from the 1973/74 season), a one-dimensional steady state cloud model was run on a daily basis (Harrison *et al*, 1978). The ultimate purpose of this model was its use as a real time forecasting tool. Unfortunately, the underlying physics of this model was far from complete and the experiment was shelved.

Harrison *et al* (1978) also stated that the above aims would only be met if a three-dimensional mesoscale model were employed. Not only would such a mesoscale model be able to overcome one-dimensional shortcomings (assumption of a simple entrainment concept and inadequate physics) and two-dimensional shortcomings

18

(the fact that convergence of airflow is not two-dimensional in cumulus clouds), but it would also be able to incorporate dynamical effects into forecasting and evaluation.

2.4.2 The Clark three-dimensional numerical cloud model

In order to understand the complicated interactions between the physical and dynamical processes at work in convective clouds over a complex terrain, a three-dimensional time-dependent mesoscale model is required. With a view to understand these processes and attempt to come a step closer to achieving the aims set out in section 2.4.1, the Clark cloud model (Clark, 1977, 1979) was utilized to conduct numerical simulations over the BPRP area. For this dissertation two severe hailstorms that occurred in the BPRP area (one a multicell case and the other a supercell case) were chosen as case study days.

Clark's three-dimensional, non-hydrostatic, anelastic model has been in various stages of development since about 1974. This model was originally developed to address a wide variety of problems in fluid dynamics and meteorology, which required a limited-area model on a small spatial scale, where the lower boundary of the model is an irregular surface.

Through the years, the Clark cloud model, has been used in a wide variety of studies. Clark and Farley (1984), Clark, Hall and Banta (1994) and Peltier and Clark (1979) used this model in severe windstorm simulations. Bruintjes, Clark and Hall (1994) made use of the model in order to study winter time cloud dynamics, while Bruintjes, Clark and Hall (1995) used the model for tracer studies. More closely related to the present study, are the convective dynamical studies by Balaji and Clark (1988) and Smolarkiewicz and Clark (1985). Other research includes: gravity wave studies by Clark, Hauf and Kuettner (1986) and Hauf and Clark (1989), the entrainment studies by Grabowski and Clark (1991, 1993a, 1993b) and the frontal dynamic studies by Gall, Williams and Clark (1987, 1988).

19

Bruintjes (1992) used the model to conduct numerical simulations of winter time storms over Arizona, USA, and summer time convective cumulus clouds over Bethlehem and Carolina, South Africa. In his study, Bruintjes found a good agreement between the modelling results and the observations. He also found that the modelling results indicated the importance of the interaction between the airflow and the orography in determining preferred areas of cloud and precipitation development.

2.4.3 Equipment required to run the Clark model

The Clark model was originally developed on a CRAY computer, but the majority of the code is portable. Model run times vary dramatically depending on how the simulation is set up (domain size, resolution, physical parameters, etc.). For operational use, a workstation with at least 256 Mb of memory will be required.

In South Africa the model was run on a variety of computers over the years. Due to a lack of computer power and the need to develop machine dependant code, the model never ran successfully on these machines. In 1993 the SAWB purchased a CRAY Y-MP, but even with this new computer research with the Clark model was a long and slow process. This was partly because this new computer was still too small to run the model optimally, and partly due to the vast number of other models that was run on it. As this study drew to a close, the SAWB purchased a CRAY J90. On this new machine it is possible to run the model in real time, given that the model domain used is not to big.

20

Table 2.1: Gross value of individual agricultural crops (excluding horticultural and animal products) 1985/86 to 1994/95 (Source: Abstract of Agricultural Statistics, 1996)

YEAR	1985/86	1986/87	1987/88	1988/89	1989/90	1990/91	1991/92	1992/93	1993/94	1994/95
CROP	R 1000									
Maize	2 008 968	1 986 303	1 960 705	3 328 612	2 814 823	3 201 580	1 489 980	4 131 470	4 860 594	2 782 929
Wheat	534 916	864 521	1 257 265	1 220 682	929 947	879 422	1 321 345	923 083	1 492 808	1 353 929
Oats	2 055	8 706	12 847	7 636	5 899	6 549	10 264	13 731	12 386	16 318
Barley	52 716	53 328	88 186	41 081	94 449	119 252	83 458	150 160	150 703	195 676
Rey	456	565	610	648	665	1 722	2 056	1 103	1 650	1 440
Grain Sorghum	111 603	165 960	169 483	124 608	92 900	119 234	56 052	240 352	208 121	117 676
Hay	675 632	626 680	760 803	789 628	863 073	876 275	1 044 230	1 620 333	1 078 306	1 225 774
Lucerne seed	1 149	3 895	2 538	426	699	9 806	9 158	2 425	1 904	4 244
Dry beans	80 190	110 658	121 029	143 375	163 082	153 283	63 545	131 755	118 131	106 441
Dry peas	4 174	6 576	8 030	11 779	4 570	3 189	8 023	8 307	4 858	4 067
Lentils	1 677	2 002	2 024	917	1 414	1 735	1 216	810	103	199
Sugar cane	578 386	658 142	687 189	816 625	942 624	1 001 644	1 140 428	1 226 359	1 123 207	1 626 199
Chicory root	11 267	13 429	7 160	9 257	15 315	9 892	12 185	15 998	31 580	31 600
Tobacco	149 242	158 222	207 217	287 599	226 447	320 928	399 916	251 153	189 234	228 563
Cotton	95 650	143 272	192 981	192 545	190 102	141 228	66 526	42 703	107 900	100 767
Groundnuts	83 349	96 149	155 873	152 415	116 369	136 705	92 771	138 312	168 246	164 327
Sunflower seed	127 923	217 447	233 522	303 917	461 033	457 164	152 596	295 825	238 438	287 738
Soya beans	16 216	18 293	32 964	47 755	72 652	100 612	51 975	66 111	54 203	34 163
Wattle bark	20 490	29 475	29 447	41 233	43 478	48 051	81 915	54 068	43 756	45 000
Sisal	4 310	6 019	7 503	7 982	7 930	7 657	8 847	6 399	5 708	6 384
Other crops	11 600	12 800	14 000	16 800	17 450	18 800	19 696	20 190	22 536	23 664
TOTAL	4 571 969	5 182 442	5 951 376	7 545 520	7 064 921	7 614 728	6 116 182	9 340 647	9 914 372	8 357 098

Fig. 2.1   Location map of South Africa. Namibia, Botswana, Zimbabwe, Mozambique, Swaziland and Lesotho are also shown.
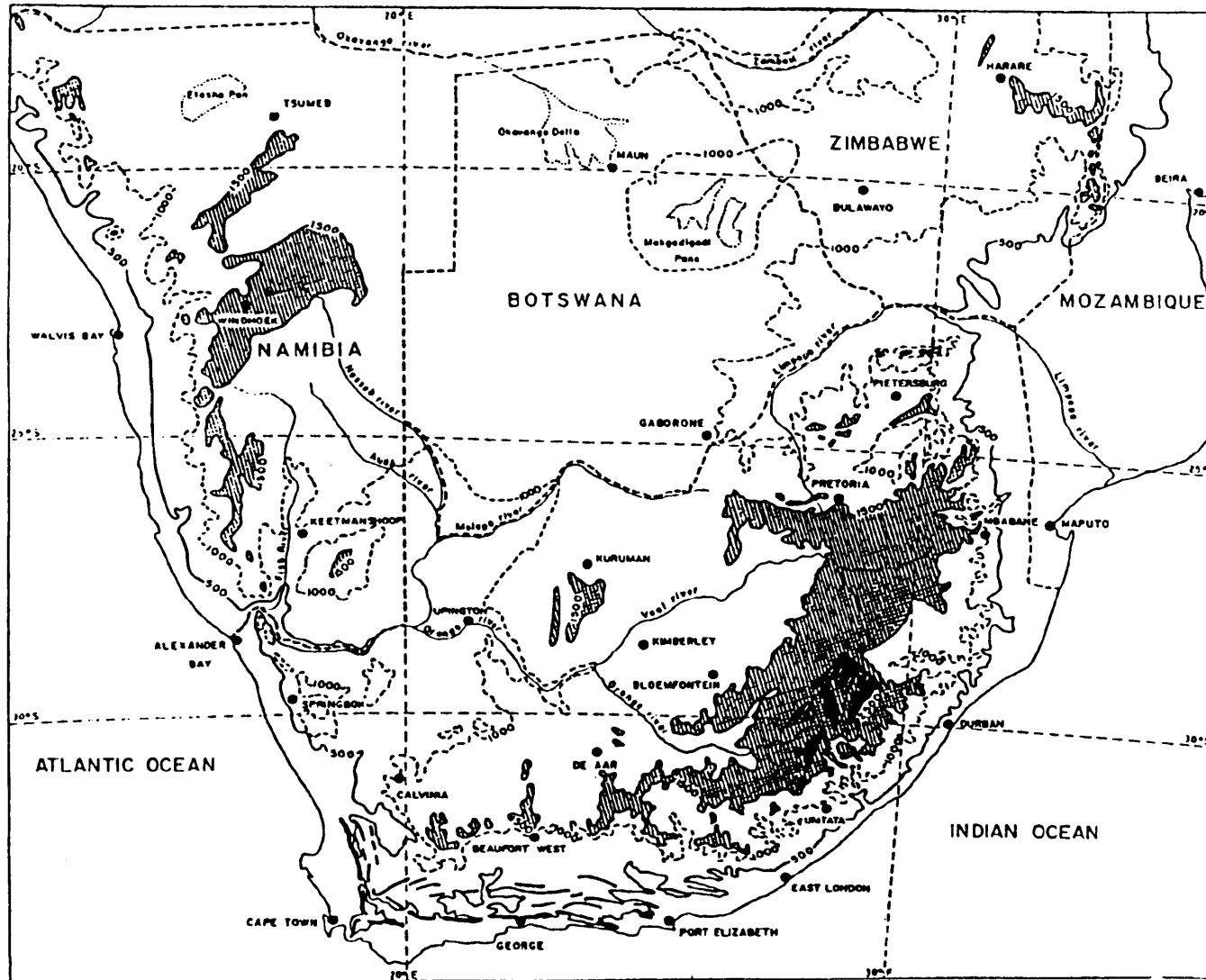
Fig. 2.2 Topographical and location map of Southern Africa. Contours are for 500, 1000, 1500 and 2500m.
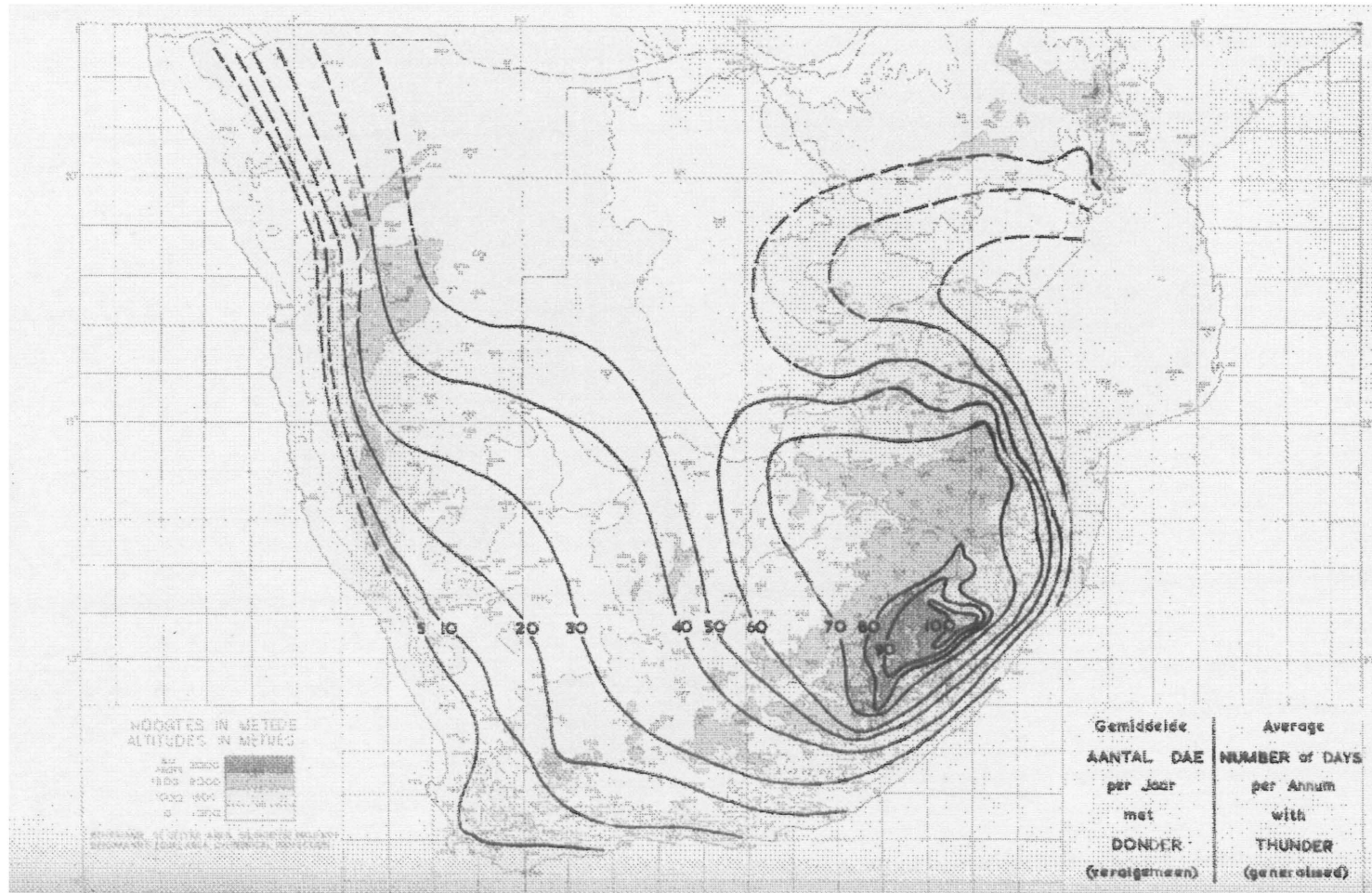
Fig. 2.3   Average number of days per annum with thunder (Schulze, 1965)
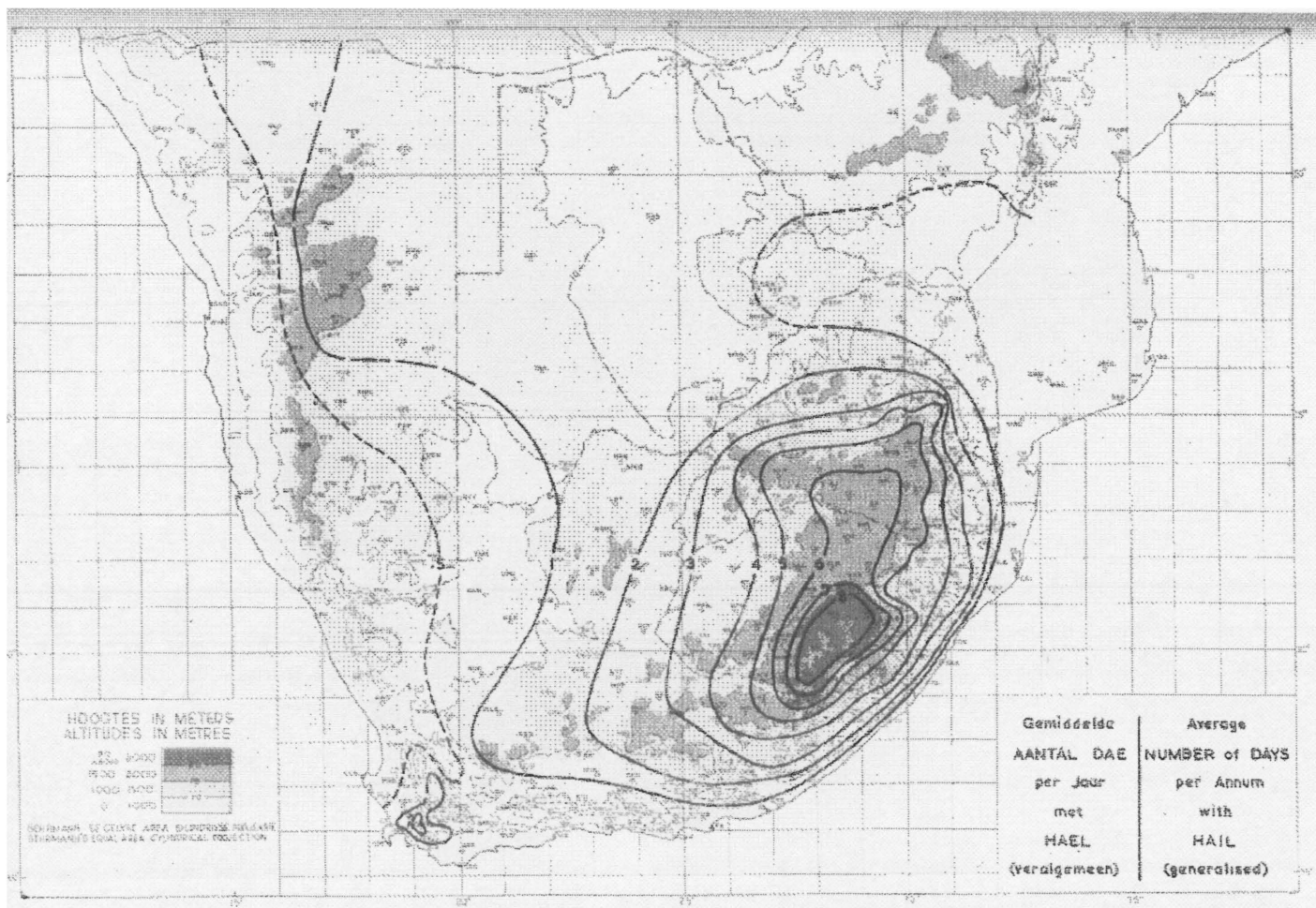
Fig. 2.4   Hail frequency - average number of days per annum with hail   (Schulze, 1965)

Fig. 2.5 The fifteen climatic regions of South Africa
(Highveld - H, Lowveld - L) (Schulze, 1965)

27
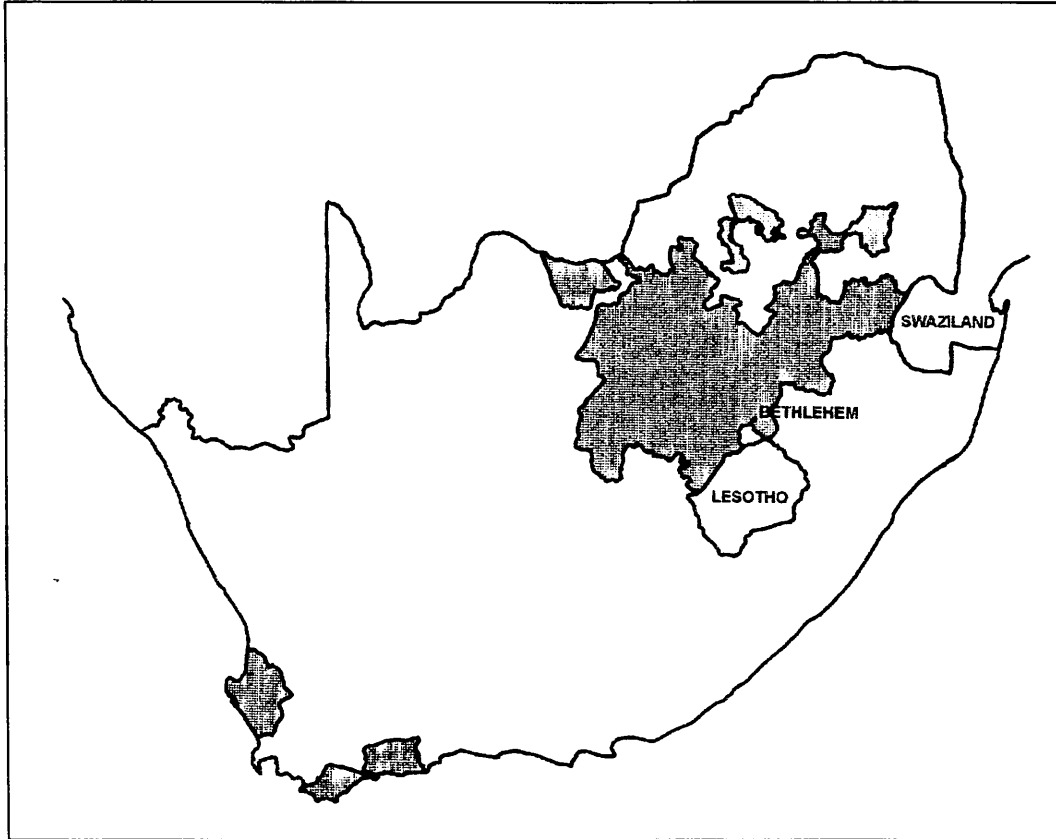
Fig. 2.6   Land utilized for cultivating crops in South Africa (shaded area)
            (Source: Reader's Digest Atlas of Southern Africa, 1982)
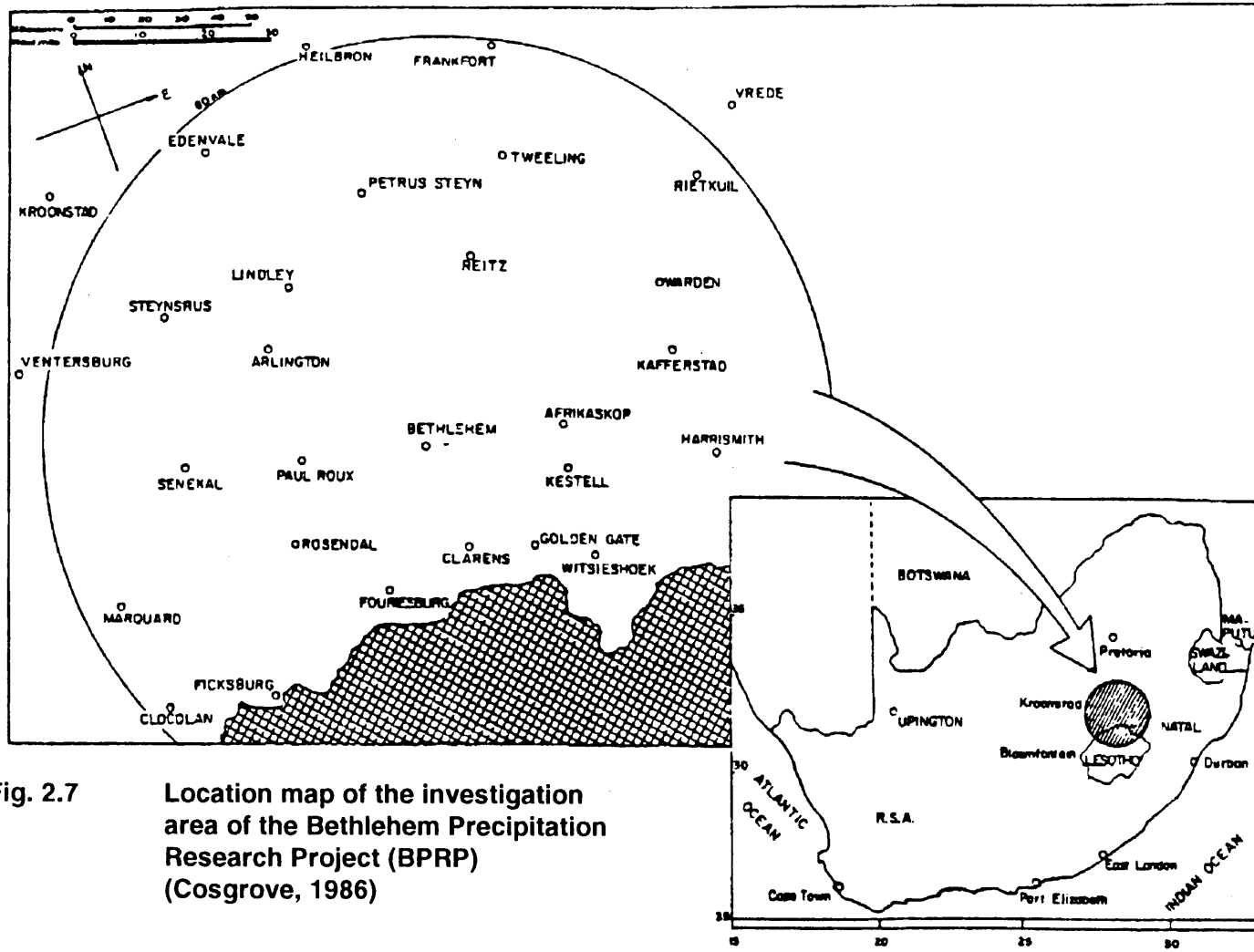
Fig. 2.7 Location map of the investigation area of the Bethlehem Precipitation Research Project (BPRP) (Cosgrove, 1986)
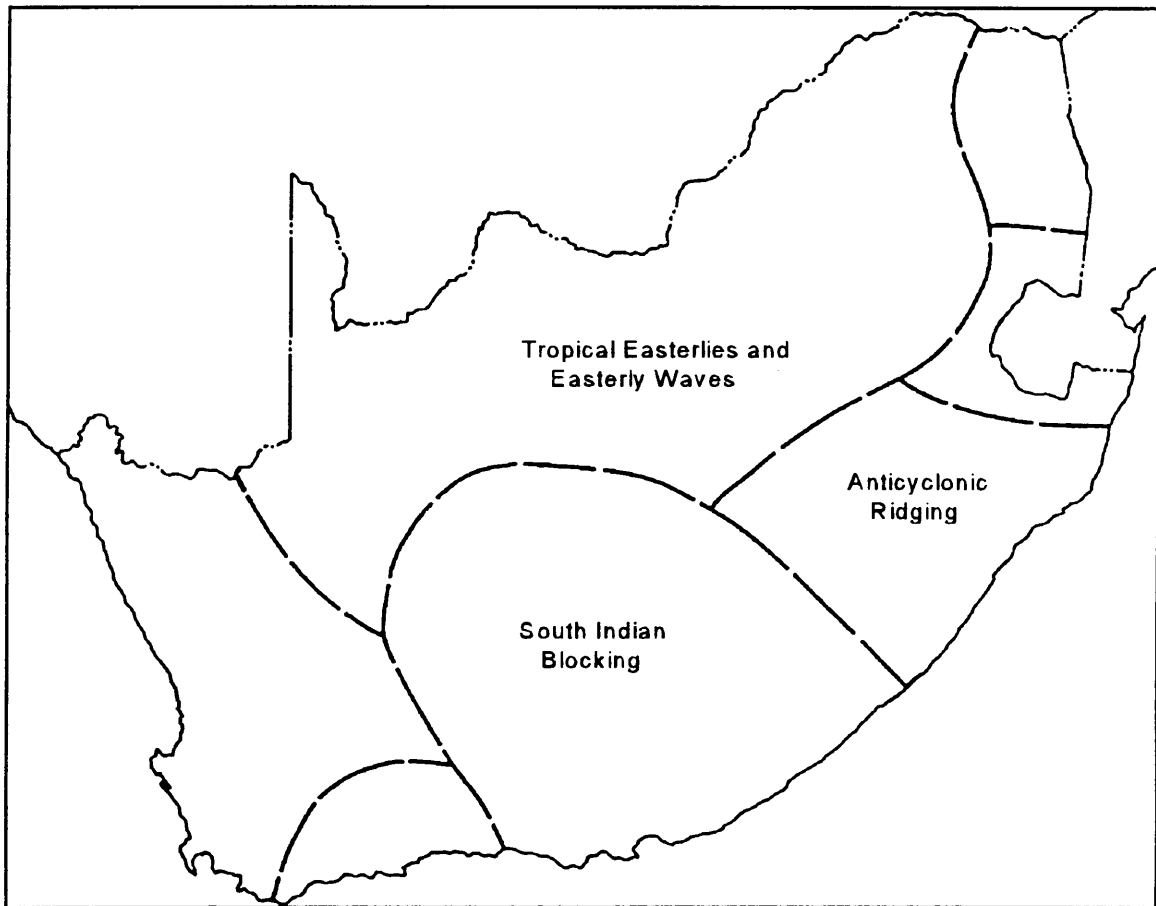
Fig. 2.8   The main atmospheric circulation patterns responsible for the rain producing systems over South Africa (after Tyson, 1984)
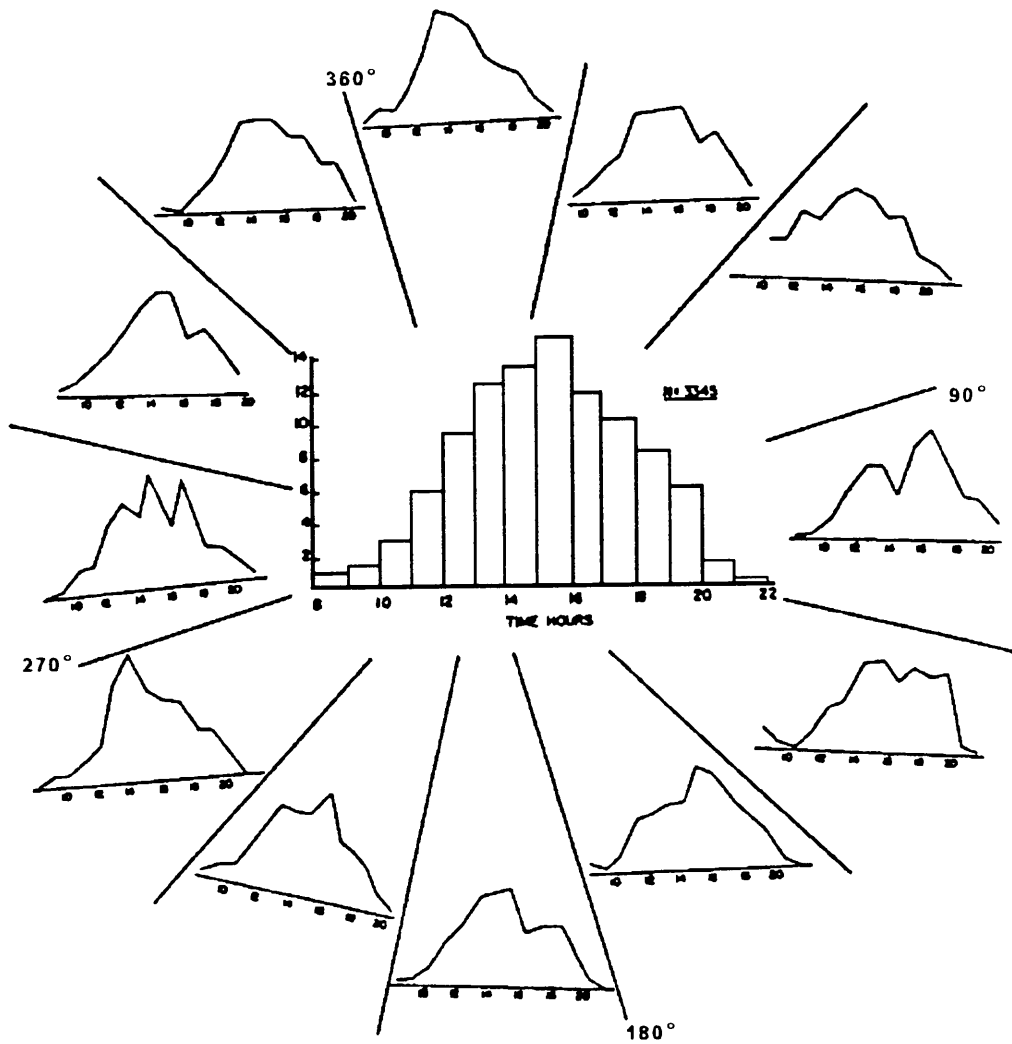
Fig. 2.9   Diurnal distribution of first echo development (inner diagram) and diurnal distribution of first echoes for different sectors (Steyn and Bruintjes, 1990).
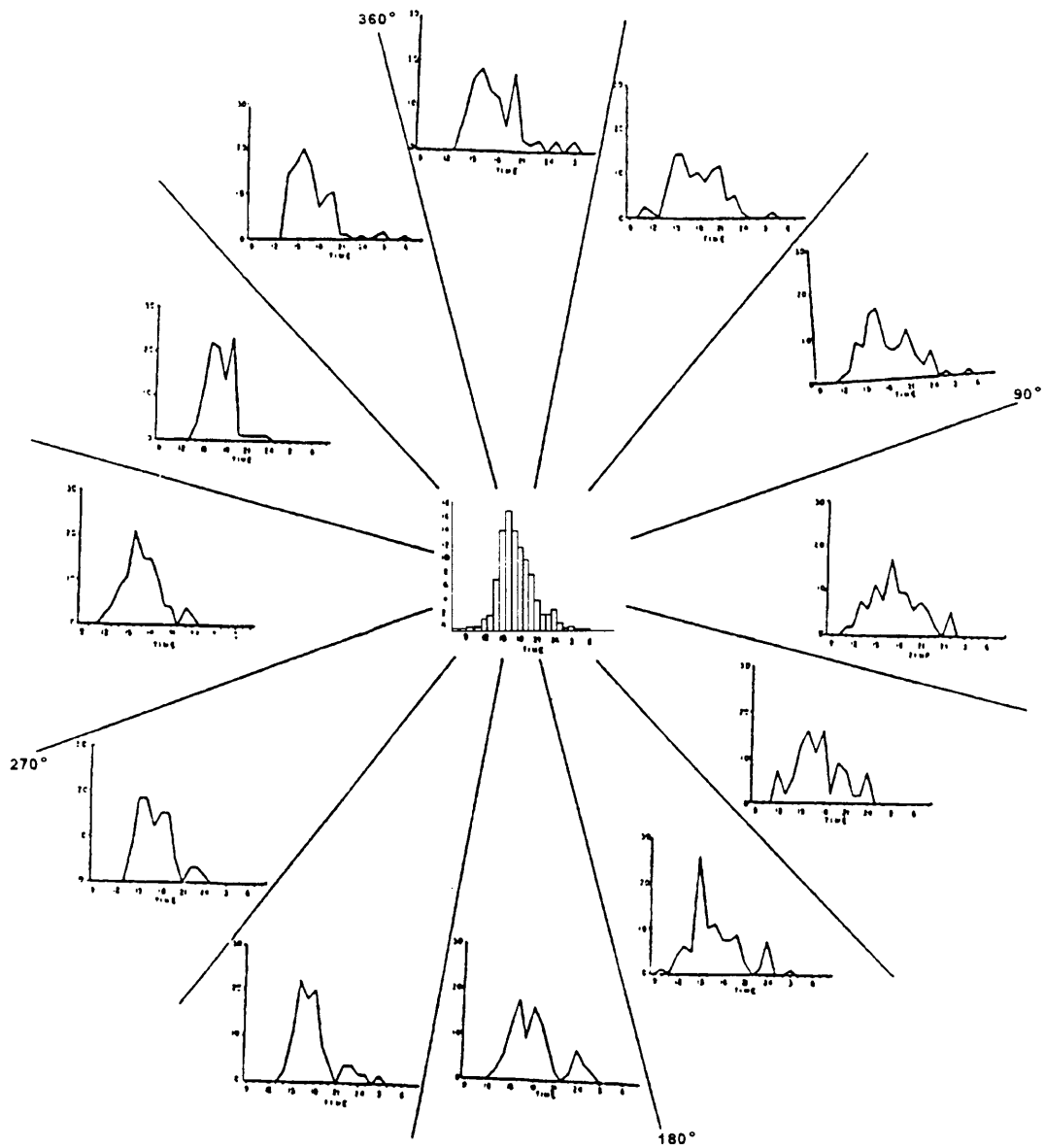
Fig. 2.10   Diurnal distribution of first echo development (inner diagram) and
diurnal distribution of first echoes for different sectors (Mather and
Terblanche, 1993)

31
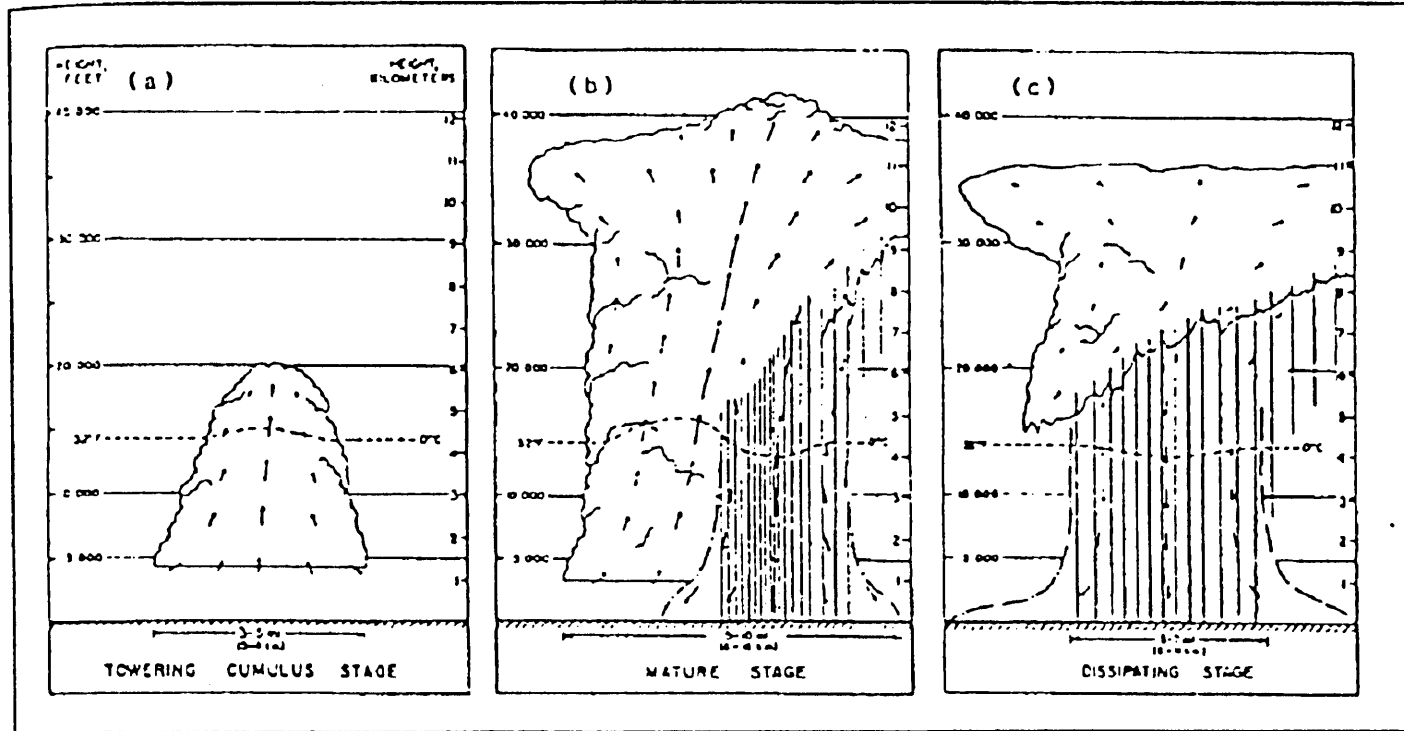
Fig. 2.11   The life cycle of a single cell a) Cumulus stage, b) Mature stage and c) Dissipating stage (Weisman and Klemp, 1986).
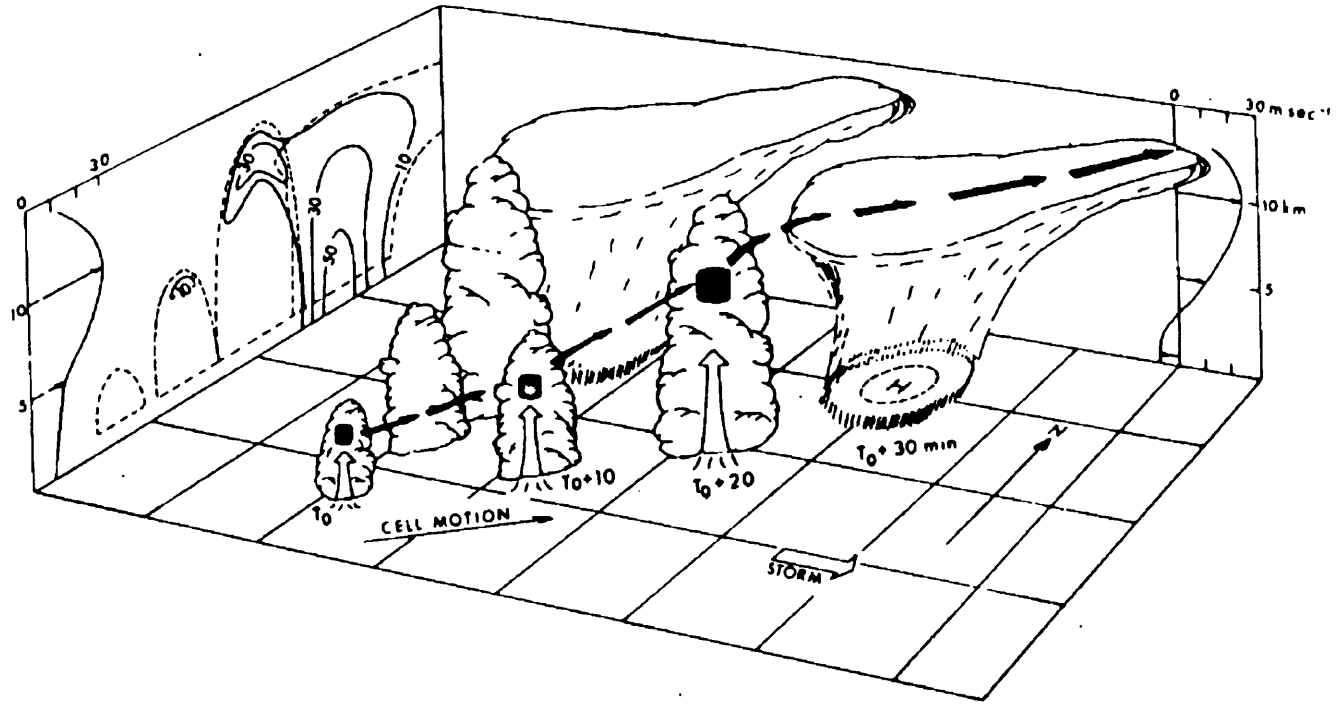
Fig. 2.12   Schematic depiction of a multicell storm. The heavy arrows depict air parcel trajectories (Chisholm and renick, 1972).
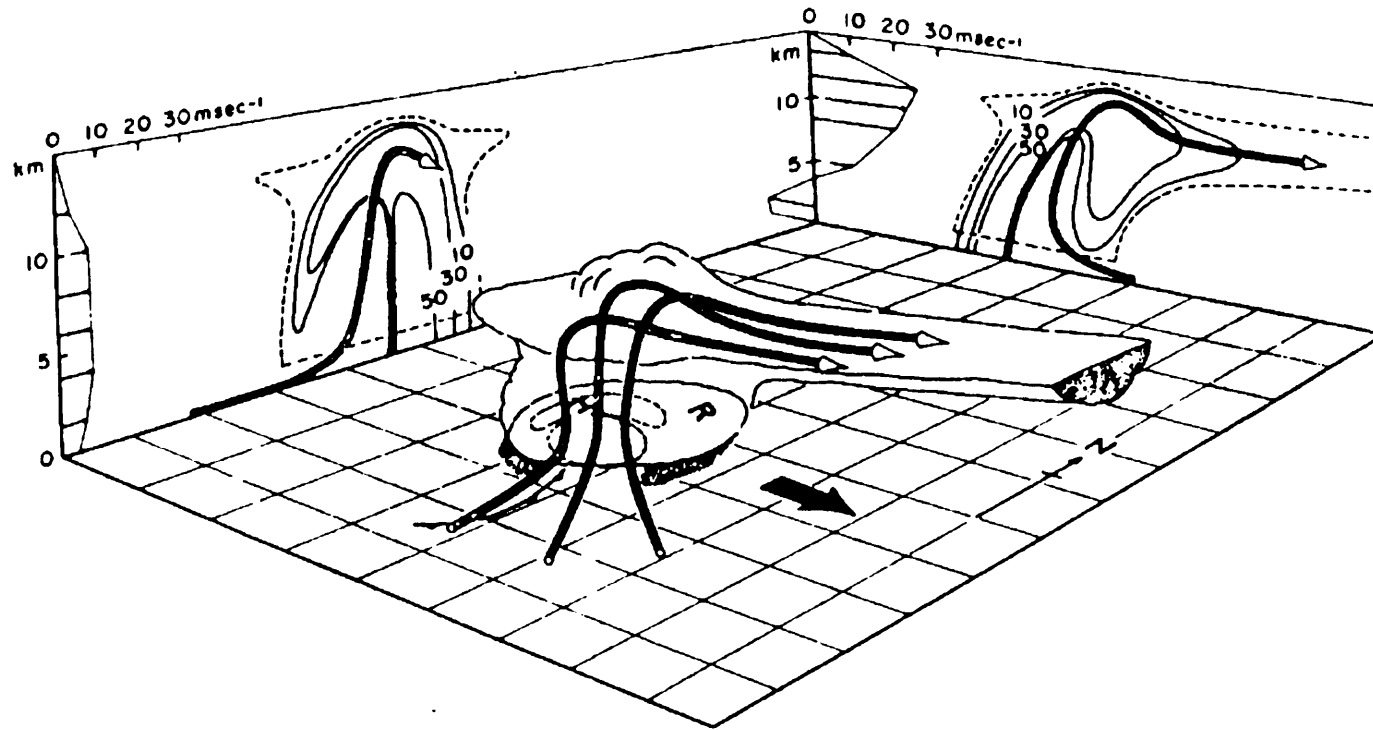
Fig. 2.13 Schematic depiction of a supercell storm. The contours Z_e are labelled in dBZ (Chisholm and Reinick, 1972).

Chapter 3

The Clark Model

In this chapter, the numerical model utilized is discussed in detail. The model used is the three-dimensional, time-dependent, non-hydrostatic, anelastic model developed by Clark (1977, 1979), Clark and Farley (1984) and Clark and Hall (1991). This model employs a terrain-following coordinate transformation, but in order to simplify the discussion, only the analytical equations will be shown. The model code is written so that the equations are solved in the transformed domain.

Section 3.1 describes the dynamics of the model and section 3.2 the physics of the model. In section 3.2, the warm rain parameterization as well as the ice microphysical processes are discussed in depth.

3.1 Dynamical equations

The momentum equations describe a balance between inertial forces, pressure gradient, Coriolis, buoyancy and friction effects. In the geospherical coordinate system, these equations (expressed in their most general form) look as follows:

$$\frac{Du}{Dt} - \frac{\tan\phi}{r}uv + \frac{uw}{r} = -\frac{1}{\rho}\frac{1}{r\cos\phi}\frac{\partial p}{\partial\lambda}$$
$$+ fv - f'w + \frac{1}{\rho}\left[(\nabla\cdot\tau)_1 - \frac{\tan\phi}{r}\tau_{12} + \frac{1}{r}\tau_{13}\right] \tag{3.1a}$$

35

$$\frac{Dv}{Dt} + \frac{\tan \phi}{r} u^2 + \frac{vw}{r} = -\frac{1}{\rho} \frac{1}{r} \frac{\partial p}{\partial \phi}$$

$$- fu + \frac{1}{\rho} \left[(\nabla \cdot \tau)_2 + \frac{\tan \phi}{r} \tau_{11} + \frac{1}{r} \tau_{23} \right] \tag{3.1b}$$

$$\frac{Dw}{Dt} - \frac{1}{r} (u^2 + v^2) = -\frac{1}{\rho} \frac{\partial p}{\partial r} + \frac{p\sigma}{\rho}$$

$$+ f^* u + gB + \frac{1}{\rho} \left[(\nabla \cdot \tau)_3 - \frac{1}{r} (\tau_{11} + \tau_{22}) \right] \tag{3.1c}$$

where

$$\frac{D}{Dt} = \frac{\partial}{\partial t} + \frac{u}{r \cos \phi} \frac{\partial}{\partial \lambda} + \frac{v}{r} \frac{\partial}{\partial \phi} + w \frac{\partial}{\partial r}$$

$$(\nabla \cdot \tau)_i = \frac{1}{r \cos \phi} \frac{\partial \tau_{i1}}{\partial \lambda} + \frac{1}{r \cos \phi} \frac{\partial}{\partial \phi} (\cos \phi\ \tau_{i2}) + \frac{1}{r^2} \frac{\partial}{\partial r} (r^2\ \tau_{i3})$$

$$B = \left(\frac{(\theta - \bar\theta)}{\bar\theta} + \epsilon(q_v - \bar{q_v}) - q_c - q_R - q_{iA} - q_{iB} \right)$$

The velocity components are u (eastwards), v (northwards) and w (along the radius). The Coriolis parameter f is equivalent to $2\Omega \sin \phi$, while f^* is equal to $2\Omega \cos \phi$. The density in the anelastic system is represented by ρ, while θ, q_v, q_c, q_R, q_{iA} and q_{iB} are the potential temperature, water vapour, cloud water, rain water, ice and graupel mixing ratios, respectively. Variables with an overbar represent the unperturbed environmental profiles. The parameter ϵ is equivalent to $(R_v / R_d - 1)$, with R_v and R_d the gas constants for dry air and water vapour, respectively. The stress tensor due to sub-grid scale turbulence and mixing processes is τ_{ij}. The stress tensor is parameterized according to the first-order theory of Smagorinsky (1963) and Lilly

36

(1962). Clark (1979) gives a description of this scheme in terms of an eddy mixing coefficient for momentum (K_m).

The anelastic continuity equation in the geospherical system is given by:

$$\frac{1}{r\,\cos\,\phi}\,\frac{\partial}{\partial\lambda}(\rho u) \;+\; \frac{1}{r\,\cos\,\phi}\,\frac{\partial}{\partial\phi}(\cos\,\phi\,\rho v) \;+\; \frac{1}{r^2}\,\frac{\partial}{\partial r}(r^2\,\rho w) \;=\; 0 \tag{3.2}$$

Equations (3.1) and (3.2) represent the smooth earth equations. The model equations are then transformed to a non-orthogonal, terrain-following system of coordinates (Clark, 1977), by making use of the following transformation,

$$z \;=\; F(\zeta)\left(1 - \frac{h}{H}\right) + h \tag{3.3}$$

$$(F(0) = 0 \;\; and \;\; F(H) = H)$$

where ζ is the new vertical coordinate. The model is formulated using $\Delta\zeta$ = constant for any particular domain. $F(\zeta)$ is chosen as a monotonically increasing function between 0 and H, so that the surface of the model follows the terrain and the model's upper boundary is at a constant level z = H. This process maps an irregular domain onto a regular domain, in which treatment of the lower boundary condition of zero normal air velocity at the height of the surface topography (z = h) is considerably simplified.

The model employs a form of the anelastic approximation with expansion of the thermodynamic variables around vertical profiles of an idealized atmosphere with constant stability. This idealized atmosphere, is considered to be in a mean flow corresponding to hydrostatic and geostrophic balance. The thermodynamic variables are separated into a basic state, plus perturbations from the basic state. The base

37

state and the sum of the base state plus perturbation, are both in hydrostatic balance (see Clark, 1979).

The finite-difference formulations of the momentum equations are solved using centred-space and centred-time differences according to the second-order conservative scheme of Arakawa (1966). The present version of the model has interactive two-way grid nesting capabilities. Currently, up to seven nested grids are allowed (Clark and Farley (1984) and Clark and Hall (1991)). Only the boundaries conditions for the outer-most of these domains are specified. The boundary conditions for the inner domains are supplied by the outer domain. The conditions at the outer-most domain, include free-slip boundary conditions for the velocity components and zero-flux conditions for all thermodynamic variables at the upper and lower surfaces of the model. To prevent the reflection of vertically propagating gravity waves from the upper boundary, a "sponge" layer is introduced in the upper portion of the model domain. This "sponge" layer employs Rayleigh damping and Newtonian cooling. The lateral boundary conditions (in the present simulations) are approximated by an open-boundary extrapolation scheme.

3.2 Physical equations

The microphysics in the model use bulk parameterizations for both the water and ice phases. The water phase is parameterized according to a modified form of the Kessler (1969) scheme. In this scheme, liquid water can exist in two forms, firstly as cloud water with mixing ratio q_c and secondly as rainwater with mixing ratio q_R. The ice phase parameterization closely follows the work of Koenig and Murray (1976), hereafter referenced as K-M. The K-M parameterization allows for the existence of two types of ice particles, Type A and Type B.

The average precipitating drop is by definition larger than the average suspended drop; similarly, the average Type B ice particle tends to be larger than the average Type A ice particle, but it need not be. (These water and ice phase parameterizations

38

will be discussed in more detail in the following sections.) Consequently five categories, denoted by subscript j, for the water substances have to be allowed for in the equations for the conservation of heat and the water and ice substances. They are:

1. Water vapour
2. Suspended droplets (cloud water)
3. Precipitating rain drops
4. Type A ice particles (heterogeneously nucleated ice particles and "splinters")
5. Type B ice particles (homogeneously nucleated ice particles; graupel).

The equations governing heat and moisture conservation are (Clark, 1979 and Bruintjes, 1992):

$$\rho \, \frac{D\theta}{Dt} = \frac{\rho L_{lv}}{c_p T} (C_{2d^1} + C_{3d^2}) + \frac{\rho L_{lv}}{c_p T} (C_{jd^1} + C_{jd^2} + C_{d^3})_{j=4,5}$$

$$+ \frac{\rho L_{il}}{c_p T} (C_{jd^4} - C_{jd^6})_{j=4,5} + \frac{\rho L_{lv}}{c_p T} (C_{jd^5})_{j=4,5} + \nabla \cdot (\rho K_H \nabla \theta) \tag{3.4}$$

$$\rho \, \frac{Dq_v}{Dt} = - \rho \, (C_{jd^1})_{j=2,4,5} + \rho \, (C_{jd^2})_{j=3,4,5} - \rho \, (C_{d^3}) + \nabla \cdot (\rho K_H \nabla q_v) \tag{3.5}$$

$$\rho \, \frac{Dq_c}{Dt} = \rho \, (C_{jd^1})_{j=2} - \rho \, (C_{jd^5})_{j=4,5} - S_{ac} - S_c + \nabla \cdot (\rho K_H \nabla q_c) \tag{3.6}$$

39

$$\rho\,\frac{Dq_R}{Dt} = -\rho\,(C_{jd^2})_{j=3} - \rho\,(C_{jd^4})_{j=5} - \rho\,(C_{jd^5})_{j=4,5}$$
$$+ \rho\,(C_{jd^6})_{j=4,5} + S_{ac} + S_c + \nabla \cdot (\rho K_H \nabla q_R) - \frac{\partial}{\partial z}(\rho \overline{V}_{T_R} q_R) \tag{3.7}$$

$$\rho\,\frac{Dq_{iA}}{Dt} = \rho\,(C_{jd^1} - C_{jd^2} - C_{jd^6})_{j=4} + \rho\,(C_{jd^5})_{j=2,3}$$
$$+ \rho\,(C_{d^3}) - \rho\,(C_{jd^4})_{j=5} + \nabla \cdot (\rho K_H \nabla q_{iA}) - \frac{\partial}{\partial z}(\rho \overline{V}_{T_A} q_{iA}) \tag{3.8}$$

$$\rho\,\frac{Dq_{iB}}{Dt} = \rho\,(C_{jd^1} - C_{jd^2} - C_{jd^6})_{j=5} + \rho\,(C_{jd^5})_{j=2,3}$$
$$+ \rho\,(C_{jd^4})_{j=3,4} + \nabla \cdot (\rho K_H \nabla q_{iB}) - \frac{\partial}{\partial z}(\rho \overline{V}_{T_B} q_{iB}) \, , \tag{3.9}$$

where C_{d^1} represents the condensation/evaporation (deposition/sublimation) due to diffusional growth of water drops (ice crystals). C_{d^2} represents the rate of evaporation/sublimation of rain drops and ice in subsaturated air. The nucleation rate of Type A and Type B ice are represented by C_{d^3} and C_{d^4}, respectively. C_{d^5} is the rate of accretional growth of Type A and Type B ice due to the collection of cloud drops and rain drops, while C_{d^6} represents the melting of Type A and Type B ice to form rain water. The transfer rate of cloud water to rain water due to autoconversion is S_{ac}, while the transfer rate of cloud water to rain water due to rain drops collecting cloud droplets is parameterized by S_c. The latent heats of condensation, sublimation and fusion are L_{lv}, L_{iv} and L_{il}. K_H is the eddy mixing coefficient used for heat and moisture. The mass-weighted average terminal velocities for rain drops, Type A and Type B ice are represented by $\overline{V}_{T_R}$, $\overline{V}_{T_A}$ and $\overline{V}_{T_B}$. During condensation/evaporation of cloud water C_{d^1} is calculated using the so-called bulk physical assumption in

40

which one attempts to maintain 100% relative humidity. Thus, during condensation q_v is equal to q_{vs} (the saturation value of q_v), while during cloud water evaporation C_{d^1} is calculated such that $q_v \leq q_{vs}$. The second-order-accurate positive-definite advection transport algorithm of Smolarkiewicz (1984) was used for the conservation equations of heat and moisture. These microphysical processes are schematically depicted in figure 3.1.

3.2.1 Warm rain parameterization

A short overview of the Kessler (1969) warm rain process will now be given. This scheme is described in detail in Clark (1979). In this scheme, the main assumptions are (1) liquid water is subdivided into cloud water with a mixing ratio q_c and rain water with a mixing ratio q_R, (2) rain water drops are assumed to exist in a Marshall-Palmer type distribution and fall with their mass-weighted mean terminal velocity, and (3) a threshold cloud water content q_{c0} must exist before autoconversion from cloud water to rain water can take place. The form taken for the distribution of rain water in terms of the diameter is,

$$f(D) = N_0 \, e^{-\lambda D} \tag{3.10}$$

where $f(D)$ represents the density function of rain drops. Following Atlas *et al* (1973) the terminal velocity of rain drops is taken as,

$$V_T(D) = \alpha_1 - \alpha_2 e^{-\beta D} \tag{3.11}$$

where $\alpha_1 = 965$ cm s^{-1}, $\alpha_2 = 1030$ cm s^{-1} and $\beta^{-1} = 0.166$ cm. Defining the mass-weighted terminal velocity as,

41

$$\overline{V}_T = \frac{\int_0^\infty D^3 f(D) V_T(D) dD}{\int_0^\infty D^3 f(D) dD} \quad , \tag{3.12}$$

and combining (3.10) to (3.12), one will find,

$$\overline{V}_T = \alpha_1 - \alpha_2/(1 + \beta/\lambda)^4 \tag{3.13}$$

and

$$\lambda = [\pi \rho_L N_0/(\rho_d q_R)]^{1/4} \tag{3.14}$$

where ρ_L is 1 g cm^{-3} and ρ_d is the density of dry air.

The formulas used for S_{AC} and S_C are similar to those used by Kessler (1969). Cloud water is converted to rainwater at a fixed rate (A_{01}) when the cloud water mixing ratio surpasses a threshold value (A_{02}). This can be expressed as:

$$S_{AC} = \begin{cases} A_{01} (q_c - A_{02}), & if \quad q_c \geq A_{02} \\ 0, & otherwise \end{cases} \tag{3.15}$$

The autoconversion rate A_{01} and the threshold cloud water amount A_{02} are constants and they are set according to the type of experiment that is being done. The treatment for S_C was taken as,

$$S_C = A_{05} E_{11} N_0^{1/8} q_c (\rho_d q_R)^{7/8} \tag{3.16}$$

42

where A_{05} equal to 0.2935 and E_{11} equal to unity were assumed. The value chosen for N_0 in the experiments was $N_0 = 10^7$ m^{-4}.

3.2.2 Ice microphysical parameterization

The current ice microphysical scheme in the three-dimensional model closely follows K-M. This formulation allows the existence of two types of ice particles. Type A ice represents ice particles that are initially small having been created either by heterogeneous ice nucleation or ice splintering. Type B ice (graupel) represents ice particles that are initially large, having been created by the freezing of rain drops. Each category of ice (Type A and Type B) is represented by two variables, the mixing ratio (q_j) and the number density or number of particles per unit volume, denoted by N_j. The average particle mass m_j, is defined in such a way that the number density is related to the mixing ratio through the expression,

$$N_j \, m_j \;=\; q_j \rho_d \tag{3.17}$$

In this application it is assumed that particles of mass m_j represent the entire spectrum of particles of category j.

The ice growth processes currently included in the model are:
   a.   Nucleation of Type A ice by a subscribed sorption nucleation spectra
   b.   Nucleation of Type B ice through the collision of Type A ice with rain drops
   c.   Diffusional and riming growth of Type A and Type B ice particles
   d.   Melting of Type A and Type B ice particles to form rain water
   e.   Homogeneous nucleation of Type A ice at temperatures below -40°C.

The physical equations describing each of these processes are now presented (in cgs units).

a. Nucleation of Type A ice by a subscribed sorption nucleation spectra (C_{d^3}).

This can occur whenever the air is saturated with respect to liquid water and the temperature is below T_0 (0°C) or whenever the air is supersaturated with respect to ice and the temperature is below a certain threshold (-12°C). It is assumed that the maximum number of new particles that can be generated by this process is a function of temperature,

$$N_{IF} = A_{06} \exp\left[\frac{\ln(10)}{A_{07}} \max[(273.15 - T), 20] \right] \qquad (3.18)$$

with a maximum value allowed at T = -20°C, and a constant number at temperatures colder than -20°C. A_{06} and A_{07} are constants that may vary for each experiment depending on the rate of nucleation desired. The actual number of particles generated will also depend on the number already present at any given time

$$\delta N_{IA} = \max[(N_{IF} - N_{IA}), 0] \qquad (3.19)$$

It is also assumed that each newly nucleated ice particle has a mass (m_3) of 10^{-11} gm (equivalent to an ice sphere having a diameter of 3 μm). Thus the nucleation rate of Type A ice particles (C_{d^3}) is,

$$C_{d^3} = \frac{\delta N_{IA} \times 10^{-11}}{\rho_d} \qquad (3.20)$$

44

b. Nucleation of Type B ice through the collision of Type A ice with rain drops (C_{d^4}).

Nucleation of Type B ice occurs when a rain drop collides with a Type A ice crystal at temperatures below $0°C$. For each drop-crystal contact one precipitating drop and one Type A ice particle are lost and one Type B ice particle (graupel particle) is gained with the average mass (m_5) equal to the sum of mass ($m_3 + m_4$) of the two colliding particles. As derived by K-M, the number of drop-Type A ice contacts during one time step is

$$\delta N_{IB} = \frac{3\delta t \ N_0^{1/4} \ (\rho_d \ q_R)^{3/4}}{4A_{08} \ \rho_l} \ | \ V_{T_R} - V_{T_A} \ | \ N_{IA} \ E_{il} \tag{3.21}$$

where ρ_l is the density of the water, A_{08} is a constant and E_{il} is the collision efficiency, which is assumed to be unity. Consequently, the nucleation rate of Type B particles is,

$$C_{d^4} = \frac{\delta N_{IB}}{\rho_d} \ (m_3 + m_4) \tag{3.22}$$

c. Diffusional and riming growth of Type A and Type B ice particles $((C_{jd^i})_{j=4,5; \ i=1,5})$.

The growth rate of the entire spectrum of Type A and Type B ice particles can be parameterized in terms of the mass of a "growth mean" ($\overline{m}_j$) particle. The model calculates the growth of ice particles by diffusion of water vapour and riming, where the growth rates depend upon the ice particles' mean mass and the liquid water mixing ratios. K-M have parameterized the growth rates into four regimes based upon the detailed ice particle calculations of Koenig (1972). The growth rates in these different growth regimes are illustrated in figure 3.2 (after Koenig, 1972).

45

In the first regime (Regime A-E), only growth through vapour diffusion occurs, because there is too little liquid water available to support riming growth ($(q_c + q_R) \leq 5 \times 10^{-2}$ gm m^{-3}). In the second regime (Regime A-B), also only growth through vapour diffusion occurs, because in this case the ice crystals are still too small for riming to occur ($\overline{m_j} > 5 \times 10^{-8}$ gm (particle sizes smaller than 50 µm)). The appropriate value of δm_j in these two regimes are as follows:

$$\delta m_j = \delta t \left(\frac{q_v - q_{vis}}{q_{vs} - q_{vis}} \right) \alpha(\overline{m_j})^\beta \qquad (3.23)$$

where α and β are functions of temperature that determine the growth rate of ice particles and q_{vs} and q_{vis} are the saturation water vapour mixing ratios for water and ice, respectively. These regimes are also active during sublimation when $q_v < q_{vis}$. This differs from the K-M approach, where an analogous to Kessler's (1969) raindrop evaporation term was used.

In the third regime (Regime B-C), diffusion and riming simultaneously take place when $(q_c + q_R) > 5 \times 10^{-2}$ gm m^{-3} and 5×10^{-8} gm $< \overline{m_j} \leq 10^{-4}$ gm (particle sizes between approximately 50 and 600 µm). Letting

$$\tan \psi = 1 + \frac{\ln(\rho_d(q_c + q_R))}{10} \qquad (3.24)$$

and

$$\gamma = \delta t\, \alpha(5 \times 10^{-8})^\beta \qquad (3.25)$$

where ψ is the angle between BC and the horizontal from B (see figure 3.2, determined from the liquid water content), and γ is the mass growth rate due to diffusion. Then

46

$$\delta m_j = \gamma \left(\frac{\overline{m_j}}{5 \times 10^{-8}} \right)^{\tan \psi} \tag{3.26}$$

As particles grow by riming, the maximum to minimum dimension of an ice particle decreases. Eventually the particles tend to a spherical shape and riming growth starts to dominate. Therefore, only riming occurs in the fourth regime (Regime C-D) when $\overline{m_j} > 10^{-4}$ gm (this is for particles sizes greater than 600 μm). Letting

and
$$\zeta = \gamma (2 \times 10^3)^{\tan \psi} \tag{3.27}$$

then
$$\xi = \frac{\ln \left[\rho_d (q_c + q_R) \times \dfrac{10^9}{\zeta} \right]}{\ln [10^4]} \tag{3.28}$$

$$\delta m_j = \zeta (\overline{m_j} \times 10^4)^\xi \tag{3.29}$$

The growth computations are determined separately for each ice category (Type A and Type B ice particles). The rate of change in terms of the mixing ratio is related to the total change in mass due to diffusional growth and riming, by the expression

$$(C_{jd}{}^i)_{j=4,5; \ i=1,5} = \frac{N_j \ \delta m_j}{\rho_d} \ , \tag{3.30}$$

47

where the subscript i denoted the type of growth (diffusional or accretional) depending on the growth regime. Once calculated, these values are then used in the governing equations for heat and moisture conservation (equations (3.4) to (3.9)).

In calculating the transfer of latent heat during growth or sublimation in the different regimes it is assumed that the latent heat of sublimation (L_{iv}) adequately approximates the processes in the first and second regimes, while the latent heat of condensation (L_{lv}) is used in regimes three and four. The assumption was therefore made that the mass added through diffusional growth is negligible compared to the mass added by riming growth. Therefore in the conservation equations for heat and moisture it is assumed that only riming growth occurs in regimes three and four. In addition, it is assumed that depletion of liquid water during riming growth only occurs in the rain water field until it is exhausted, where after water will be removed from the cloud water field.

d.   **Melting of Type A and Type B ice particles to form rain water** ($(C_{jd^6})_{j=4,5}$). Melting occurs when the particles fall or are advected into a region where the ambient temperature is above 0°C. If the average particle mass is less than 10^{-8} gm, it is assumed that it will melt instantly. For larger particles, the mass change during one time step, due to melting is

$$\delta m_j = A_{10} \delta t \, \overline{R}_j \, (T - 273.15) \, [1 + A_{11}(-\overline{R}_j \overline{V}_{T_j} \, \rho_d)^{1/2}] \qquad (3.31)$$

where $\overline{R}_j$ represents the average radius of the entire ice particle spectrum. A_{10} and A_{11} are constants. $\overline{R}_j$ is calculated with the aid of the following equation,

$$\overline{R}_j = \left(\frac{3 q_{i_j} \rho}{4 \pi N_j \rho_i} \right)^{1/3} \qquad (3.32)$$

48

The rate of change due to melting of ice particles in the mixing ratio field is then given by

$$(C_{jd^6})_{j=4,5} = \frac{\delta N_j \, \delta m_j}{\rho_d} \tag{3.33}$$

where

$$\delta N_j = \frac{N_j \, \delta q_j}{q_j} \tag{3.34}$$

Melting in the model is currently based upon the following assumptions:

- all melted ice is converted to rain water;

- during melting, the number of ice particles decreases but the mean ice particle size does not change; and

- the heat capacity of ice particles is neglected - only latent heat due to melting is considered.

e.   Homogeneous nucleation of Type A ice at temperatures below -40°C.

At temperatures below -40°C, cloud water is assumed to freeze homogeneously. Cloud observations suggest that initial nucleation is associated with a very high concentration of small crystals (between 10^3 - 10^4 per litre), and that larger crystals - once they are formed by diffusional growth - typically occur in much smaller concentrations (10 and 100 per litre). The simple parameterization of homogeneous freezing results in the transfer of all cloud water into Type A ice particles, with a corresponding change in the number of crystals per gram of air based on the crystal mass of 4 x 10^{-9} g (mass of a 10 μm radius droplet). However, this change cannot lead to concentrations larger than, approximately 100 per litre. In addition, Heymsfield *et al* (1993) suggested that water saturation may only be reached at

49

-40°C; for colder temperatures, the water vapour mixing ratio should be forced not to exceed a prescribed value between water and ice saturation. Based on this suggestion, the highest possible mixing ratio for water vapour at temperatures below -40°C is that of water saturation at -40°C, thereafter it will decrease linearly to the value of (q_i +0.1(q_v - q_i)) (i.e. only 10% of the difference between water and ice saturation above saturation with respect to ice) at -60°C.

50
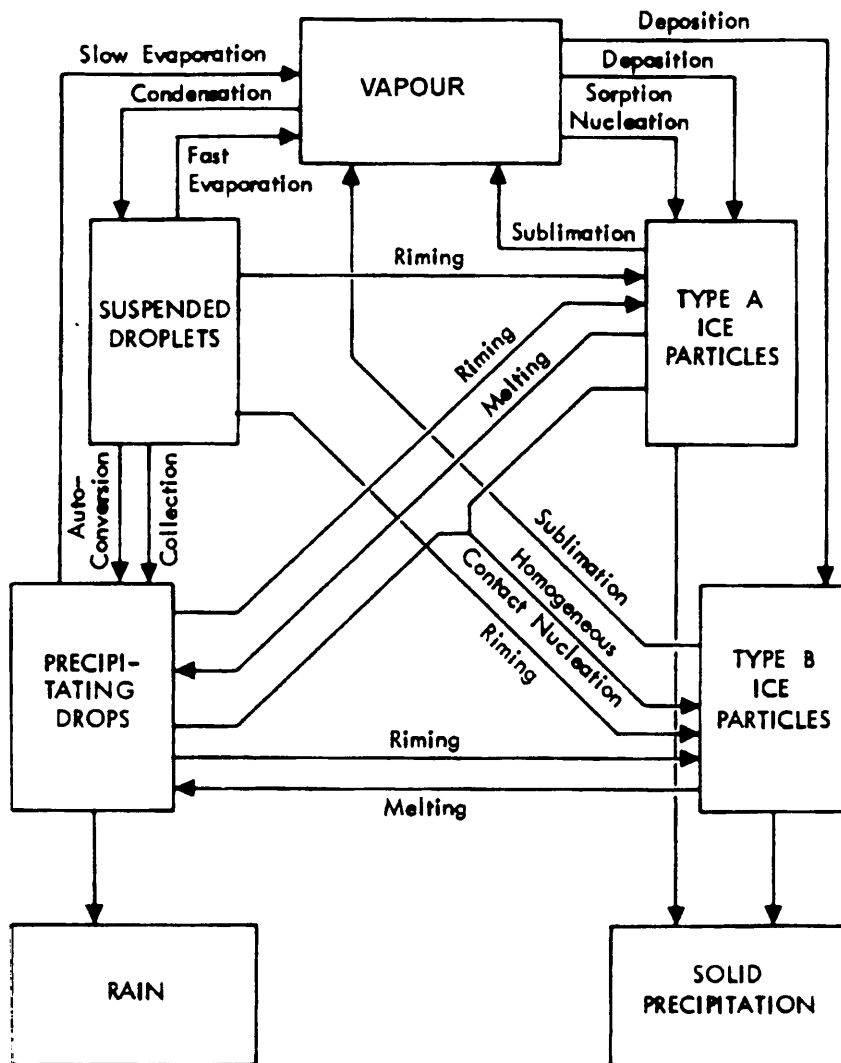
Fig. 3.1   Schematic depiction of microphysical processes
included in the model.

51
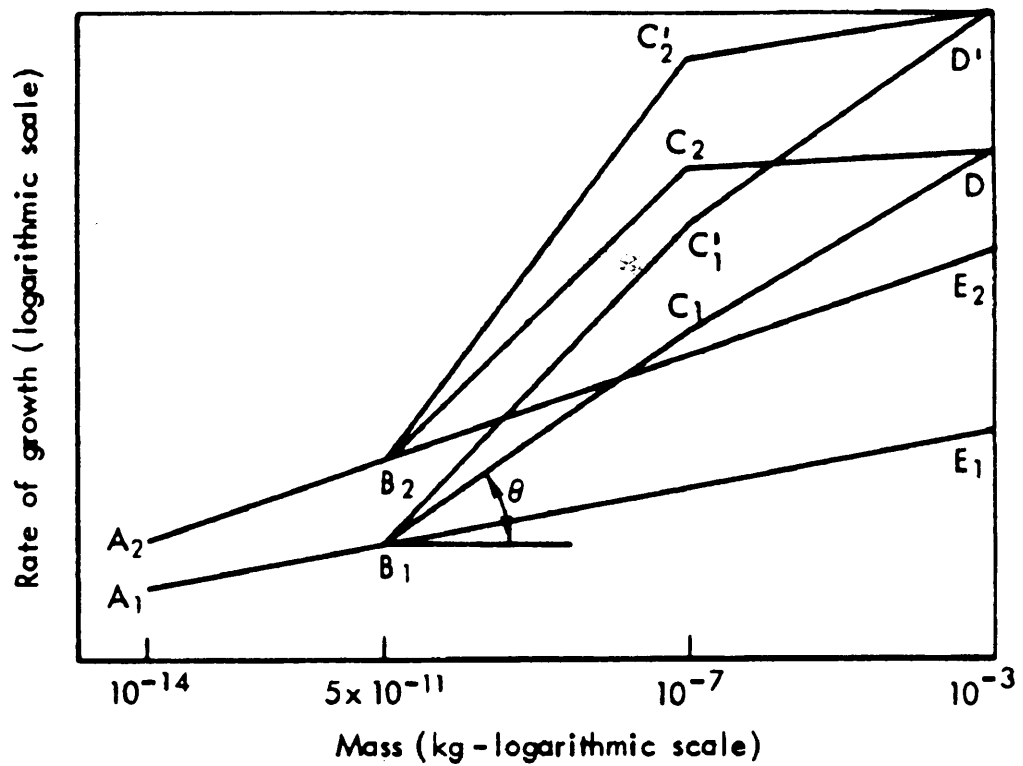
Fig. 3.2   Schematic depiction of ice-particle growth regimes. Growth at constant temperature and liquid water content follows path ABCD. Subscripts indicate growth properties at different temperatures; primed and unprimed points indicate growth properties at different liquid water contents. (Koenig, 1972)

52

Chapter 4

24 November 1992

On 24 November 1992 a severe multicell storm moved over the BPRP area and caused hail damage in the Reitz area, north of Bethlehem. In this chapter, this case day, and the results obtained from the numerical simulation will be discussed in detail.

In sections 4.1 and 4.2, the weather patterns leading up to the severe hailstorm on the afternoon of the 24 November 1992 are discussed. In section 4.2.2, the mesoscale conditions within which this hailstorm developed, are discussed, using C-band radar data.

Sections 4.3 and 4.4 deal with the numerical simulation of the hailstorm. Section 4.3 deals with the set-ups and initialization of the model, while in section 4.4 the results obtained during the model runs, including those to isolate the effect of solar heating and orography, are discussed. Section 4.5 contains the conclusions drawn from this case study.

4.1   Weather patterns for 23 November 1992

On 23 November 1992 an upper-air trough was situated over the western part of the country (figure 4.1). Isolated thunderstorms developed over the Free State, to the east of the trough, and scattered thunderstorms occurred in the moist air north of the Vaal River. An approaching cold front to the south-west of the country, caused scattered prefrontal showers over the western and south-western Cape. A coastal

low developed between Port Elizabeth and Durban, while dry and hot conditions prevailed over the central and western interior.

A surface high pressure system was situated to the west of the country and one to the south-east of the country. The latter moved to the east during the course of the day. A third high pressure system developed over the interior. This system was advecting moisture from the north-west.

For the greater part of the day, the Highveld regions were partly cloudy. Bloemfontein had only two eighths cloud cover throughout the day. No rain was reported at Bethlehem, Pretoria or Bloemfontein. Bethlehem reported stratocumulus and a moderate northwesterly wind. The pressure at the station decreased steadily.

The upper air was mostly dry, the only exception being some moisture at the 500 hPa level. At this level moist air was in circulation over the extreme northern and north-western parts of the subcontinent with a tongue of moisture extending southeastwards.

4.2   Weather patterns for 24 November 1992

4.2.1 Synoptic circulation

On the 24 November 1992 (the case day), the upper-air trough over the western part of the country moved slowly eastwards. The approaching cold front moved in over the south-western Cape and continued its eastward movement during the day (figure 4.2). By 18:00 UT the front had passed Port Elizabeth and was moving away in a south-easterly direction. The surface high pressure system to the west of the country intensified slightly and started to ridge along the south coast behind the cold front. The high pressure system prevailed over the interior. The coastal low moved slowly north-eastwards along the coast and by 12:00 UT its centre was just south of Durban. By 18:00 UT it had already reached Maputo. Undercutting took place over the eastern parts of the country due to the pressure rises behind the coastal low.

54

Moist air was in circulation to the east of the surface trough over the interior of the country, where fairly general falls of rain occurred. The moisture at the surface and in the upper air moved eastwards in sympathy with the surface front, resulting in a marked discontinuity in the moisture field between Upington and Bloemfontein.

For the greater part of the day Bloemfontein and Bethlehem were overcast, while Pretoria was partly cloudy. The clouds over the Bethlehem region were mainly stratocumulus with embedded convective cells. Rain and thunderstorm activity was reported from several stations, including Bethlehem and Pretoria. Hail was reported from stations in the Bethlehem area. The 12:00 UT Bethlehem sounding (figure 4.3) indicates unstable and moist conditions, with a surface temperature of 16°C. By 18:00 UT the Bethlehem area was cloudless, but there was still some rain and thunderstorm activity to the north-east. The wind over the Bethlehem region at that stage was light north-westerly.

4.2.2 Mesoscale conditions

The satellite images (figures 4.4a and 4.4b) for the afternoon of 24 November 1992 clearly show the position and movement of the cloud band over the project area. During the afternoon a severe multicell storm developed 50 km northwest of Bethlehem and propagated eastwards. This storm intensified and regenerated, maintaining radar reflectivities in excess of 50 dBZ for most of its life. During its lifetime this storm produced hail and left a path of destruction in its wake, causing crop damages of approximately two million Rand. The life cycle of this storm was recorded on a C-band Enterprise radar. The radar is situated in Bethlehem and is operated in volume-scan mode (Terblanche *et al*, 1994).

This severe multicell storm developed between 16:00 and 16:30 SAST in the Lindley area. After the initial radar echo appeared, the storm rapidly developed into a well-structured band with a northwest-southeast orientation, which persisted during its eastwards movement. The storm band and its propagation can clearly be seen on

55

the series of radar-rain-rate plots for the day (figure 4.5a to 4.5f). Note that the y-axis on these plots is orientated with regard to magnetic north. A secondary coordinate system, indicating true north (18° east of magnetic north for Bethlehem) has also been drawn in on these plots.

During the hailstorm's lifetime, a series of intense cells developed and dissipated within the well-structured storm band. The intense cell responsible for the widespread crop damages was at its most intense stage when it was situated over the Reitz area. From here it moved in an eastwards direction towards Warden where it started to dissipate. Between the most intense stage (at around 17:00 SAST) and the dissipating stage this cell lived for approximately 30 to 45 minutes. A second intense cell developed to the north of the original intense cell and with time merged with it. Other less intense cells developed to the north-west and south-east of Bethlehem throughout the hailstorm's lifetime.

4.3   The model set-up and initialization

In order to simulate this hailstorm, the non-hydrostatic, anelastic, three-dimensional Clark model was used. The domain within which the simulation was performed was a 240 x 240 km window over the Bethlehem area, centred at -28°N and 28°E (figure 4.6). In this two-by-two degree window, the topography changes from below 1500 m in the west to above 3000 m over the mountains in the south-east. A three-dimensional plot of the domain, as viewed from the north-east, is displayed in figure 4.7.

The model's horizontal grid resolution was set to 4 km, which gave 62 grid points in both the x (east) and y (north) directions. It is desirable to reduce this grid resolution to 2 km or smaller to resolve the microphysical processes active in the cloud more accurately. Unfortunately, at the time these model runs were performed, computer resources limited the grid resolution to a minimum of 4 km. Even with such a coarse resolution, it is still possible to distinguish the main dynamical and physical aspects

56

of the model generated storms. Keeping in mind that these simulations were done as an initial phase in the process of testing the model's capabilities over South Africa, this limitation is acceptable. In future studies this limitation will be addressed.

The model's vertical dimension (z) also consisted of 62 grid points. Vertical stretching was applied in the z-direction and this resulted in a resolution which varied from about 0.2 km between grid points in the lower layers, to about 1 km in the upper layers. This gave a vertical extent of approximately 23 km. The upper 18 grid points were used as a buffer zone to prevent gravity waves from propagating from the upper lid of the model domain into the research area and thereby affecting the results.

The model was initialized with the original 12:00 UT Bethlehem sounding for 24 November 1992 (figure 4.3). Test runs were also performed using the 06:00 UT Bethlehem sounding, but these model runs produced no significant storm development. It was therefore argued that the trigger mechanism responsible for the development of the multicell storm that afternoon was advected into the area after the 06:00 UT sounding. For this reason, only results obtained using the 12:00 UT sounding will be discussed.

4.4   Results

Section 4.4.1 contains the results from the basic model run, while in sections 4.4.2 and 4.4.3 the results from some sensitivity studies are discussed.

Steyn and Bruintjes (1990) and Mather and Terblanche (1993) found that the two major local factors controlling the development of convective activity in the BPRP area are surface heating and topography (refer to section 2.2.2). In order to see whether the Clark model is able to confirm these results, sensitivity studies on surface heating and topography were conducted. In section 4.4.2 the effect of surface heating is discussed, while section 4.4.3 deals with the effect topography has on the model results.

57

4.4.1 Basic model run

The observed storm and the numerically simulated storm compare very well. The model's first signs of storm development took place in the Lindley area. This development occurred between 120 and 150 minutes simulated time. Converted to local time, it places the first storm development between 16:00 and 16:30 SAST. The model thus not only predicted the area of first convection correctly, it also predicted the initial development time accurately.

Figures 4.8a to 4.8f are a series of the model's predicted surface rain water mixing ratio fields over a period of 50 minutes. In these plots the topography contours are depicted as bold lines. The contour intervals for the rain mixing ratio (thin lines) are 0.1 g kg^{-1}. The towns Lindley (L), Reitz (R), Warden (W), Bethlehem (Be), Clarens (C) and Fouriesburg (F) are also shown for reference.

The model storm developed into a northwest-southeast orientated band structure, which corresponds well with the observations. This band structure can be seen best on the 2.13 km above MSL rain water mixing ratio field plots (figure 4.9a,b). With time, the model storm band moved due east, similarly to the movement of the observed storm. As for the observed storm, the leading edge of the model predicted storm band was where the major new development took place. This was especially true during the early stages of storm development. Later, new cells started to develop further back, also conforming to the observations.

Corresponding to the observations, model development also occurred over the Fouriesburg/Clarens area. The predicted development over this area is especially discernable in the plots of the graupel mixing ratio fields at 4.33 km above MSL (figure 4.10a,b). The model predicted this development to be almost as intense as the development over the Reitz area. From observations it is obvious that although cell development did occur over this area, it was never as intense as the cell development over the Reitz area. It would therefore seem that the model is overestimating the development over the Fouriesburg/Clarens area slightly. The

58

reason for this overestimation seems to lie in the fact that this area is close to very steep topographical contours. This, coupled with a north-westerly surface flow, might well lead to the overestimation of development in this particular area.

The model simulation also predicted intense storm development over the mountainous areas. This does not correspond well with the observations. The reason for this might be, again, due to overestimation because of the steep topographical contours in this area, or the radar might be underestimating development over the mountains because they are so high and so far away from the location of the radar.

The model's first cell development in the Reitz area occurred just after 180 minutes of simulation. This places the time of development at around 17:00 SAST, in line with the observed cell development. On the radar plots (figures 4.5a to 4.5f) a second intense cell, to the north of the original, can be seen. With time, this cell merged with the original cell. The model did develop this second cell and the merge between these two intense cells was also accurately predicted.

The model predicted the intense cell responsible for the hail damage to lie over the Reitz/Warden area during its most intense stage. This corresponds well with the area of greatest hail damage. The model started to dissipate this intense cell after approximately 225 minutes of simulation (local time of 17:45 SAST). Thus a lifetime of approximately 45 minutes was predicted for this cell, which correlates well with the lifetime (30 to 45 minutes) recorded for the observed cell. There were two major differences noted between the model cell and the observed cell. Firstly, the model developed the intense cell too far north. Secondly, the model predicted a more south-easterly direction of movement, while the observed cell moved almost due east.

Throughout the lifetime of the observed storm other cells developed to the north-west and south-east of Bethlehem. New cells also developed behind the intense cell which was responsible for the hail damage. All these cells were less intense and had

59

shorter lifetimes than the cell over the Reitz/Warden area. This pattern of development was also noted in the model storm.

Figures 4.11a to 4.11f are a series of model predicted graupel mixing ratio fields at 3.72 km above MSL. From these plots it can be seen that the development and movement of the graupel mixing ratio fields followed the same patterns as were noted for the rain water mixing ratio fields. The lines AB in these plots are vertical sections that run through the centre of the intense cell responsible for the hail damage. The vertical plots along these lines are depicted in figures 4.12a to 4.12f. Here the vertical extent of the graupel development in the most intense cell is clearly visible. A problem observed with the model's predicted graupel development is that the model failed to precipitate the graupel. Never in the lifetime of the model storm did hail reach the ground.

This problem has been highlighted to some extent by other authors. Bruintjes (1992) states that the classical heterogeneous nucleus concepts, which are used in the Clark model, may result in the under-production of ice particle concentrations. According to Orville (1990) hail, hailstone sizes and associated parameters are still a problem in most mesoscale models. Work on a better parameterization scheme to solve this problem has been done by Farley and Orville (1986).

Since this study is only the first step in implementing the Clark model to support the precipitation research programme, no attempt has been made to incorporate such a parameterization scheme into the current version of the model. This is a research area that must be addressed in future before the model will be ready to be used operationally in South Africa.

60

4.4.2 Effect of surface heating

The treatment of surface heating in the Clark model was parameterized according to the method of Clark and Gall (1982). A time varying sensible heating rate, taking into account the effects of the sloping terrain, is used. Sensible heat rate according to the sun's zenith angle is given by:

$$S = \mu S_0 \cos Z \tag{4.1}$$

where S_0 is the solar constant, taken to be 1395 Wm^{-2}, Z is the sun's zenith angle, while μ, set to 0.5 for this study (after Clark and Gall, 1982), is a factor to account for absorption and reflection.

When the effects of the sloping terrain are taken into account, equation 4.1 is modified to:

$$S = \mu S_0 [\cos Z - h_x \cos \delta \sin \phi_r$$
$$- h_y (\sin \varphi \cos \delta \cos \phi_r - \cos \varphi \sin \delta)] (1 + h_x^2 + h_y^2)^{-\frac{1}{2}}, \tag{4.2}$$

where h_x and h_y represent the terrain slope in the x and y directions respectively. The declination angle is δ, while the latitude and the hour angle are φ and ϕ_r, respectively. According to Clark and Gall (1982), the difference between equations 4.1 and 4.2 could be as much as 100 Wm^{-2}.

For the basic model run (section 4.4.1) the latent heat fluxes were taken as half the value of the sensible heat fluxes (after Bruintjes, 1992). This resulted in a maximum of 600 Wm^{-2} for sensible heat fluxes and 300 Wm^{-2} for latent heat fluxes at the sun's maximum inclination. For the sensitivity study discussed below the surface sensible heat fluxes were set to zero.

61

During this sensitivity study, the first storm development took place only after 390 minutes of simulation (local time 20:30 SAST). Since the actual development took place at around 16:30 SAST, the model's predicted initial development time lagged the observations by four hours. Although the start time was not predicted accurately, it is interesting to note that the model nevertheless predicted the area of most intense development over Lindley correctly.

Figures 4.13a to 4.13d are a series of the model's predicted surface rain water mixing ratio fields over a period of 90 minutes. As before, the topography contours are depicted as bold lines and the towns Lindley (L), Reitz (R), Warden (W), Bethlehem (Be), Clarens (C) and Fouriesburg (F) are indicated.

Although the development started late, the model storm again developed into a northwest-southeast orientated band structure, which moved east with time in line with the observed storm. What was missing during this model run was the detail observed during the basic model run. During this model run the storm band was the main feature, while the individual cells that developed and dissipated during the lifetime of the storm were less well defined. Again the development over the mountains was overestimated.

The first signs of severe cell development in the Reitz area took place after 420 minutes of simulation (local time 21:00 SAST), again approximately four hours later than the observed development. This development started to dissipate after 540 minutes of simulation (23:00 SAST), giving it a predicted lifetime of approximately two hours. This is more than double the lifetime of the observed cell (30 to 45 minutes). The second intense cell, which developed to the north of the original intense cell and later merged with it, did not develope during this model run, emphasising again that the model was able to predict the general development and movement of the storm but not the detail.

62

As for the basic model run, during the sensitivity study the model predicted the initial development of the intense cell too far to the north, although it placed this cell over the correct area (Reitz/Warden) during its most intense stage. This again resulted in a predicted south-eastern movement, rather than the almost due easterly direction followed by the observed cell.

Figures 4.14a to 4.14d are a series of model predicted graupel mixing ratio fields at 3.72 km above MSL. Again the development and movement of the graupel mixing ratio fields followed the same patterns as were observed for the rain water mixing ratio fields. It can be seen that during this run, the model underpredicted the development of the graupel even more than was noted during the basic model run. Note that although this underestimation was again a serious problem and that hail again did not reach the ground, the model correctly predicted the most intense graupel development over the Reitz/Warden area.

Comparing this model run with the basic model run, one notices that the dynamical aspects of the storm were well predicted by the sensitivity run. In other words, the model correctly predicted the area of initial development, the development of the storm into a northwest-southeast orientated storm band, as well as the eastern movement of this storm band and the area of most severe development. The effect of no surface heating on the model was noted in the physical aspects of the storm. In other words, detail about individual cell development and dissipation was missing and the predicted time of development lagged behind that of the basic model run by four hours. Also, not only did the initial development lag, but once the storm developed it moved very slowly with a lifetime more than twice as long as was observed during the basic model run.

63

4.4.3 Effect of topography

That topography plays a role in the development and movement of storms and particularly in severe hail producing storms, is well known. As far back as 1965 Schulze showed that the isopleths of hail incidence in South Africa conform well with the general topography of the country (see chapter two). The question here is thus not whether topography has an effect on the development of storms, but rather to what *extent.*

This is a question that is impossible to try to answer without the aid of a detailed mesoscale model. In order to find answers to this question, the Clark model was used to simulate the 24 November 1992 multicell storm over a smoothed topography. These results were then compared with those obtained during the basic run (section 4.4.1) in order to see the effect of a smoothed topography on the dynamical and physical aspects associated with this storm.

In this sensitivity study the model was run on a topography similar to the original, only smoothed by making use of the following equation:

$$S(h) = F(h) - \left[\frac{F(h) - h_0}{\kappa} \right] F(h), \qquad (4.3)$$

where S(h) is the smoothed, F(h) the original and h_0 the lowest surface topographical value in the chosen model domain. The value of κ determines the desired smoothing required. This operation has the effect that the lower surface topographical values remain almost unchanged, while the higher values are smoothed considerably. In this study κ was chosen in such a manner that the highest topographical value (around 3000 m) was smoothed by approximately 25 percent. [Some studies, where the topography was smoothed by 100 percent - i.e. representing a flat topography, were also done. During these studies the only development that took place was line storms orientated perpendicularly to the prevailing wind direction.] The smoothed

64

topography is depicted in figure 4.15, while figure 4.16 shows a three-dimensional plot of the area as viewed from the north-east. The model results obtained from this sensitivity study are discussed below.

As for the basic model run, this sensitivity run correctly predicted the first signs of storm development to be between 120 and 150 minutes simulated time (local time between 16:00 and 16:30 SAST), in the vicinity of Lindley. Figures 4.17a to 4.17f are a series of the model's predicted surface rain water mixing ratio fields over a period of 50 minutes. The topography contours are depicted as bold lines.

During this run the model storm did develop into a more or less northwest-southeast orientated band structure, but this band structure was never as well defined as was noted during the basic run. Again the storm band, with its leading edge the area of most intense development, moved eastwards with time. As time progressed new cell development took place further back in the storm band, but this development was weak in comparison to that noted for the basic model run.

The development seen previously over the Fouriesburg/Clarens area developed during this run, but was not as strong. Emphasising that the steep topographical contours in this area are a dominant factor in the overestimation of cell development. This can also be seen in the fact that the development over the mountains in the south was now much weaker.

The first model cell development in the Reitz area occurred shortly after 180 minutes of simulation (local time around 17:00 SAST). This places it in line with both the observations and the basic model run. The area of development, as well as the predicted movement of this cell, were similar to that observed in section 4.4.1. A difference noted between the two runs was that this time the developed cell was less well-defined. During the sensitivity study this cell was no longer an intense well-developed entity, but weaker and more spread-out. This "scaling down" of development can also be seen in the weak development over the mountains. This

65

weaker, more spread-out development seems to be a direct consequence of the smoothing of the topography.

Again, during this model run, a second intense cell developed to the north of the initial intense cell, with a merging between these two intense cells with time.

Figures 4.18a to 4.18f are a series of the model's predicted graupel mixing ratio fields at 3.72 km above MSL. Again the development and movement of the graupel mixing ratio fields follow the same patterns as were observed for the rain water mixing ratio fields. A difference between this run and the basic model run was that on average even less graupel developed during the sensitivity study. The graupel that did develop was also dissipated faster. Again, as anticipated, no graupel precipitated.

This run compares very well with the basic model run. The sensitivity run predicted the dynamical aspects of the storm - both development and movement - just as well as the basic model run. Most of the physical aspects of the storm also corresponded well with those predicted by the basic model run. The difference between the two runs was that the sensitivity run lacked detail. The developed cells were less intense, and more spread-out compared to the well-defined intense entities of the basic model run. Also less graupel developed and it dissipated faster than was observed during the basic model run.

The smoothing of the topography resulted only in dampening the cell development. This was emphasised by running the model at different levels of smoothing. The value of κ in equation 4.3 was altered so that the highest topographical values in the model domain were decreased by between 10 and 25 percent. Each time the basic results were similar. The model developed the storms in the same area, at the same time and moved them through the model domain in the same manner. It thus seems that the topography contours is the dominant factor in establishing preferred areas of storm development. As the level of smoothing increased, the intensity of cell

66

development decreased. Increasing the level of smoothing also resulted in more spread-out cells instead of well-defined entities. This thus leads to the conclusion that the steepness of the topographical gradient is the dominant factor in storm detail and intensity. In summary, during this study it was established that the topography controls the preferred areas of development, while the steepness of the topographical gradients controls the intensity of the storms.

4.5 Summary

The Clark model predicted the development and movement of the multicell storm on 24 November 1992 accurately in space and time. As seen in section 4.4.1, the model predicted most of the dynamical and physical aspects of the storm correctly:

-      the area and time of initial storm development;

-      the development of the storm into a well-structured northwest-southeast orientated band;

-      the movement of the storm band to the east;

-      the fact that the leading edge of the storm band was where the major new development took place;

-      the development of an intense hail-producing cell over the Reitz area;

-      the time of development of the intense hail-producing cell as well as the duration of this cell, and

-      the development of a second intense cell to the north of the initial intense cell and the merging of these two cells.

The major problems encountered during the model run were:

-      the overestimation of cell development close to, or over, mountainous areas;

-      the fact that developed graupel never precipitated, and

-      the intense cell responsible for the hail damage was developed too far to the north and moved in a southeastern direction instead of the almost due east direction that the observed cell followed.

During the course of this case study two sensitivity studies were conducted. The effects that surface heating and topography have on the dynamical and physical aspects of the multicell storm were studied. From these studies it was concluded that:

- The dynamical aspects of the storm (development and movement) were controlled by the topography. In the absence of topography, the development and movement of the clouds were controlled by the prevailing wind. When topography was present, the preferred areas of development remained the same for both the smoothed and unsmoothed topographical surfaces.

- The physical aspects of the storm were strongly influenced by both surface heating and topographical smoothing. It was seen that surface heating strongly controlled the time of initial development and the duration of the storm, while having a smaller influence over the details of the developed cells. On the other hand, the steepness of the topographical gradient strongly controlled the intensity level of the developed cells as well as their definition.
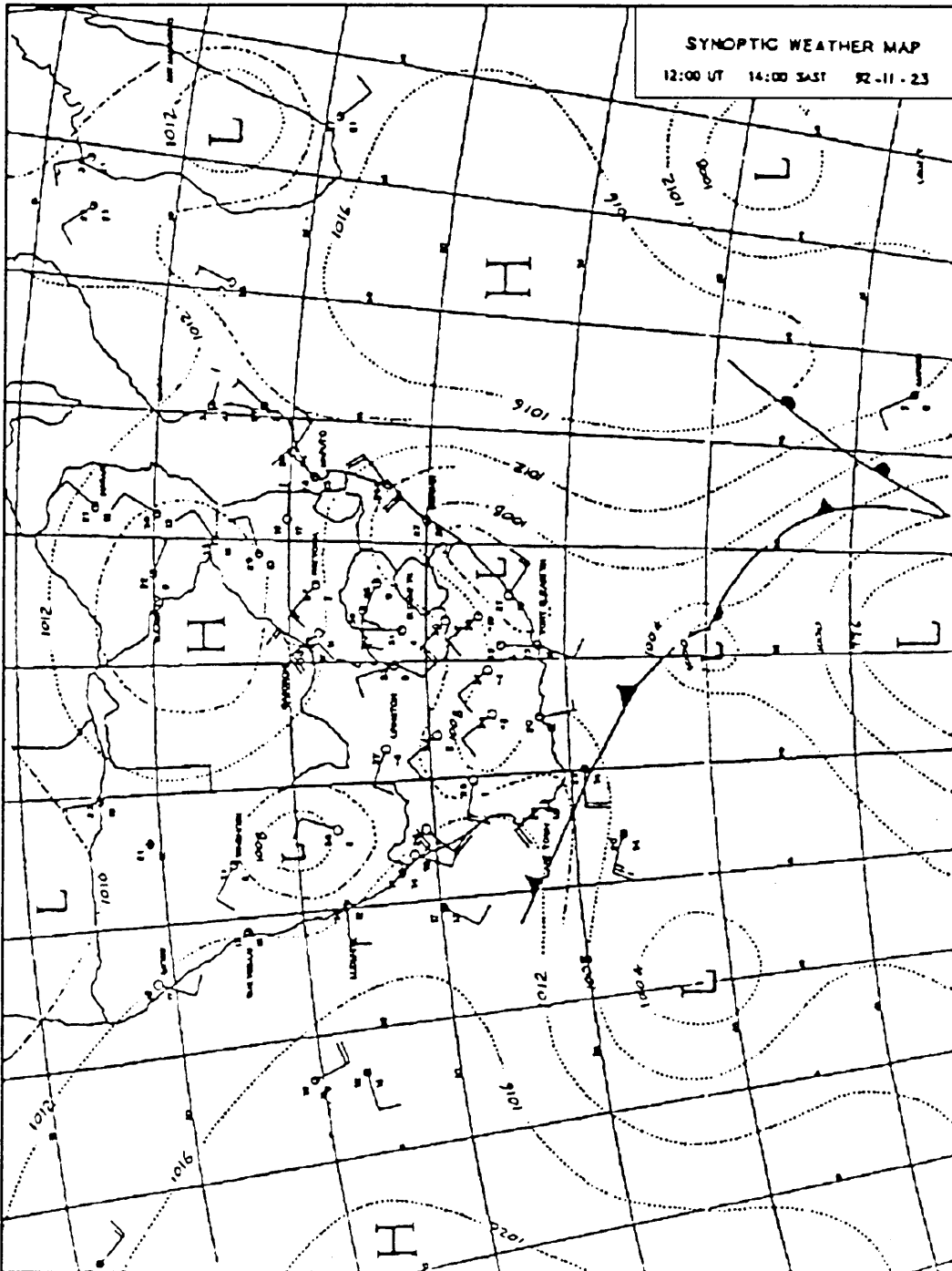
Fig. 4.1   Synoptic weather map for 12:00 UT, 23 November 1992
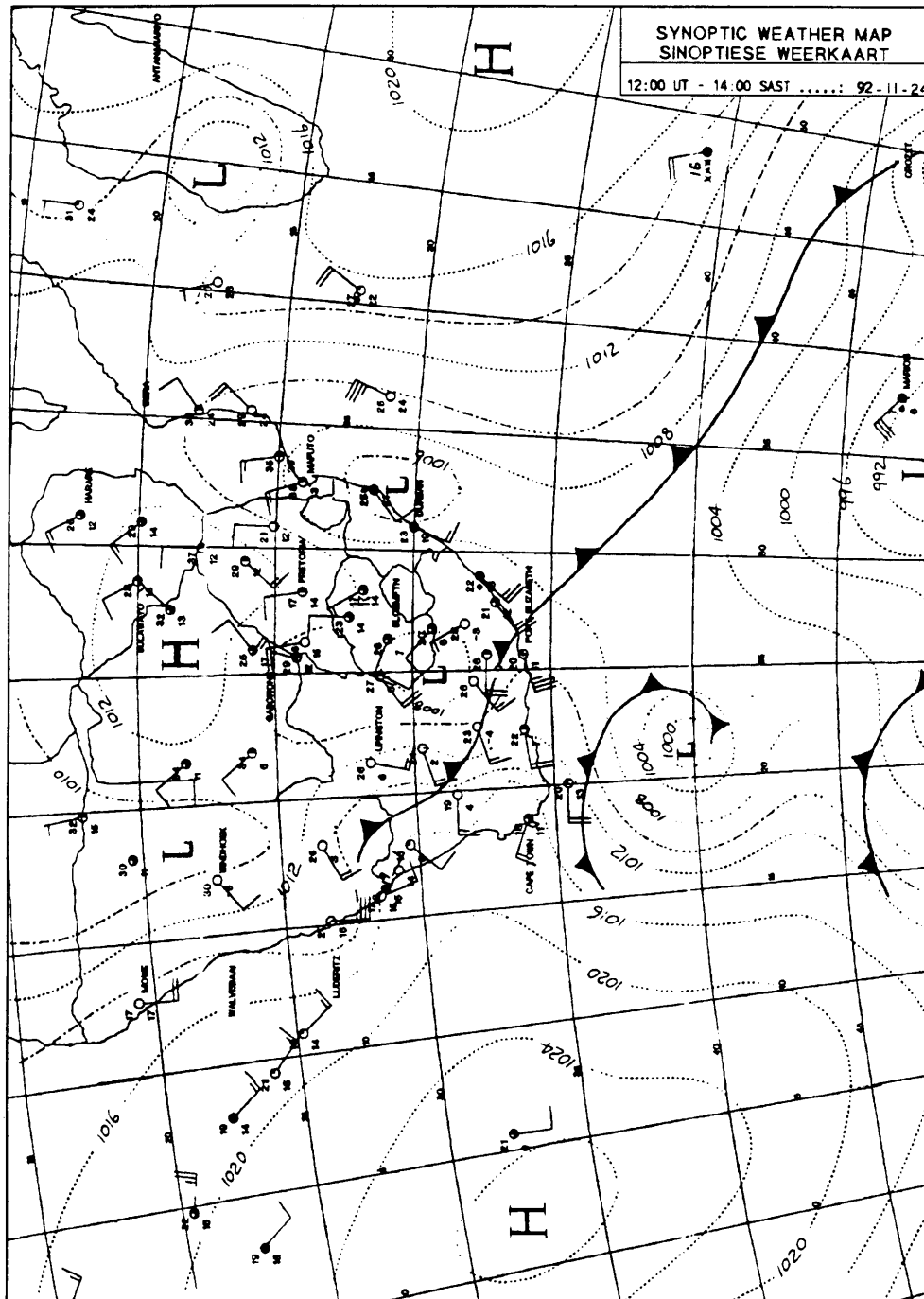
Fig. 4.2   Synoptic weather map for 12:00 UT, 24 November 1992
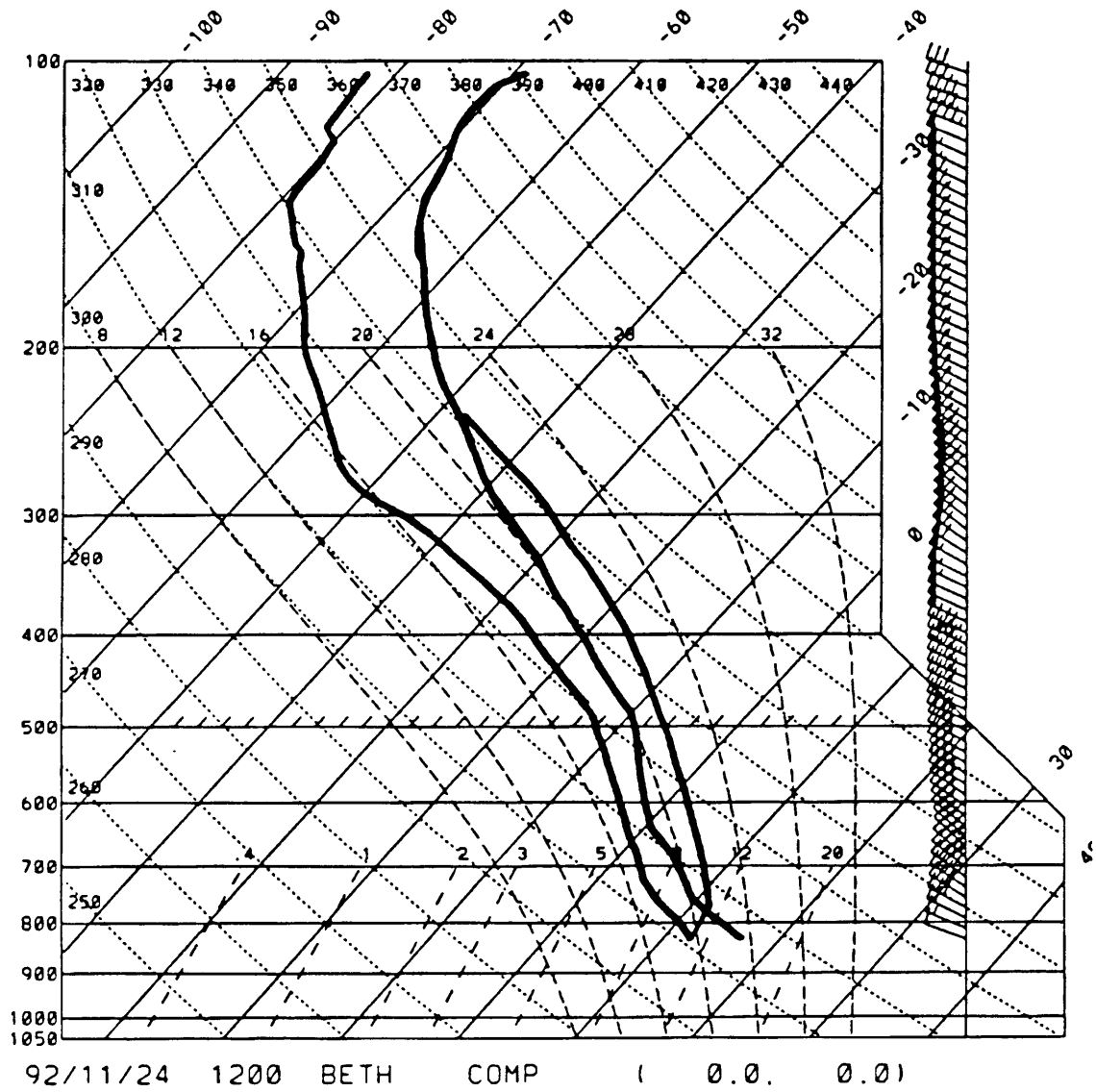
Fig. 4.3   Bethlehem sounding for 12:00 UT, 24 November 1992

71
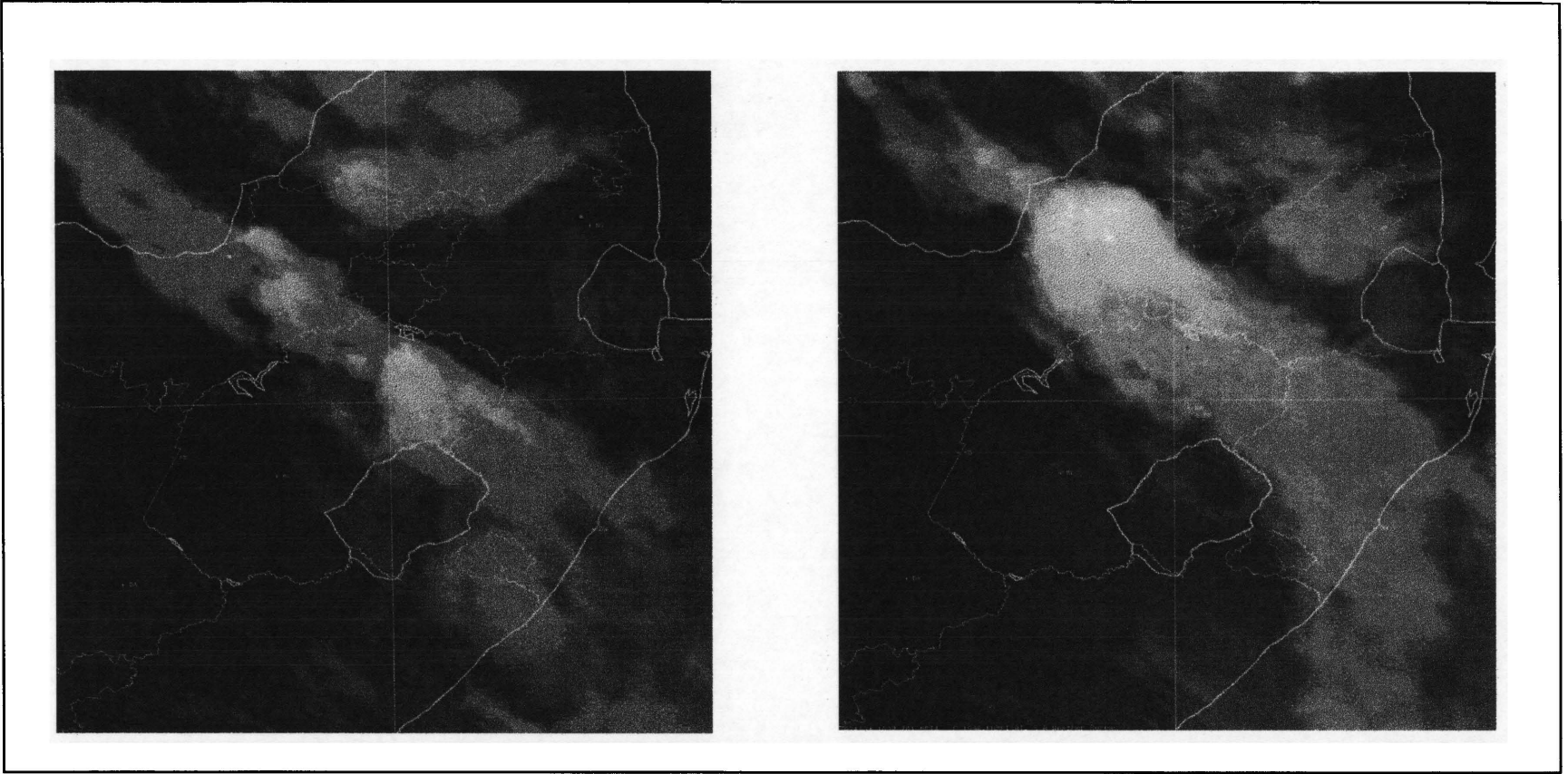
Fig. 4.4a,b   **Satellite image of cloud clover over the Free State for 24 November 1992 (16:30 and 18:30 SAST)**

73
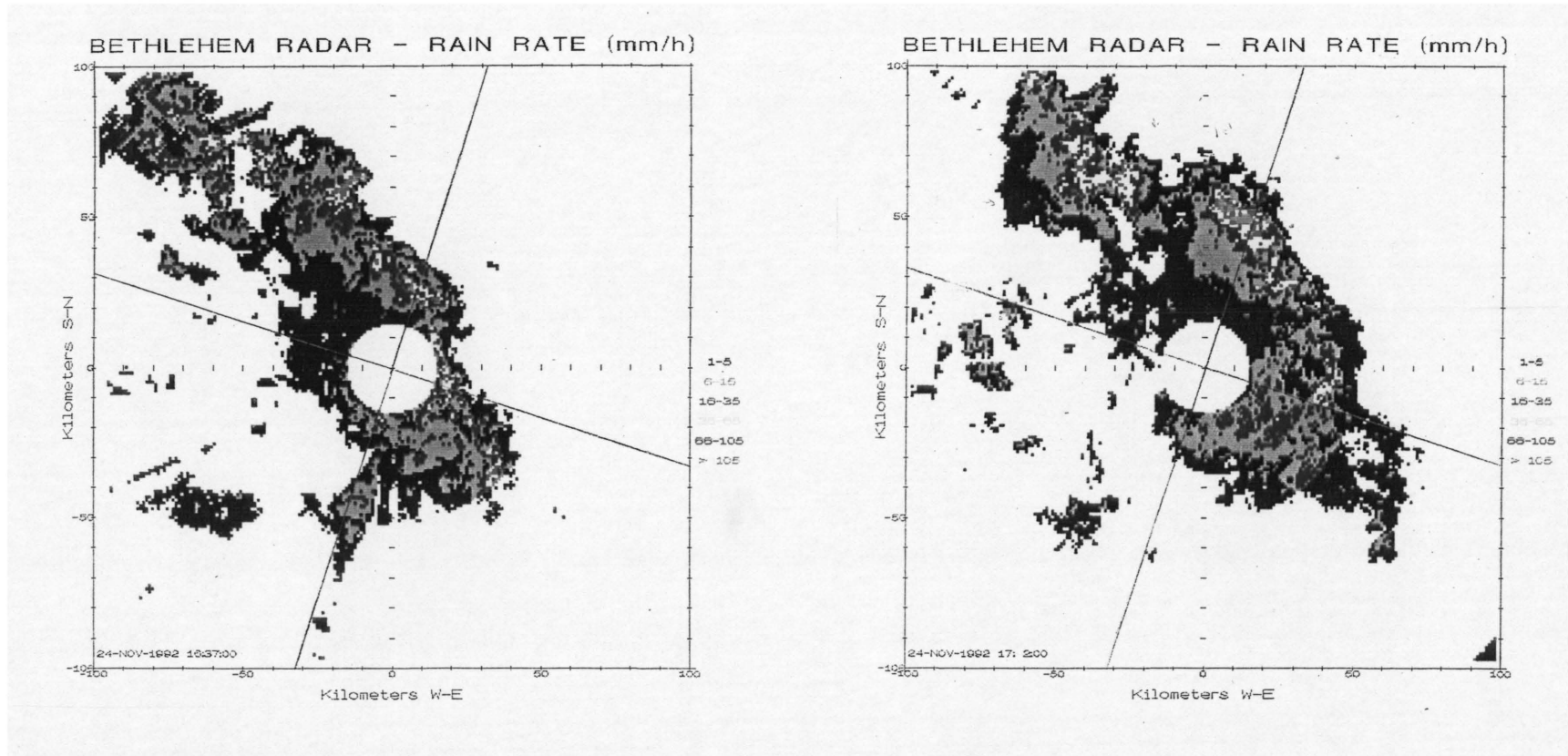
4.5a,b   Radar-rain-rate over the Bethlehem area for 24 November 1992 (16:37 and 17:02 SAST)
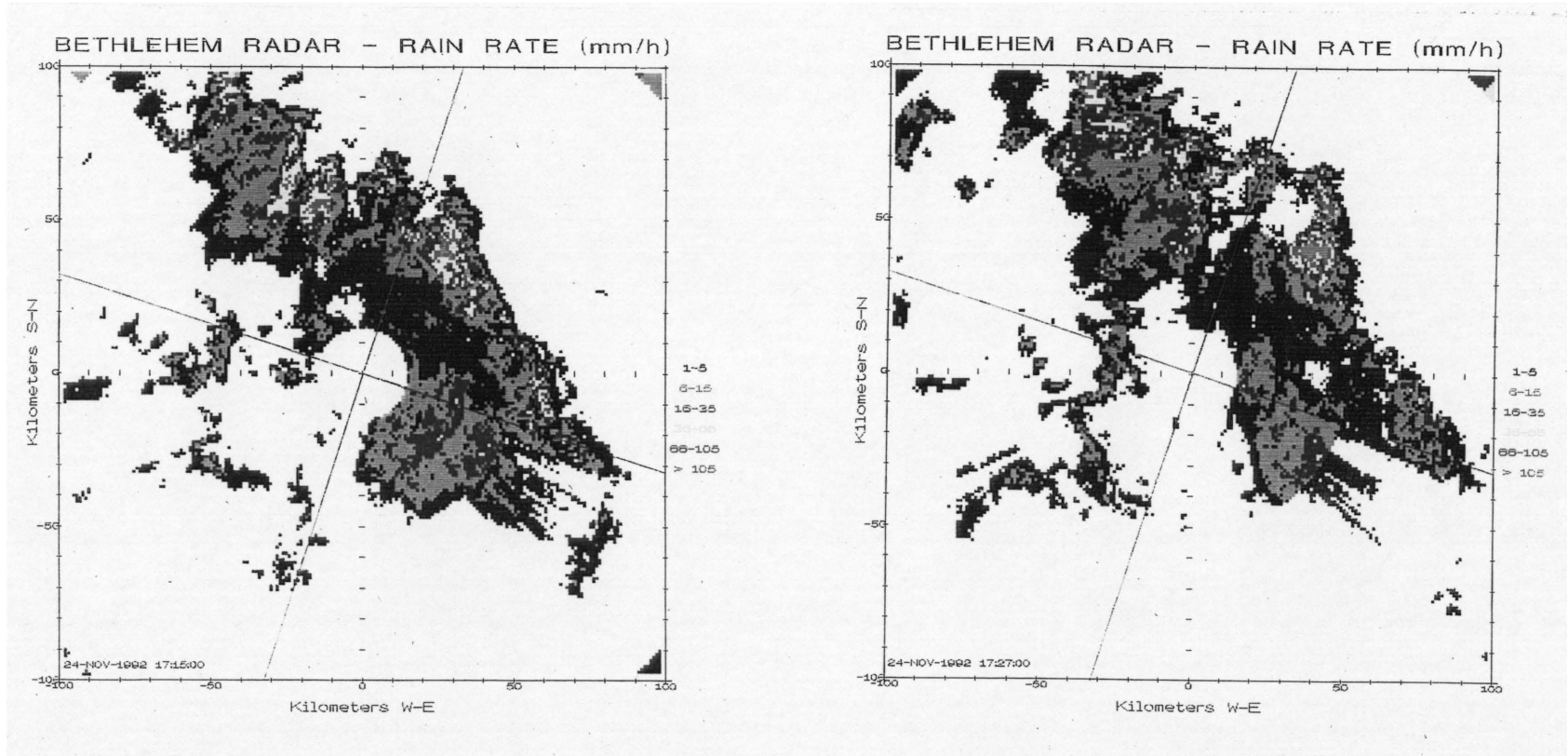
Fig. 4.5c,d   Radar-rain-rate over the Bethlehem area for 24 November 1992 (17:15 and 17:27 SAST)
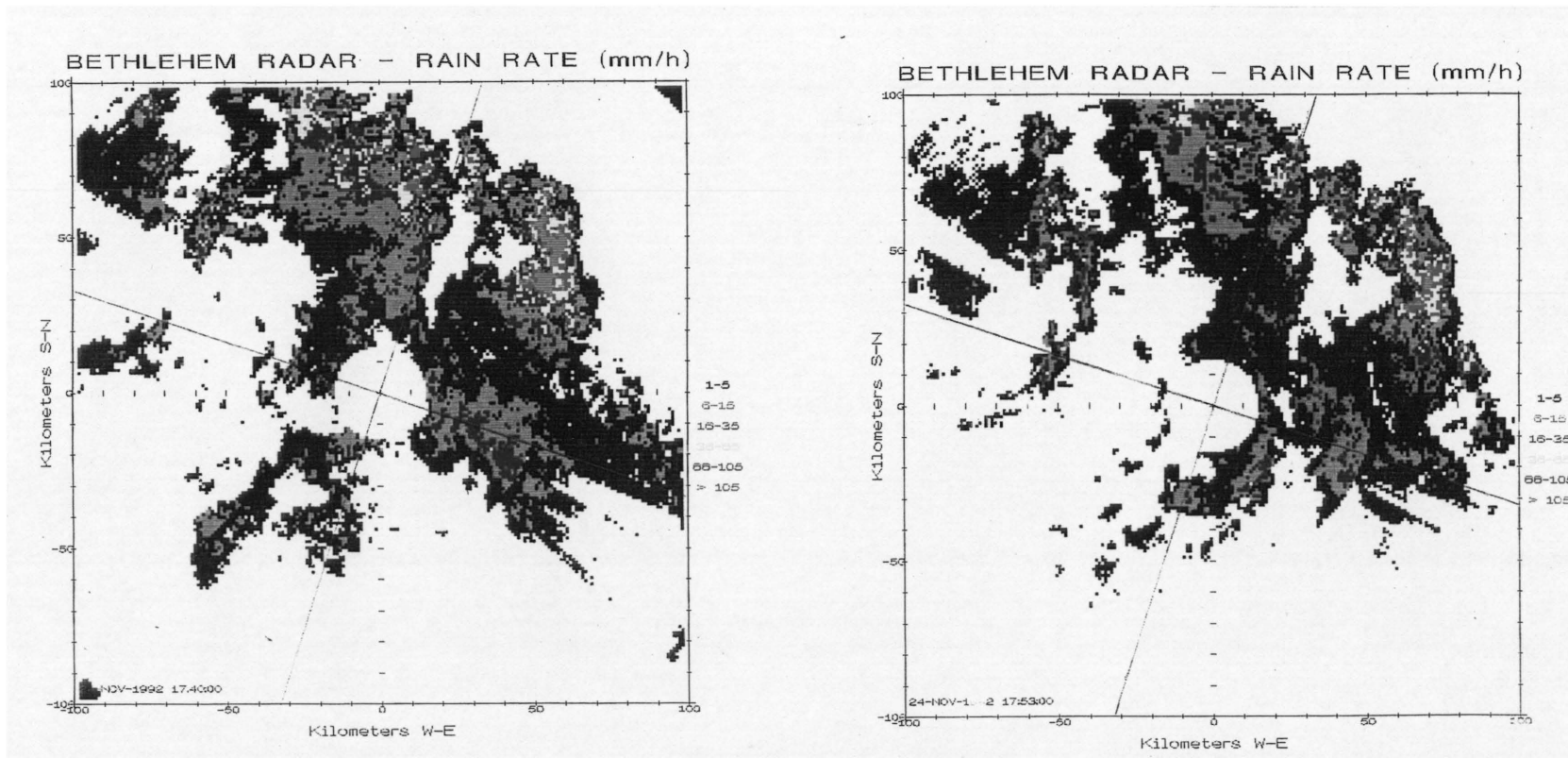
Fig. 4.5e,f   Radar-rain-rate over the Bethlehem area for 24 November 1992 (17:40 and 17:53 SAST)
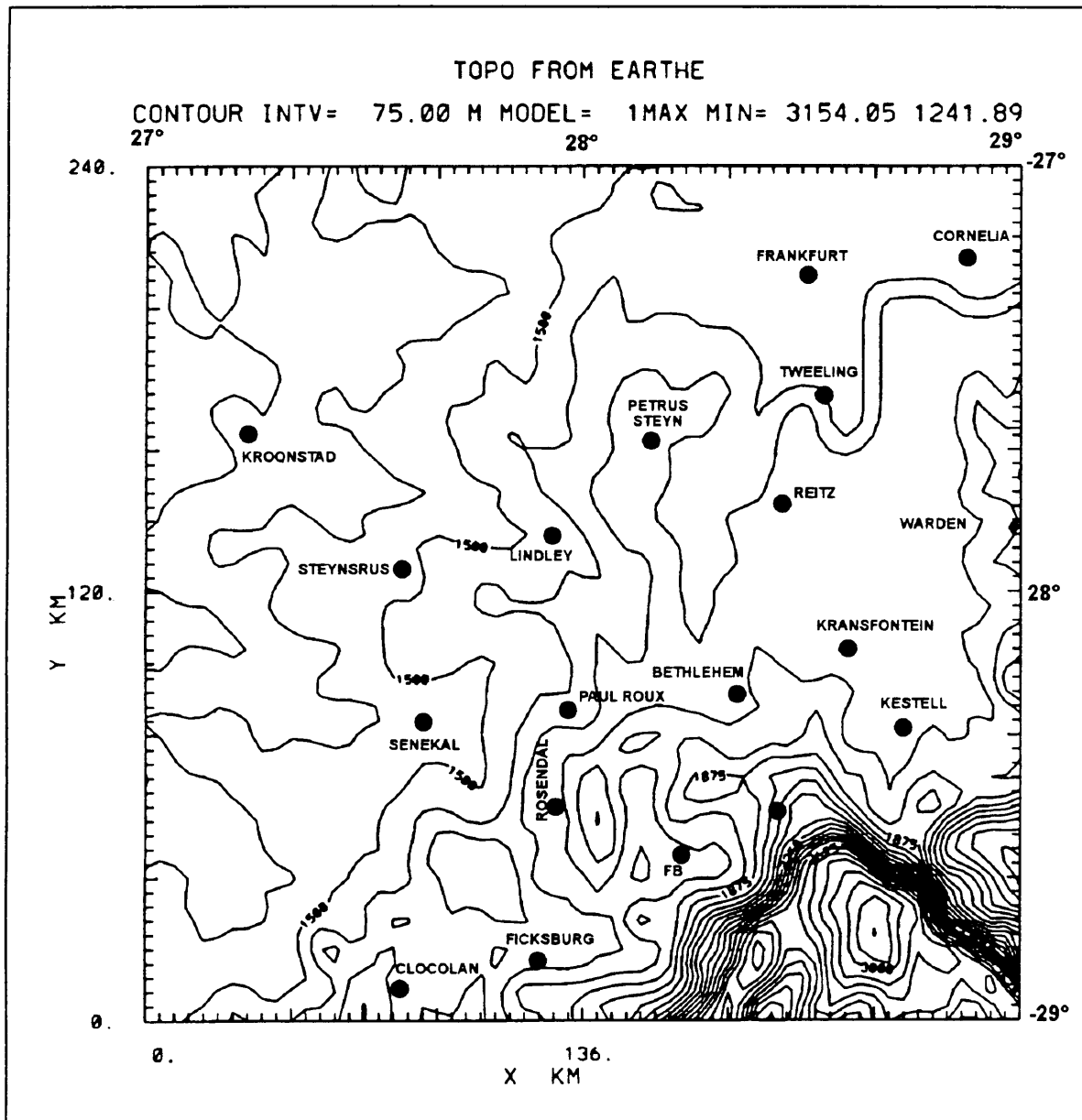
Fig. 4.6   A 240 x 240 km, two-dimensional topography plot of the model domain over the Bethlehem area. This is the topography that was used during the simulation of the multicell storm of 24 November 1992 for both the basic model run as well as the surface heating studies.

Fig. 4.7   A 240 x 240 km, three-dimensional topography plot of the model
            domain over the Bethlehem area. This is the topography that was used
            during the simulation of the multicell storm of 24 November 1992 for
            both the basic model run as well as the surface heating studies.

77

78

SURFACE PLOT AT TIME= 180.00MIN
QR FIELD (GR/KG)
TOPO CONT INT=788.50(M)

SURFACE PLOT AT TIME= 190.00MIN
QR FIELD (GR/KG)
TOPO CONT INT=788.50(M)

FIELD MAX.MIN.DEL 1.03709E+00 0.00000E+00 1.00000E-01
CONT. MAX.MIN.LEV 1.00000E+00 1.00000E-01 9

FIELD MAX.MIN.DEL 1.05363E+00 0.00000E+00 1.00000E-01
CONT. MAX.MIN.LEV 1.00000E+00 1.00000E-01 9

Fig. 4.8a,b   Model generated surface rain water mixing ratio fields after 180 and 190 minutes of simulation (17:00 and 17:10 SAST). The topograhy contours are depicted as bold lines and the contour intervals for the rain water mixing ratio (thin lines) are 0.1 g kg^{-1} (basic model run)

SURFACE PLOT AT TIME= 200.00MIN
QR FIELD (GR/KG)
TOPO CONT INT=788.50(M)

FIELD MAX.MIN.DEL 7.42358E-01 0.00000E+00 1.00000E-01
CONT. MAX.MIN.LEV 7.00000E-01 1.00000E-01 6

SURFACE PLOT AT TIME= 210.00MIN
QR FIELD (GR/KG)
TOPO CONT INT=788.50(M)

FIELD MAX.MIN.DEL 5.15892E-01 0.00000E+00 1.00000E-01
CONT. MAX.MIN.LEV 5.00000E-01 1.00000E-01 4

Fig. 4.8c,d Model generated surface rain water mixing ratio fields after 200 and 210 minutes of simulation (17:20 and 17:30 SAST). The topograhy contours are depicted as bold lines and the contour intervals for the rain water mixing ratio (thin lines) are 0.1 g kg^{-1} (basic model run)

SURFACE PLOT AT TIME= 220.00MIN
QR FIELD (GR/KG)
TOPO CONT INT=788.50(M)

SURFACE PLOT AT TIME= 230.00MIN
QR FIELD (GR/KG)
TOPO CONT INT=788.50(M)

FIELD MAX.MIN.DEL 6.89181E-01 0.00000E+00 1.00000E-01
CONT. MAX.MIN.LEV 6.00000E-01 1.00000E-01 5

FIELD MAX.MIN.DEL 5.43205E-01 0.00000E+00 1.00000E-01
CONT. MAX.MIN.LEV 5.00000E-01 1.00000E-01 4

Fig. 4.8e,f   Model generated surface rain water mixing ratio fields after 220 and 230 minutes of simulation (17:40 and 17:50 SAST). The topograhy contours are depicted as bold lines and the contour intervals for the rain water mixing ratio (thin lines) are 0.1 g kg⁻¹ (basic model run)

81

X-Y PLOT AT Z= 2.13KM TIME= 180.00MIN
QR FIELD (GR/KG)

X-Y PLOT AT Z= 2.13KM TIME= 190.00MIN
QR FIELD (GR/KG)

FIELD MAX.MIN.DEL 1.03709E+00 0.00000E+00 1.00000E-01
CONT. MAX.MIN.LEV 1.00000E+00 1.00000E-01 9

FIELD MAX.MIN.DEL 1.05363E+00 0.00000E+00 1.00000E-01
CONT. MAX.MIN.LEV 1.00000E+00 1.00000E-01 9

Fig. 4.9a,b Model generated rain water mixing ratio fields at 2.13 km above MSL after 180 and 190 minutes of simulation (17:00 and 17:10 SAST). The contour intervals for the rain water mixing ratio are 0.1 g kg^{-1} (basic model run)

X-Y PLOT AT Z= 4.33KM TIME= 210.00MIN
CLOUD ICE -B- MIXING RATIO (G/KG)

X-Y PLOT AT Z= 4.33KM TIME= 220.00MIN
CLOUD ICE -B- MIXING RATIO (G/KG)

FIELD MAX.MIN.DEL 3.16682E+00 0.00000E+00 1.00000E-01
CONT. MAX.MIN.LEV 3.10000E+00 1.00000E-01 30

FIELD MAX.MIN.DEL 3.42450E+00 0.00000E+00 1.00000E-01
CONT. MAX.MIN.LEV 3.40000E+00 1.00000E-01 33

Fig. 4.10a,b   Model generated graupel mixing ratio fields at 4.33 km above MSL after 210 and 220 minutes of simulation (17:30 and 17:40 SAST). The contour intervals for the graupel mixing ratio are 0.1 g kg^{-1} (basic model run)

X-Y PLOT AT Z= 3.72KM TIME= 180.00MIN
CLOUD ICE -B- MIXING RATIO (G/KG)

X-Y PLOT AT Z= 3.72KM TIME= 190.00MIN
CLOUD ICE -B- MIXING RATIO (G/KG)

FIELD MAX.MIN.DEL 5.58921E+00 0.00000E+00 1.00000E-01
CONT. MAX.MIN.LEV 5.50000E+00 1.00000E-01 54

FIELD MAX.MIN.DEL 5.23185E+00 0.00000E+00 1.00000E-01
CONT. MAX.MIN.LEV 5.20000E+00 1.00000E-01 51
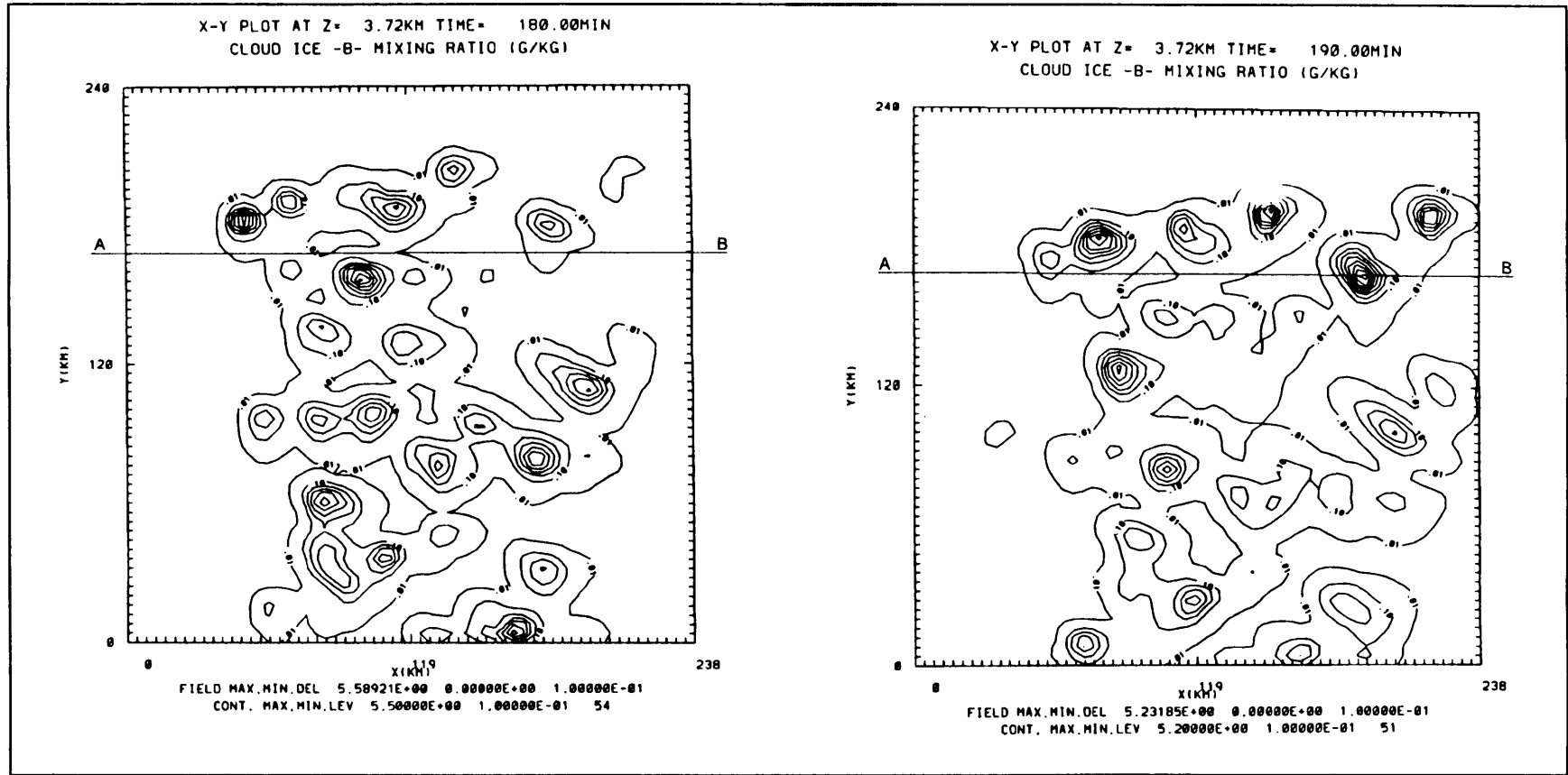
Fig. 4.11a,b   Model generated graupel mixing ratio fields at 3.72 km above MSL after 180 and 190 minutes of simulation (17:00 and 17:10 SAST). The contour intervals for the graupel mixing ratio are 0.1 g kg⁻¹ (basic model run)

X-Y PLOT AT Z= 3.72KM TIME= 200.00MIN
CLOUD ICE -B- MIXING RATIO (G/KG)

X-Y PLOT AT Z= 3.72KM TIME= 210.00MIN
CLOUD ICE -B- MIXING RATIO (G/KG)

FIELD MAX.MIN.DEL 3.50151E+00 0.00000E+00 1.00000E-01
CONT. MAX.MIN.LEV 3.50000E+00 1.00000E-01 34

FIELD MAX.MIN.DEL 3.16682E+00 0.00000E+00 1.00000E-01
CONT. MAX.MIN.LEV 3.10000E+00 1.00000E-01 30

Fig. 4.11c,d   Model generated graupel mixing ratio fields at 3.72 km above MSL after 200 and 210 minutes of simulation (17:20 and 17:30 SAST). The contour intervals for the graupel mixing ratio are 0.1 g kg^{-1} (basic model run)

X-Y PLOT AT Z= 3.72KM TIME= 220.00MIN
CLOUD ICE -B- MIXING RATIO (G/KG)

X-Y PLOT AT Z= 3.72KM TIME= 230.00MIN
CLOUD ICE -B- MIXING RATIO (G/KG)

FIELD MAX.MIN.DEL 3.42458E+00 0.00000E+00 1.00000E-01
CONT. MAX.MIN.LEV 3.40000E+00 1.00000E-01 33

FIELD MAX.MIN.DEL 4.16157E+00 0.00000E+00 1.00000E-01
CONT. MAX.MIN.LEV 4.10000E+00 1.00000E-01 40

Fig. 4.11e,f   Model generated graupel mixing ratio fields at 3.72 km above MSL after 220 and 230 minutes of simulation (17:40 and 17:50 SAST). The contour intervals for the graupel mixing ratio are 0.1 g kg^{-1} (basic model run)

X-Z PLOT AT Y= 168.00KM TIME= 180.00MIN
CLOUD ICE -B- MIXING RATIO (G/KG)

X-Z PLOT AT Y= 168.00KM TIME= 190.00MIN
CLOUD ICE -B- MIXING RATIO (G/KG)

FIELD MAX.MIN.DEL 5.58921E+00 0.00000E+00 1.00000E-01
CONT. MAX.MIN.LEV 5.50000E+00 1.00000E-01   54

FIELD MAX.MIN.DEL 5.23185E+00 0.00000E+00 1.00000E-01
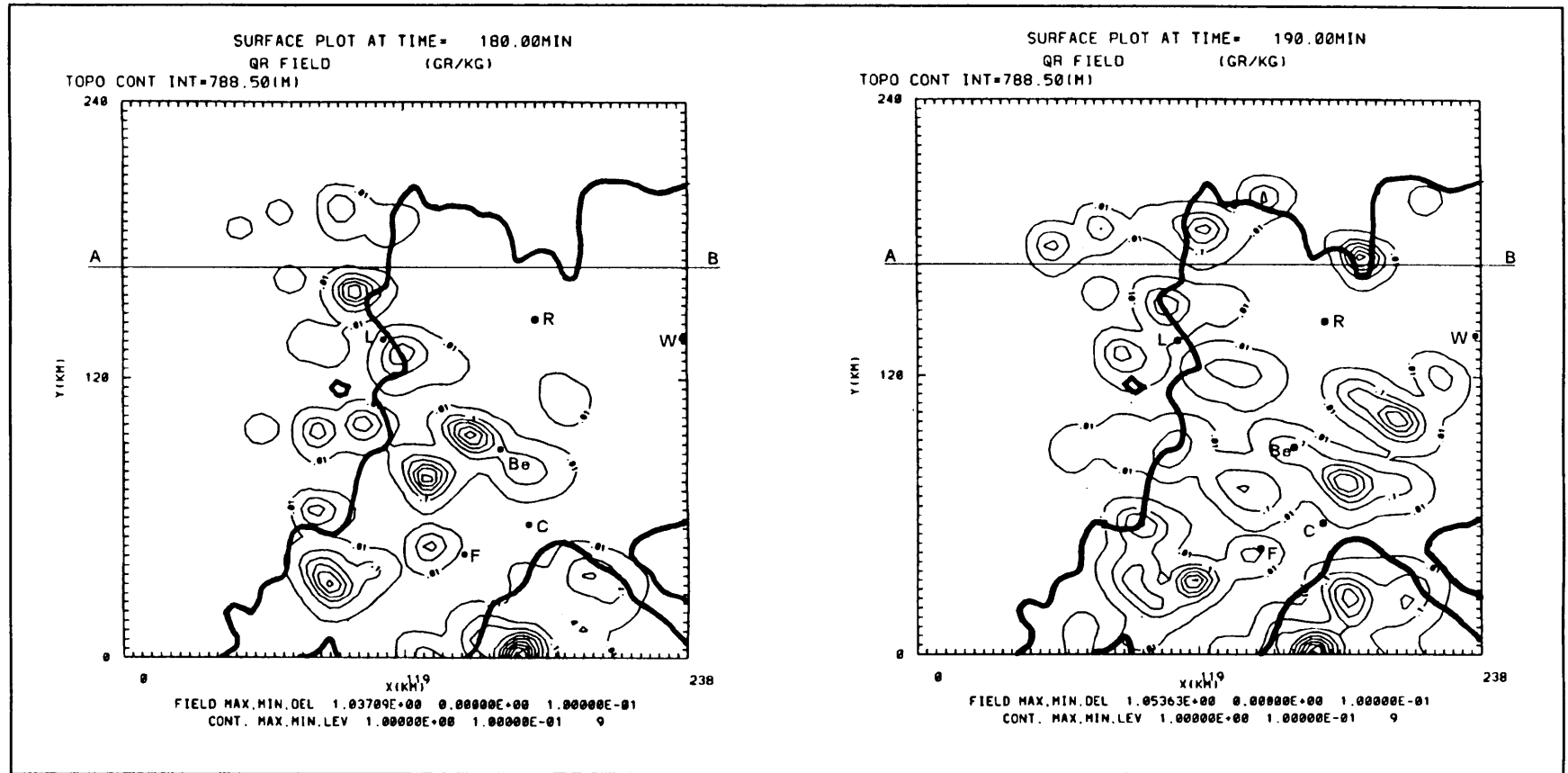CONT. MAX.MIN.LEV 5.20000E+00 1.00000E-01   51

Fig. 4.12a,b   Model generated graupel mixing ratio fields after 180 and 190 minutes of simulation (17:00 and 17:10 SAST). The plots depict the vertical segment through line AB shown in all the previous figures. The contour intervals for the graupel mixing ratio are 0.1 g kg^{-1} (basic model run)

87

X-Z PLOT AT Y= 168.00KM TIME= 200.00MIN
CLOUD ICE -B- MIXING RATIO (G/KG)

X-Z PLOT AT Y= 160.00KM TIME= 210.00MIN
CLOUD ICE -B- MIXING RATIO (G/KG)

FIELD MAX.MIN.DEL 3.50151E+00 0.00000E+00 1.00000E-01
CONT. MAX.MIN.LEV 3.50000E+00 1.00000E-01 34

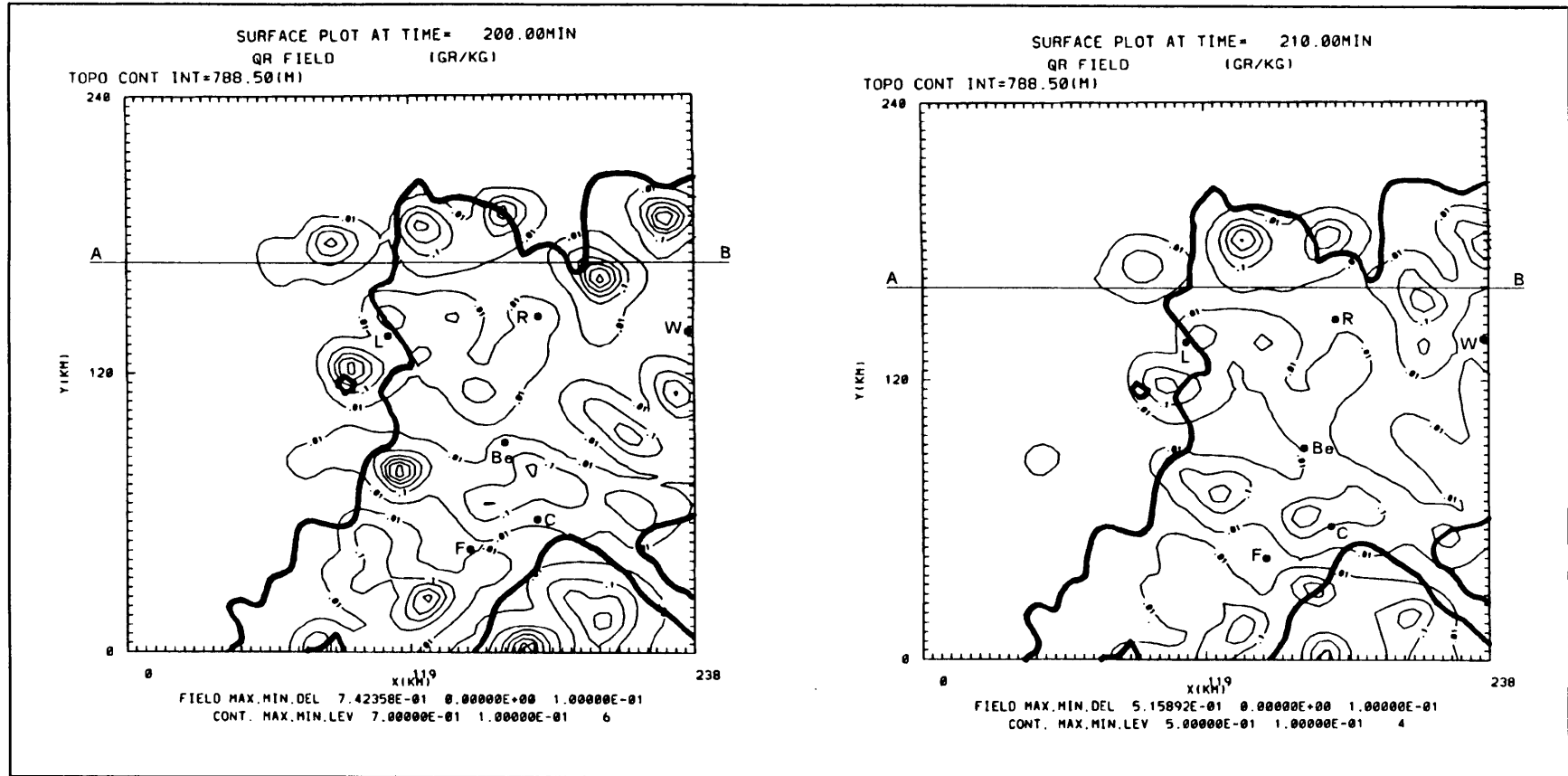FIELD MAX.MIN.DEL 3.16682E+00 0.00000E+00 1.00000E-01
CONT. MAX.MIN.LEV 3.10000E+00 1.00000E-01 30
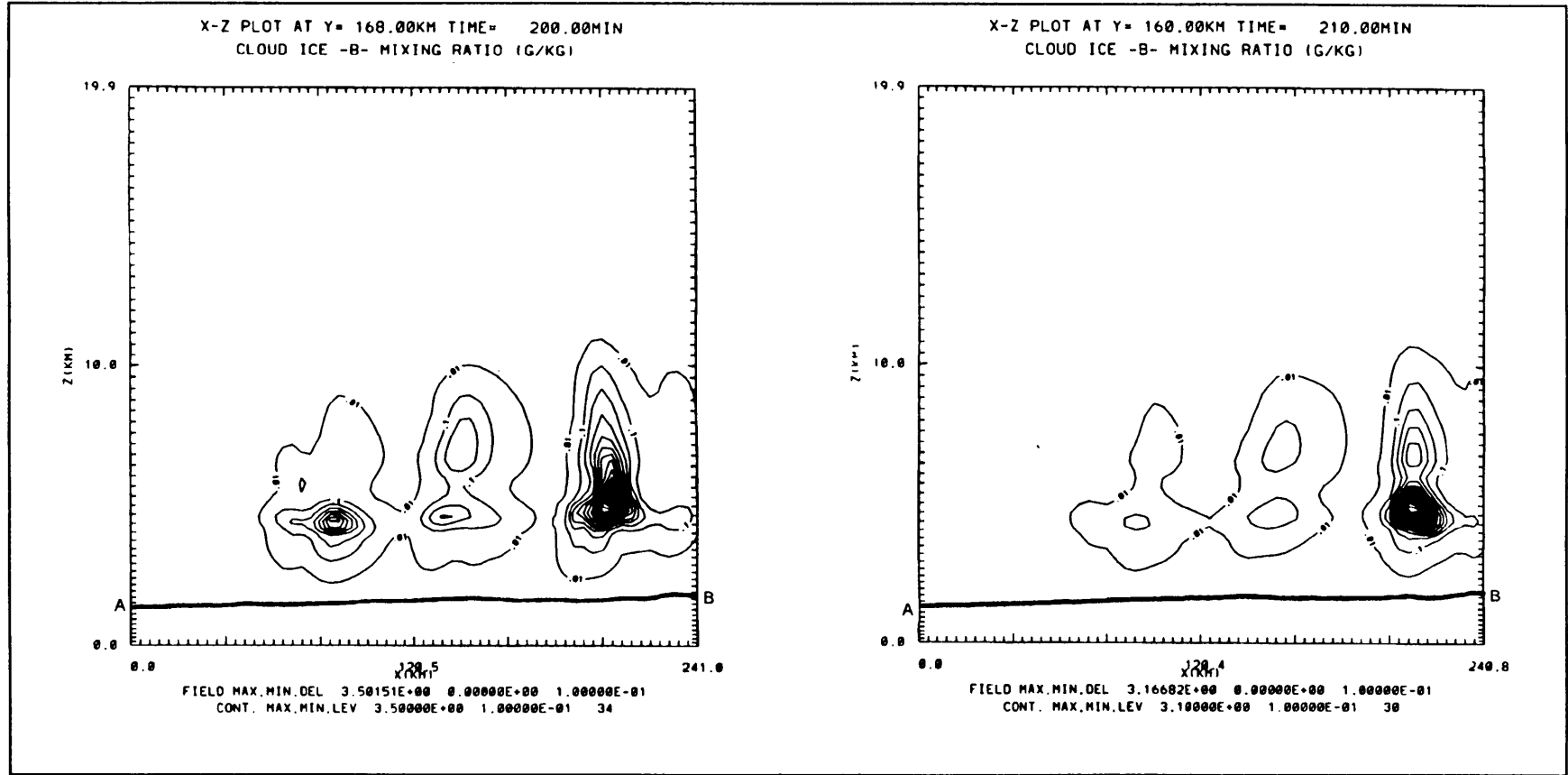
Fig. 4.12c,d   Model generated graupel mixing ratio fields after 200 and 210 minutes of simulation (17:20 and 17:30 SAST). The plots depict the vertical segment through line AB shown in all the previous figures. The contour intervals for the graupel mixing ratio are 0.1 g kg^{-1} (basic model run)

88

X-Z PLOT AT Y= 152.00KM TIME= 220.00MIN
CLOUD ICE -B- MIXING RATIO (G/KG)

X-Z PLOT AT Y= 152.00KM TIME= 230.00MIN
CLOUD ICE -B- MIXING RATIO (G/KG)

FIELD MAX.MIN.DEL 3.42458E+00 0.00000E+00 1.00000E-01
CONT. MAX.MIN.LEV 3.40000E+00 1.00000E-01   33

FIELD MAX.MIN.DEL 4.16157E+00 0.00000E+00 1.00000E-01
CONT. MAX.MIN.LEV 4.10000E+00 1.00000E-01   40
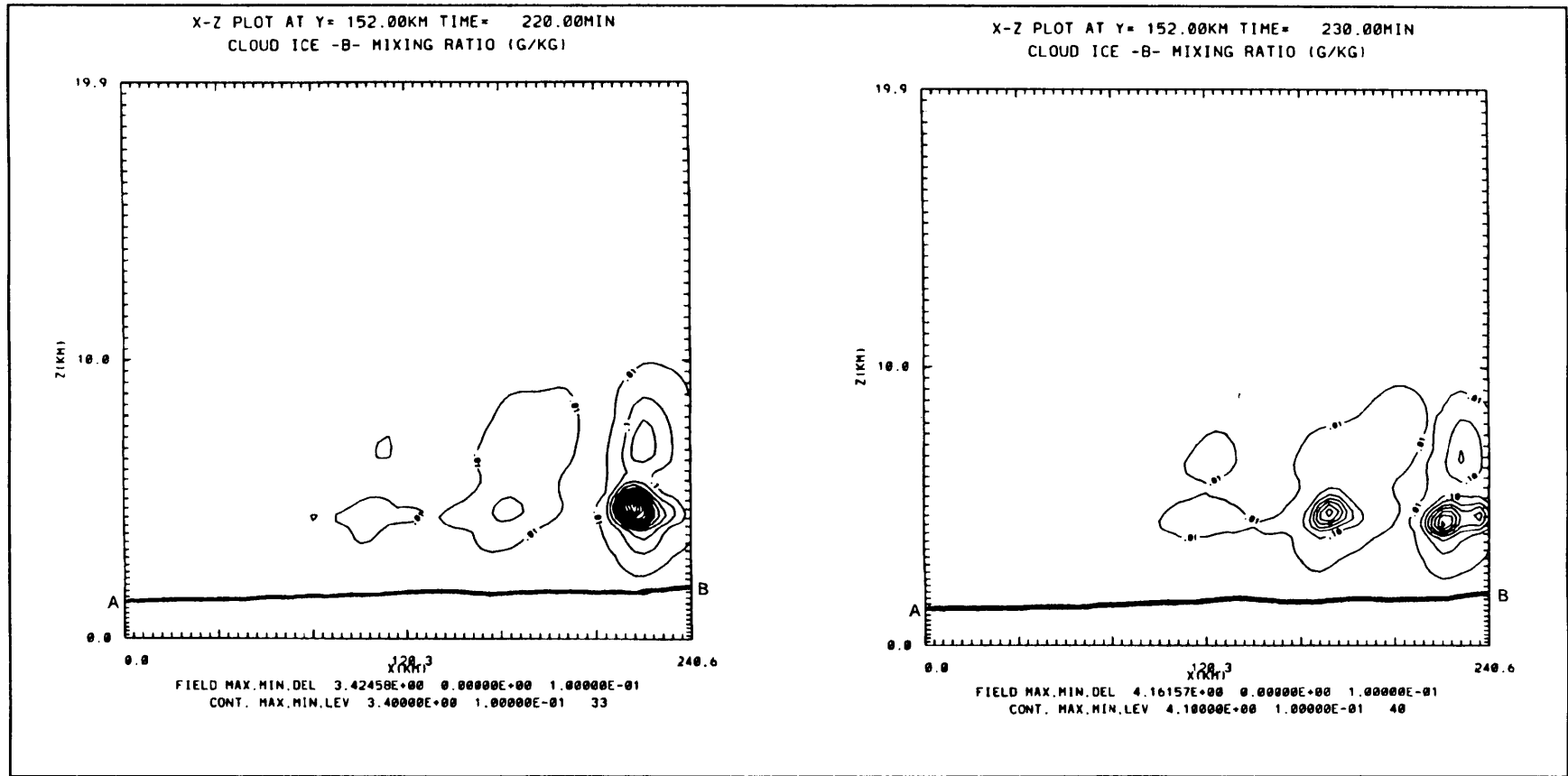
Fig. 4.12e,f   Model generated graupel mixing ratio fields after 220 and 230 minutes of simulation (17:40 and 17:50 SAST).
The plots depict the vertical segment through line AB shown in all the previous figures. The contour intervals
for the graupel mixing ratio are 0.1 g kg^{-1} (basic model run)

Fig. 4.13a,b Model generated surface rain water mixing ratio fields after 450 and 480 minutes of simulation (21:30 and 22:00 SAST). The topograhy contours are depicted as bold lines and the contour intervals for the rain water mixing ratio (thin lines) are 0.1 g kg^{-1} (effect of surface heating)
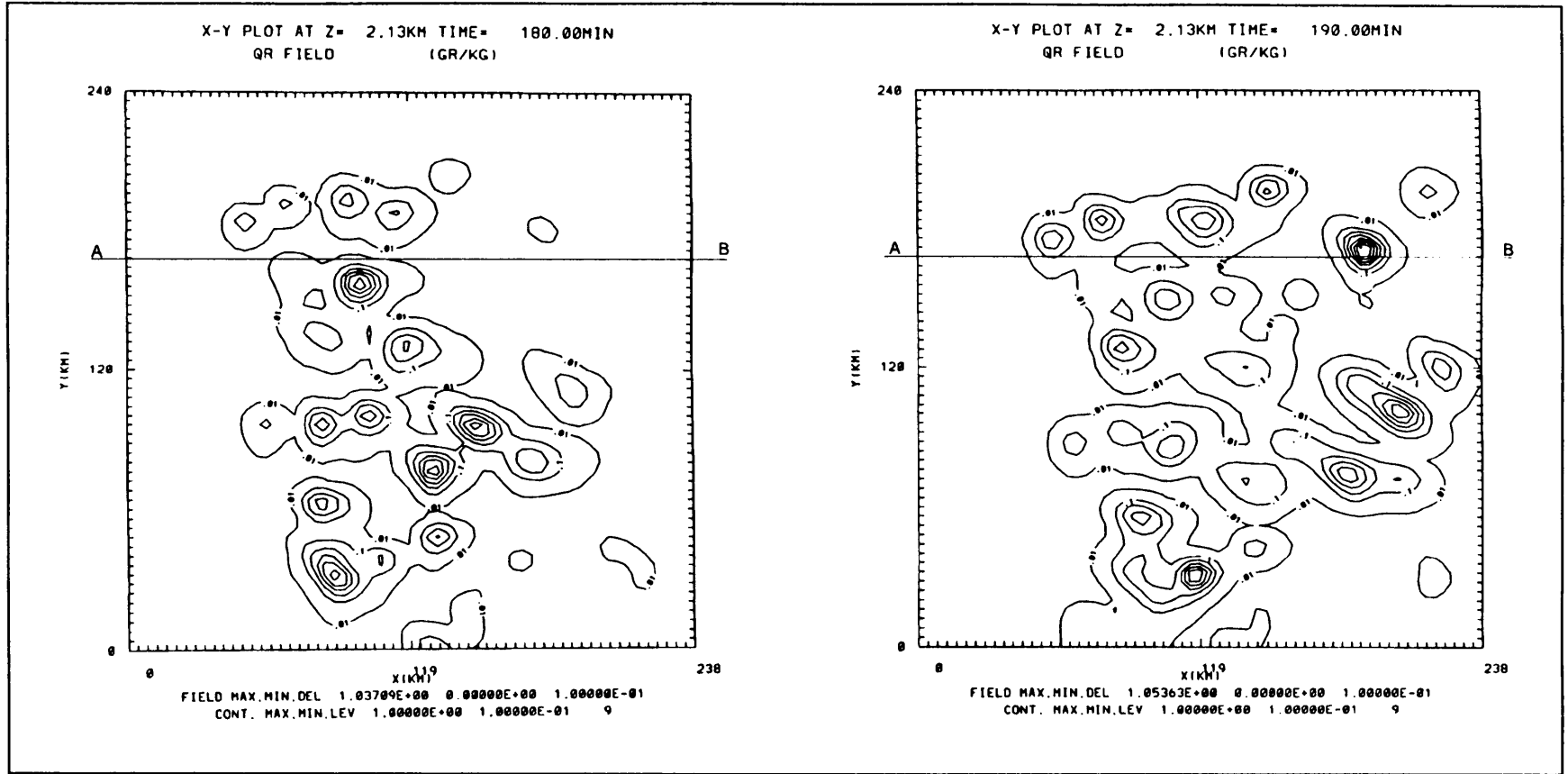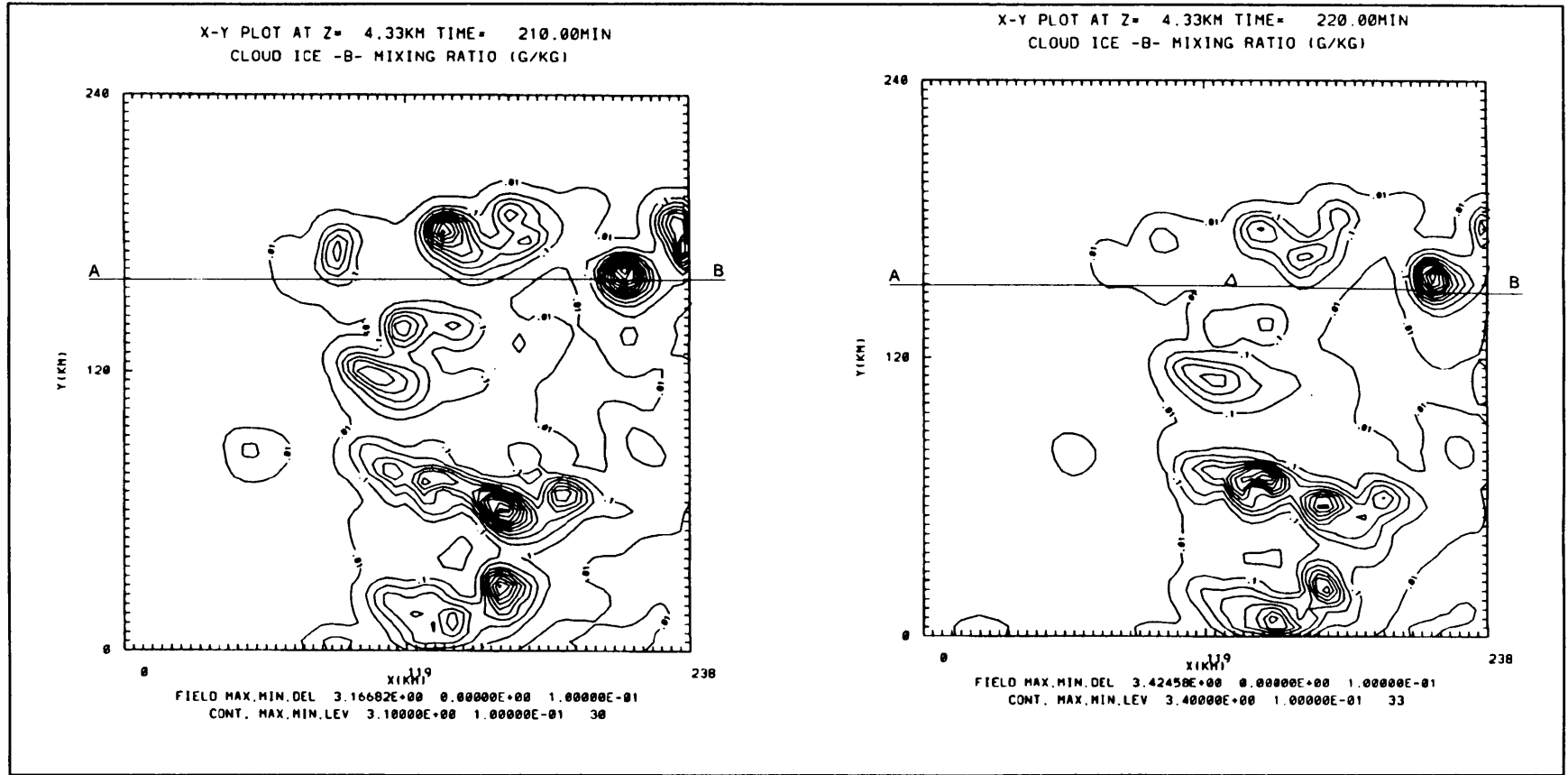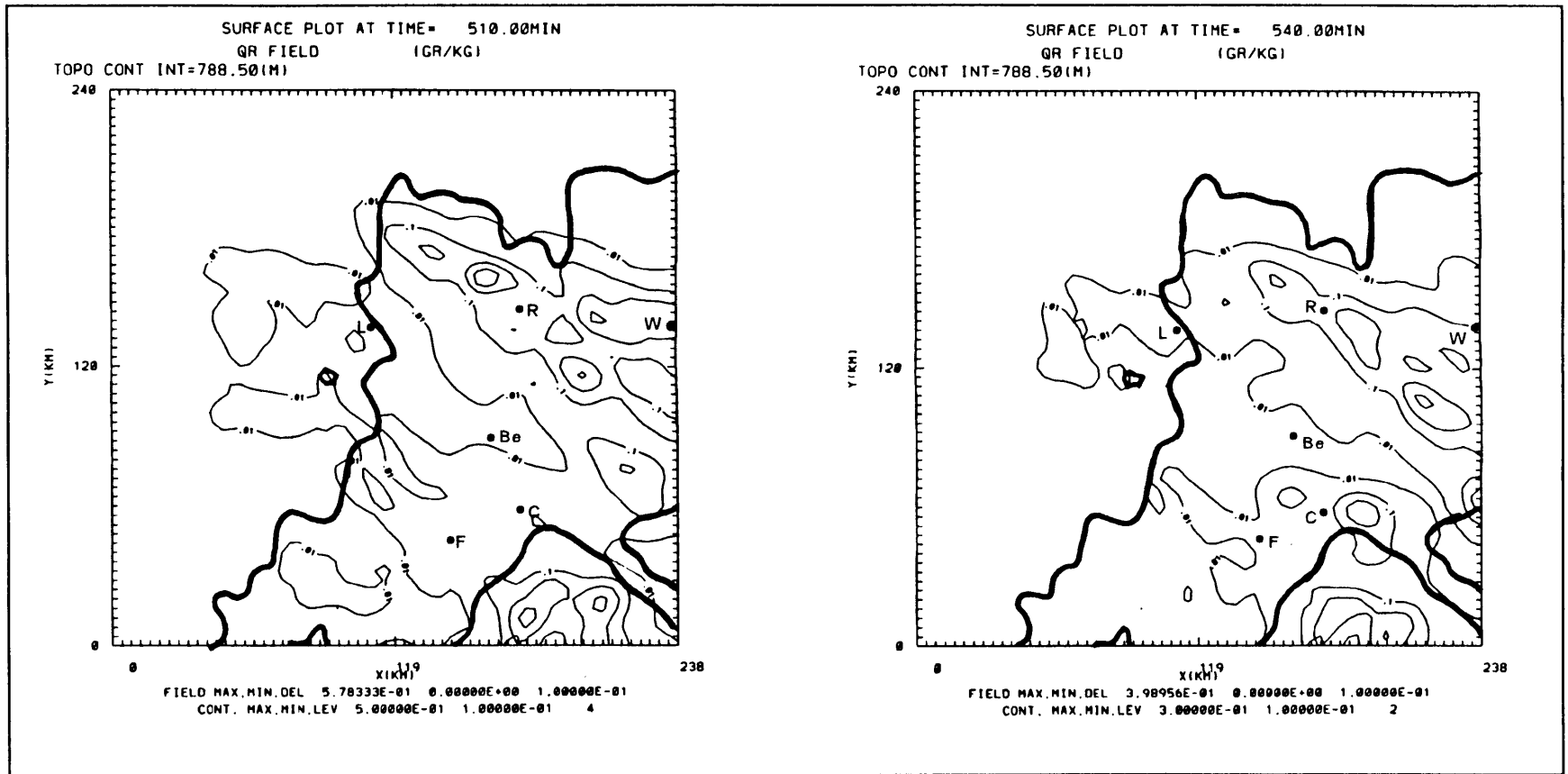
Fig. 4.13c,d   Model generated surface rain water mixing ratio fields after 510 and 540 minutes of simulation (22:30 and 23:00 SAST). The topograhy contours are depicted as bold lines and the contour intervals for the rain water mixing ratio (thin lines) are 0.1 g kg^{-1} (effect of surface heating)

91

X-Y PLOT AT Z= 3.72KM TIME= 450.00MIN
CLOUD ICE -B- MIXING RATIO (G/KG)

X-Y PLOT AT Z= 3.72KM TIME= 480.00MIN
CLOUD ICE -B- MIXING RATIO (G/KG)

FIELD MAX.MIN.DEL 2.50005E+00 0.00000E+00 1.00000E-01
CONT. MAX.MIN.LEV 2.50000E+00 1.00000E-01   24

FIELD MAX.MIN.DEL 1.02123E+00 0.00000E+00 1.00000E-01
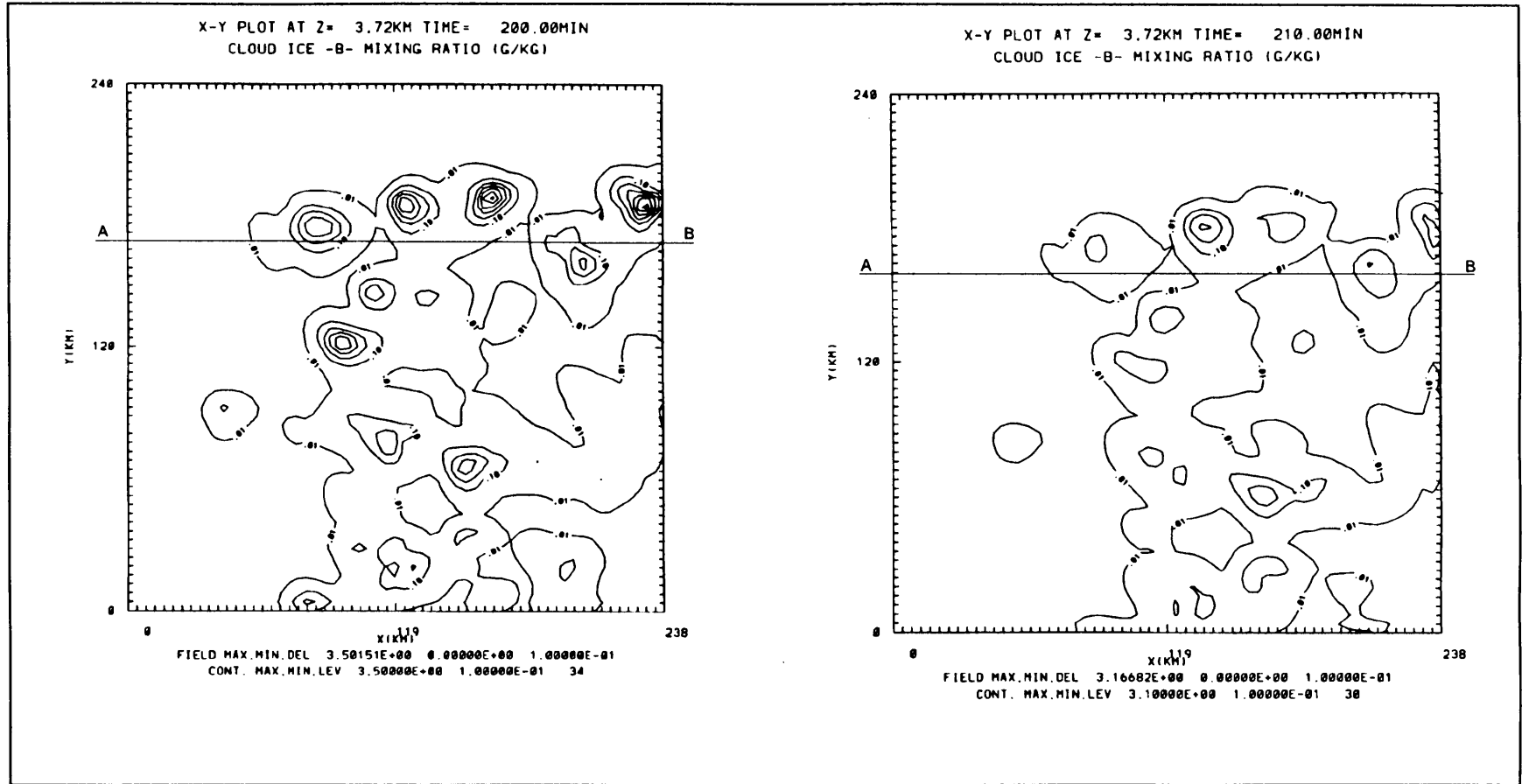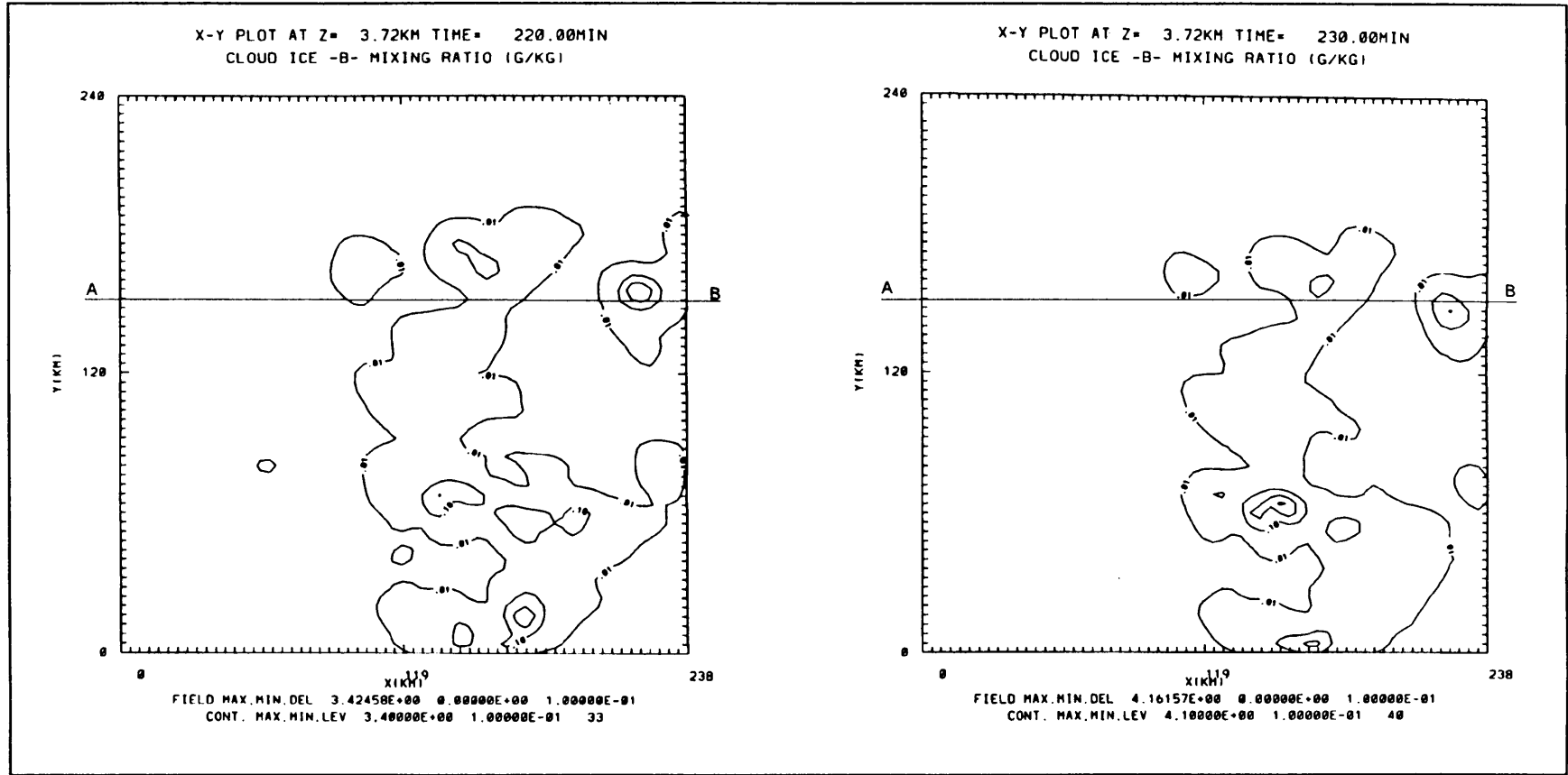CONT. MAX.MIN.LEV 1.00000E+00 1.00000E-01   9

Fig. 4.14a,b   Model generated graupel mixing ratio fields at 3.72 km above MSL after 450 and 480 minutes of simulation (21:30 and 22:00 SAST). The contour intervals for the graupel mixing ratio are 0.1 g kg^{-1} (effect of surface heating)

92

X-Y PLOT AT Z= 3.72KM TIME= 510.00MIN
CLOUD ICE -B- MIXING RATIO (G/KG)

X-Y PLOT AT Z= 3.72KM TIME= 540.00MIN
CLOUD ICE -B- MIXING RATIO (G/KG)

FIELD MAX.MIN.DEL 1.08903E+00 0.00000E+00 1.00000E-01
CONT. MAX.MIN.LEV 1.00000E+00 1.00000E-01 9

FIELD MAX.MIN.DEL 1.02477E+00 0.00000E+00 1.00000E-01
CONT. MAX.MIN.LEV 1.00000E+00 1.00000E-01 9

Fig. 4.14c,d Model generated graupel mixing ratio fields at 3.72 km above MSL after 510 and 540 minutes of simulation (22:30 and 23:00 SAST). The contour intervals for the graupel mixing ratio are 0.1 g kg^{-1} (effect of surface heating)
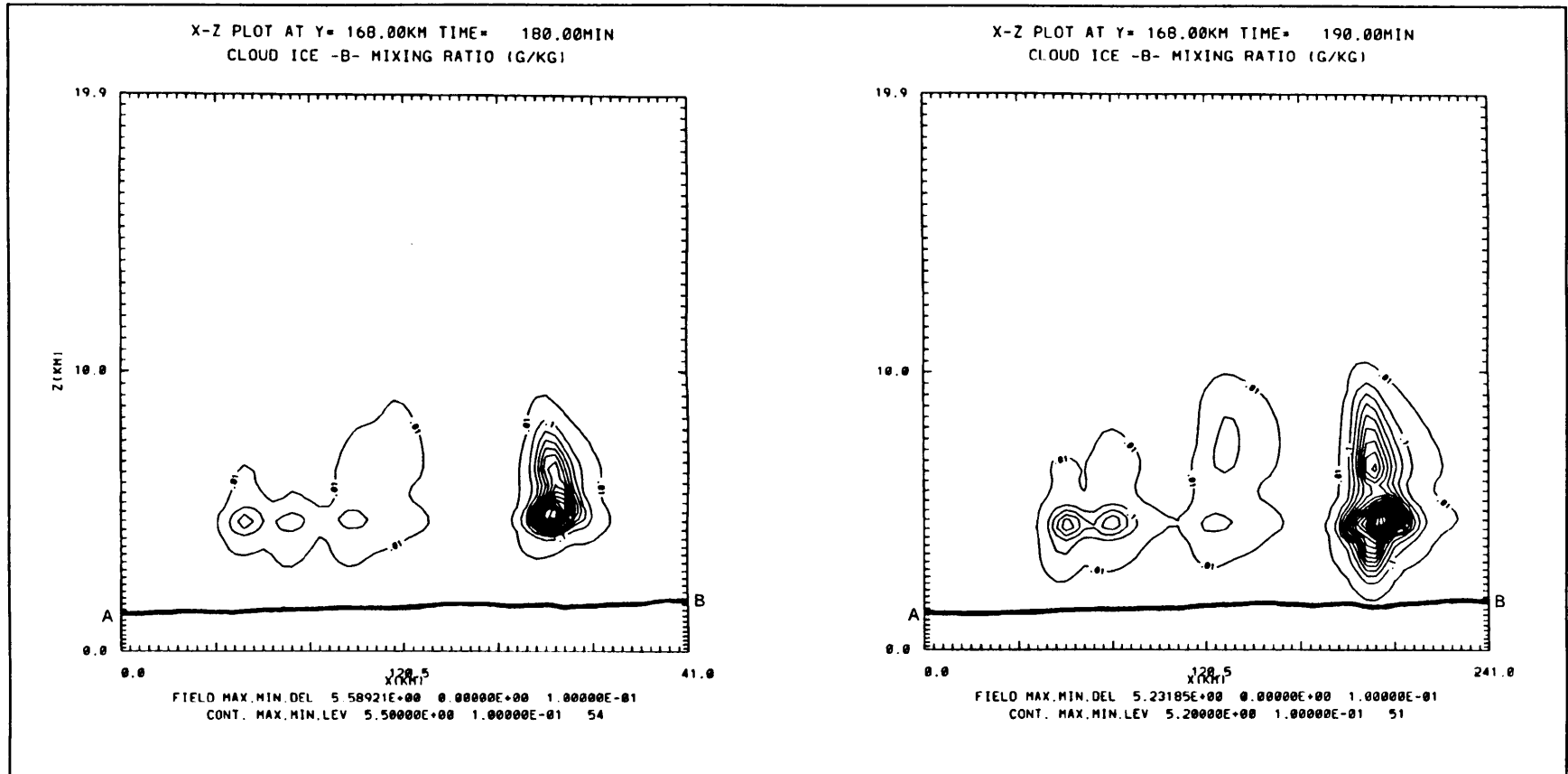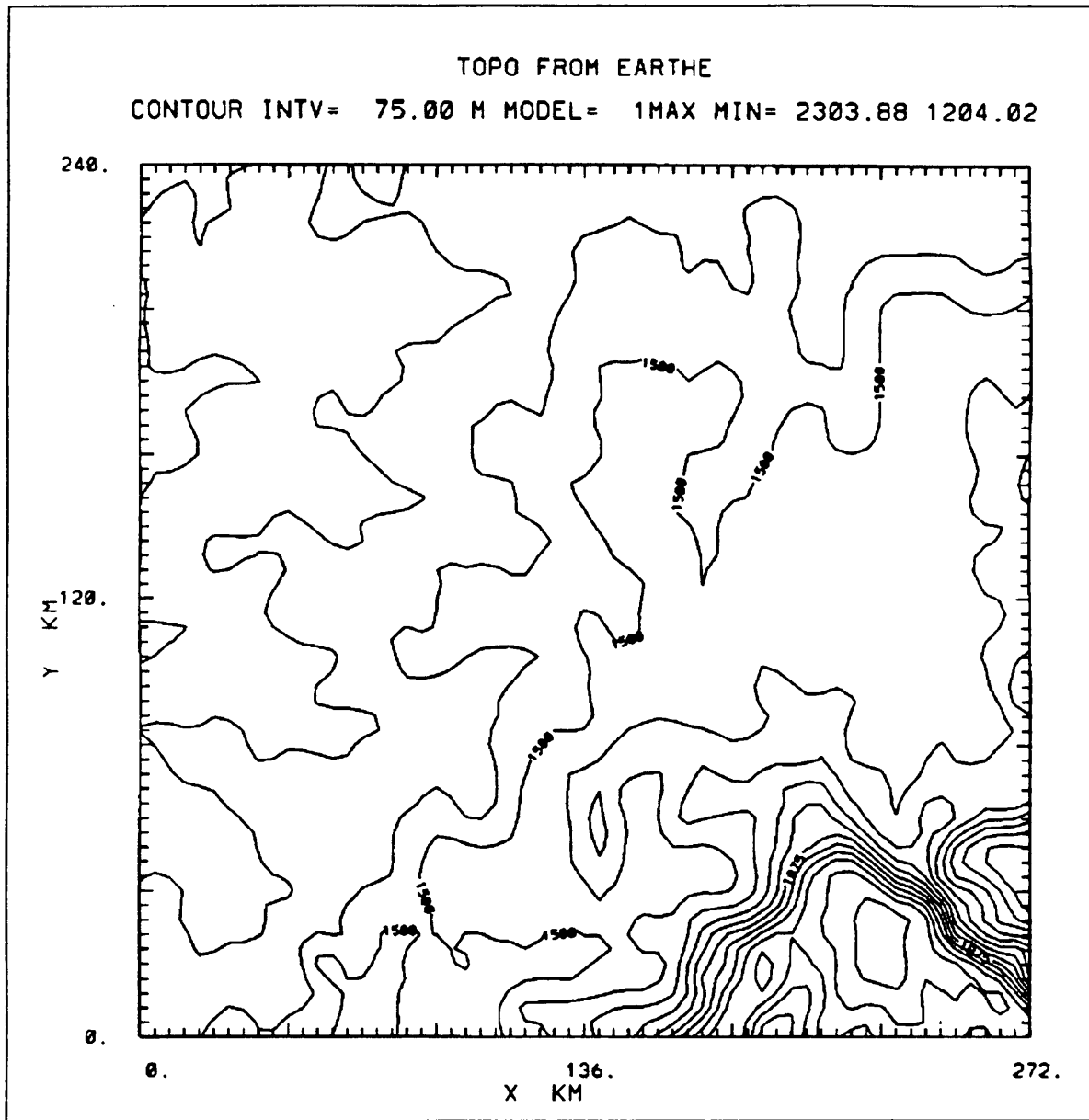
Fig. 4.15   A 240 x 240 km, two-dimensional smoothed topography plot of the model domain over the Bethlehem area.
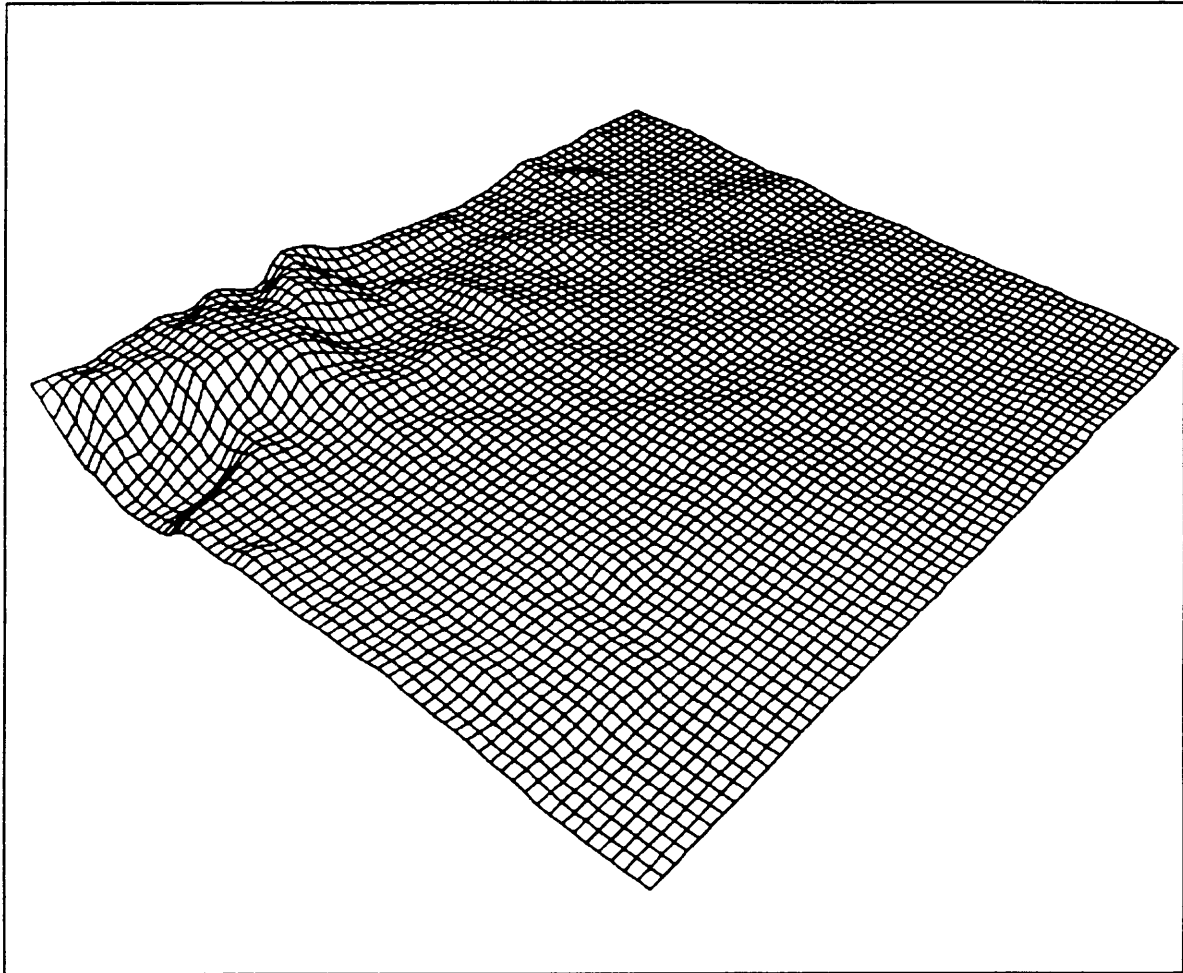
Fig. 4.16   A 240 x 240 km, three-dimensional smoothed topography plot of the
            model domain over the Bethlehem area.

95

SURFACE PLOT AT TIME= 180.00MIN
QR FIELD (GR/KG)
TOPO CONT INT=576.00(M)

FIELD MAX.MIN.DEL 6.75695E-01 0.00000E+00 1.00000E-01
CONT. MAX.MIN.LEV 6.00000E-01 1.00000E-01 5

SURFACE PLOT AT TIME= 190.00MIN
QR FIELD (GR/KG)
TOPO CONT INT=576.00(M)

FIELD MAX.MIN.DEL 8.35239E-01 0.00000E+00 1.00000E-01
CONT. MAX.MIN.LEV 8.00000E-01 1.00000E-01 7
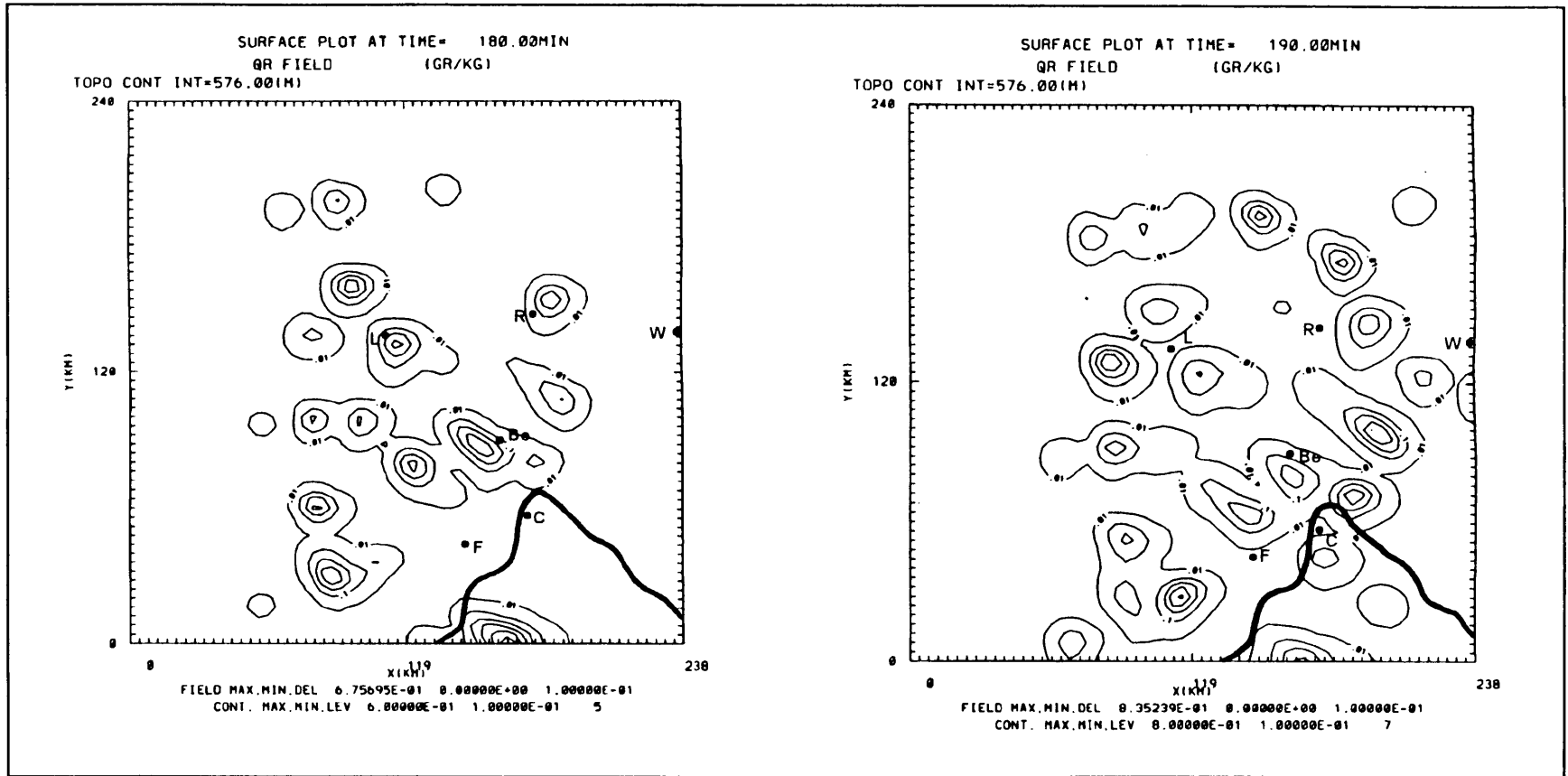
Fig. 4.17a,b Model generated surface rain water mixing ratio fields after 180 and 190 minutes of simulation (17:00 and 17:10 SAST). The topograhy contours are depicted as bold lines and the contour intervals for the rain water mixing ratio (thin lines) are 0.1 g kg^{-1} (effect of topography)
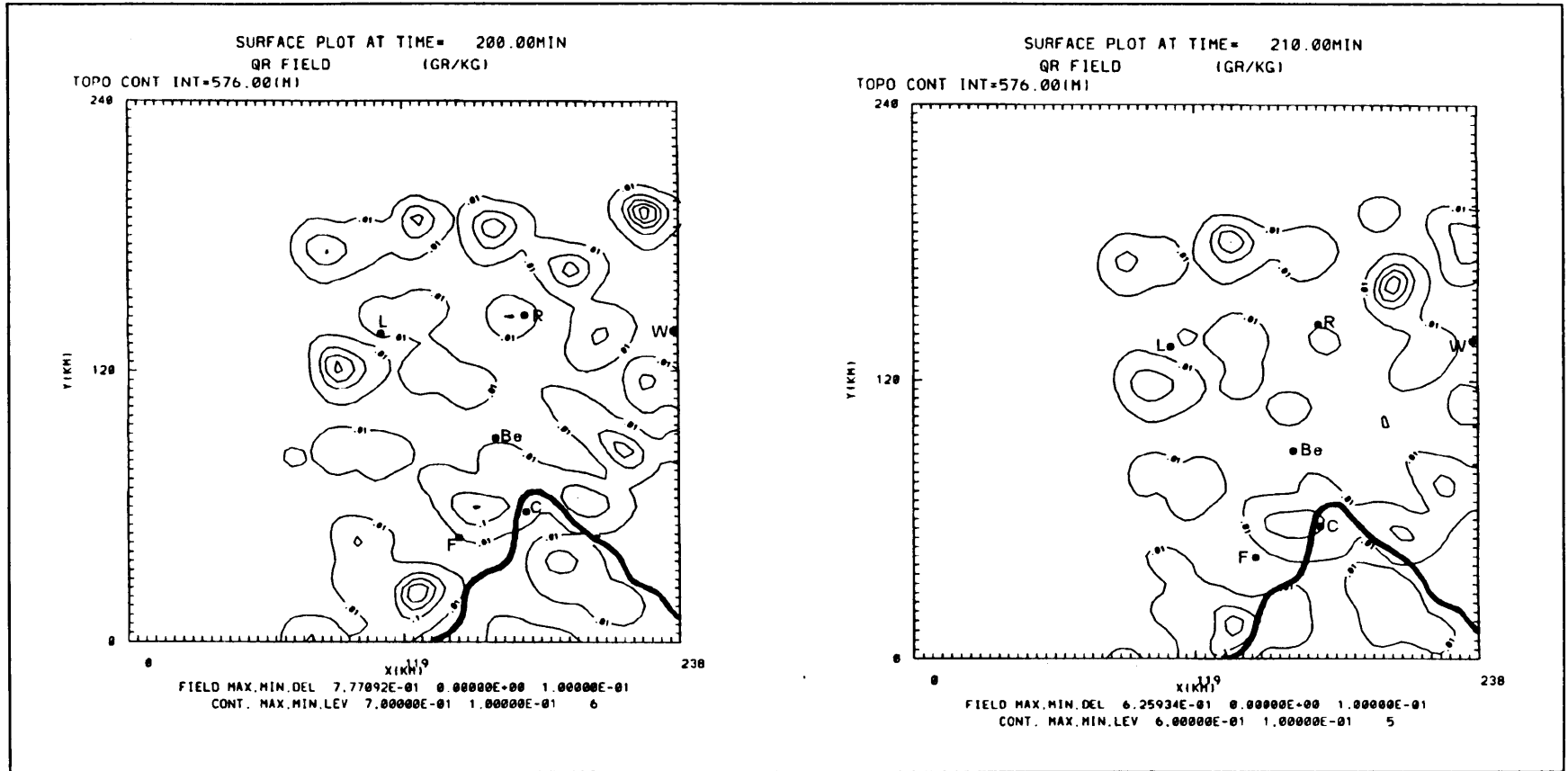
Fig. 4.17c,d   Model generated surface rain water mixing ratio fields after 200 and 210 minutes of simulation (17:20 and 17:30 SAST). The topograhy contours are depicted as bold lines and the contour intervals for the rain water mixing ratio (thin lines) are 0.1 g kg^{-1} (effect of topography)
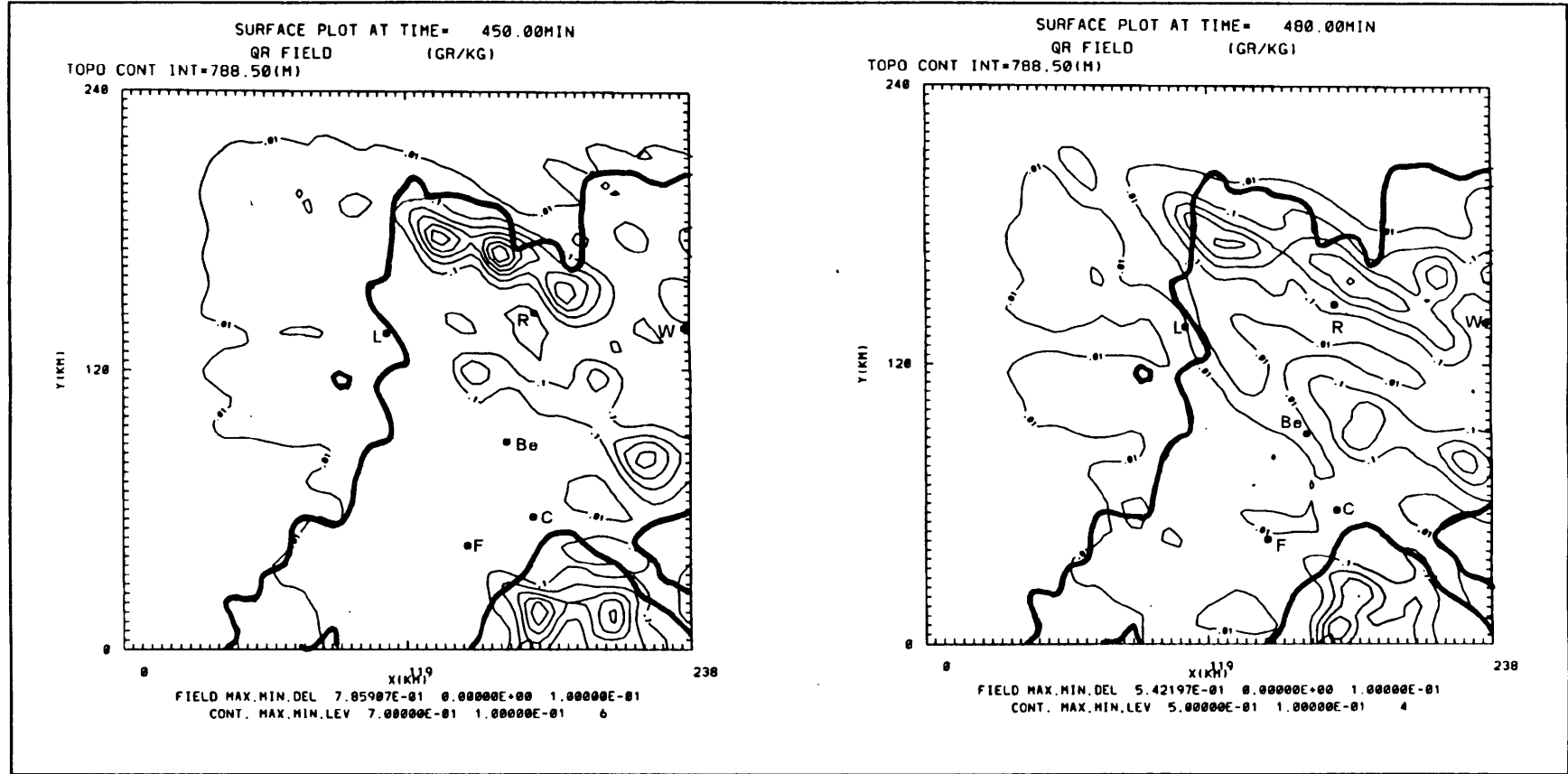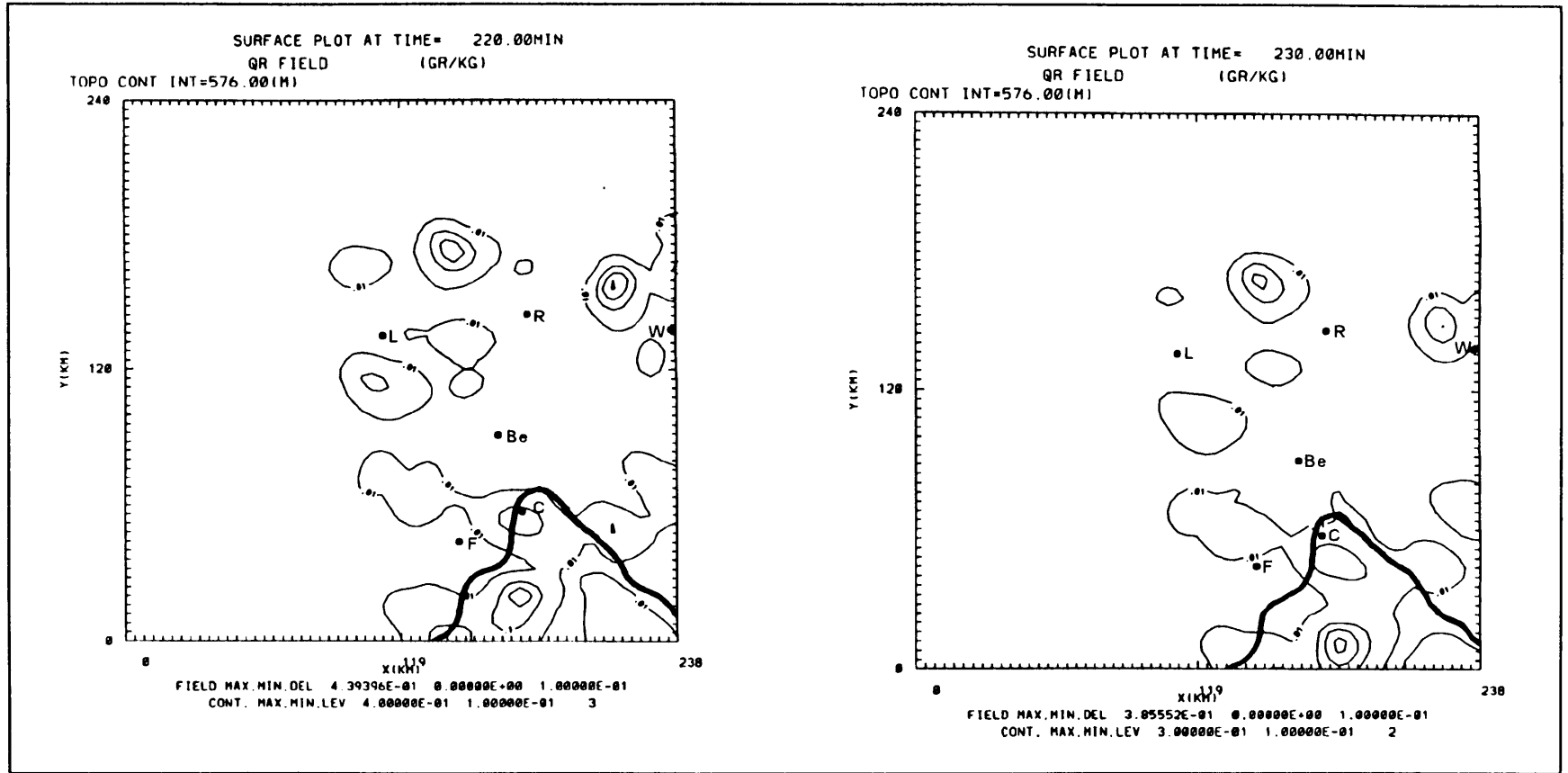
Fig. 4.17e,f   Model generated surface rain water mixing ratio fields after 220 and 230 minutes of simulation (17:40 and 17:50 SAST). The topograhy contours are depicted as bold lines and the contour intervals for the rain water mixing ratio (thin lines) are 0.1 g kg^{-1} (effect of topography)
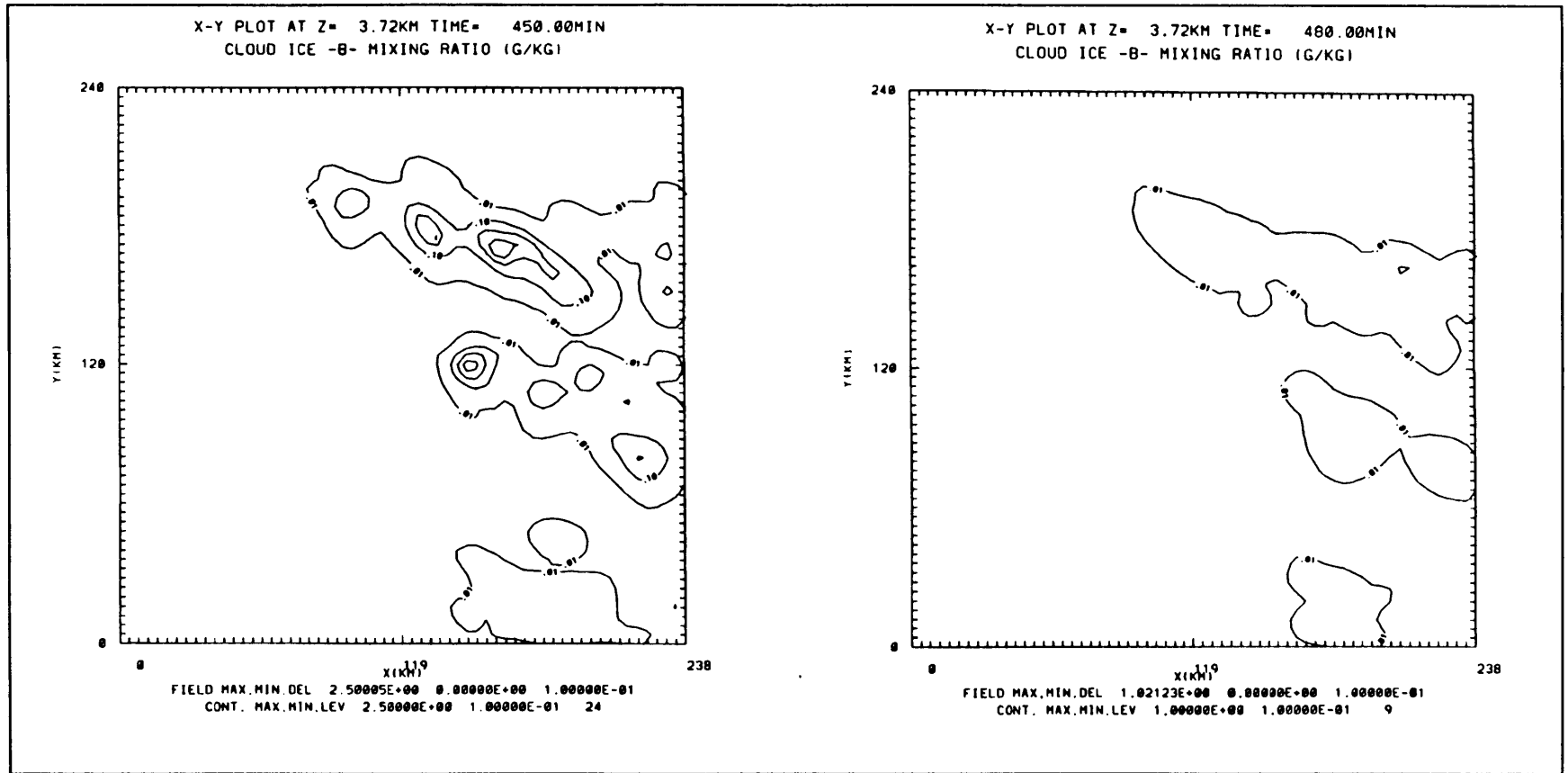
X-Y PLOT AT Z= 3.72KM TIME= 180.00MIN
CLOUD ICE -B- MIXING RATIO (G/KG)

X-Y PLOT AT Z= 3.72KM TIME= 190.00MIN
CLOUD ICE -B- MIXING RATIO (G/KG)

FIELD MAX.MIN.DEL 6.48522E+00 0.00000E+00 1.00000E-01
CONT. MAX.MIN.LEV 6.40000E+00 1.00000E-01 63

FIELD MAX.MIN.DEL 4.98194E+00 0.00000E+00 1.00000E-01
CONT. MAX.MIN.LEV 4.90000E+00 1.00000E-01 48

Fig. 4.18a,b   Model generated graupel mixing ratio fields at 3.72 km above MSL after 180 and 190 minutes of simulation (17:00 and 17:10 SAST). The contour intervals for the graupel mixing ratio are 0.1 g kg^{-1} (effect of topography)

X-Y PLOT AT Z= 3.72KM TIME= 200.00MIN
CLOUD ICE -B- MIXING RATIO (G/KG)

FIELD MAX.MIN.DEL 2.77577E+00 0.00000E+00 1.00000E-01
CONT. MAX.MIN.LEV 2.70000E+00 1.00000E-01 26

X-Y PLOT AT Z= 3.72KM TIME= 210.00MIN
CLOUD ICE -B- MIXING RATIO (G/KG)

FIELD MAX.MIN.DEL 2.22188E+00 0.00000E+00 1.00000E-01
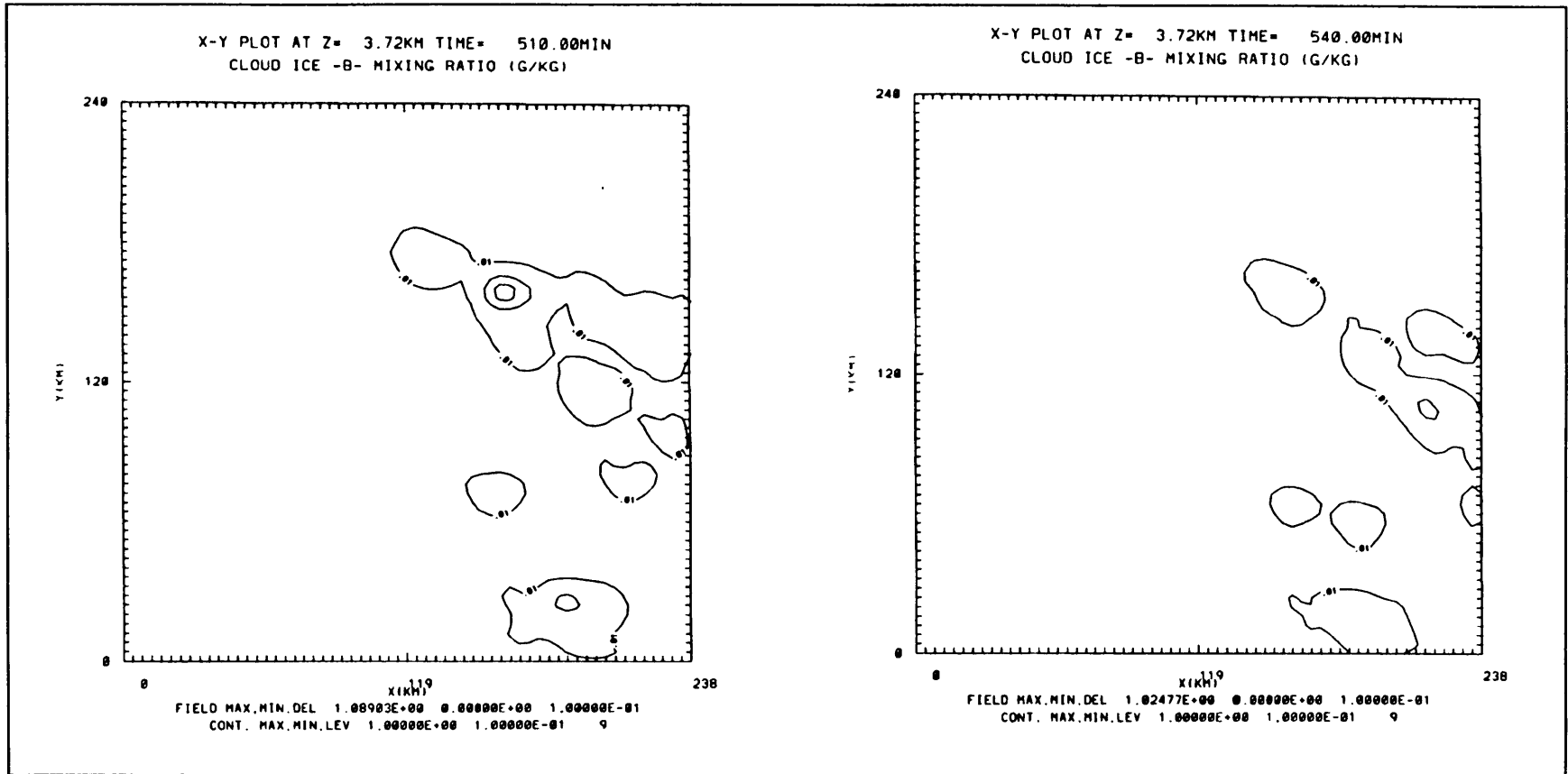CONT. MAX.MIN.LEV 2.20000E+00 1.00000E-01 21

Fig. 4.18c,d Model generated graupel mixing ratio fields at 3.72 km above MSL after 200 and 210 minutes of simulation (17:20 and 17:30 SAST). The contour intervals for the graupel mixing ratio are 0.1 g kg^{-1} (effect of topography)

X-Y PLOT AT Z= 3.72KM TIME= 220.00MIN
CLOUD ICE -B- MIXING RATIO (G/KG)

X-Y PLOT AT Z= 3.72KM TIME= 230.00MIN
CLOUD ICE -B- MIXING RATIO (G/KG)

FIELD MAX.MIN.DEL 2.41230E+00 0.00000E+00 1.00000E-01
CONT. MAX.MIN.LEV 2.40000E+00 1.00000E-01 23

FIELD MAX.MIN.DEL 1.94282E+00 0.00000E+00 1.00000E-01
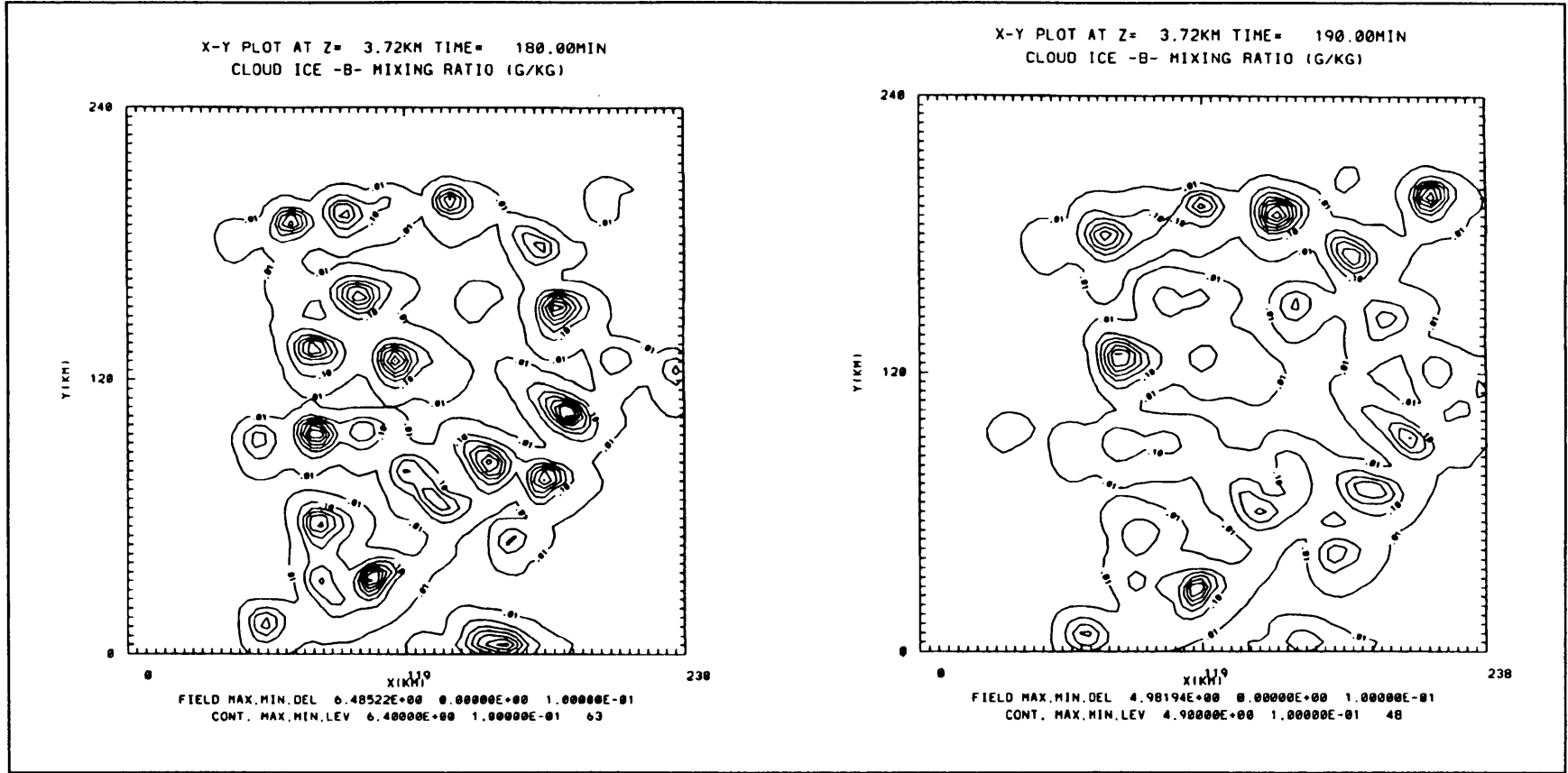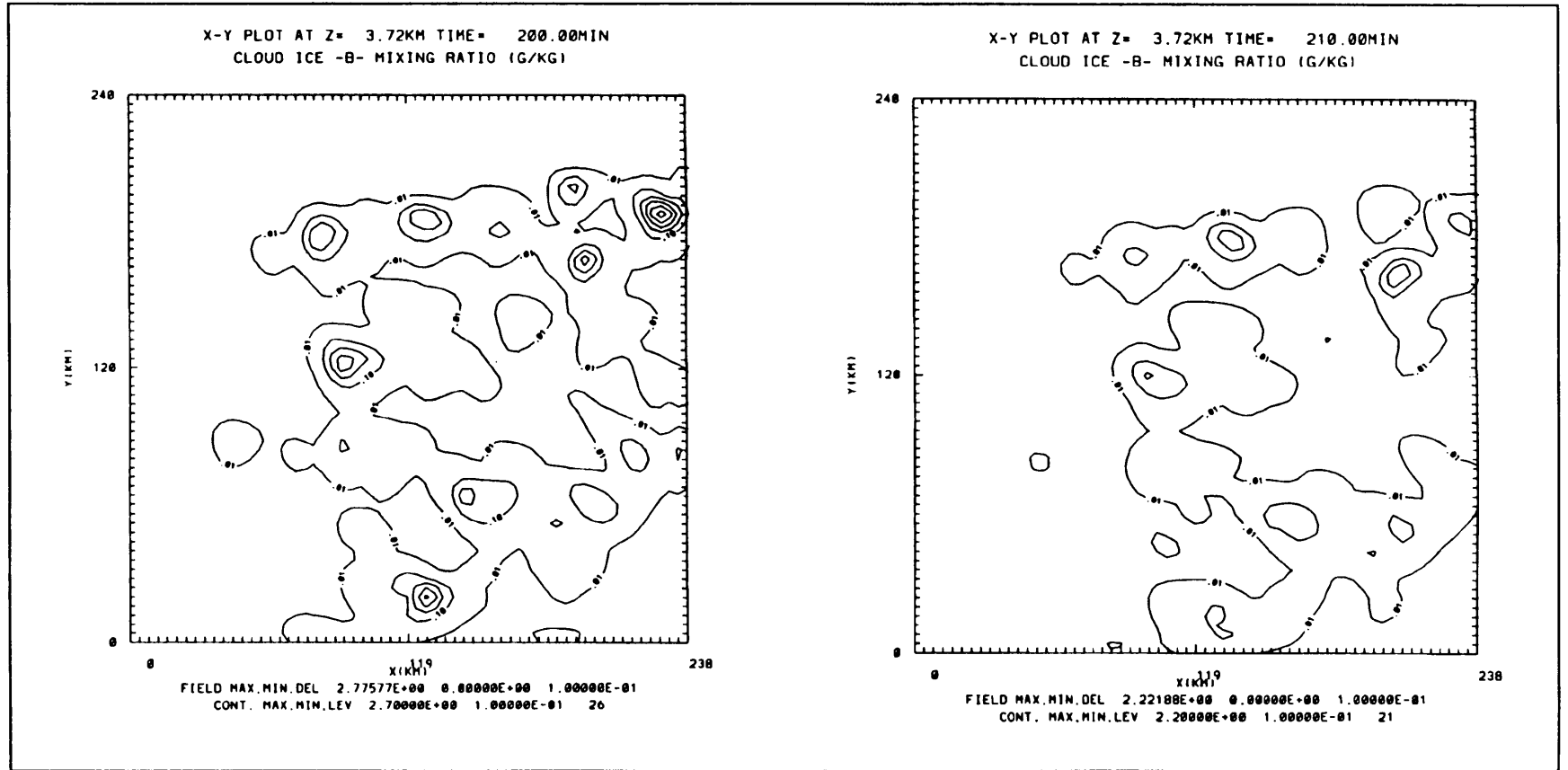CONT. MAX.MIN.LEV 1.90000E+00 1.00000E-01 18

Fig. 4.18e,f   Model generated graupel mixing ratio fields at 3.72 km above MSL after 220 and 230 minutes of simulation (17:40 and 17:50 SAST). The contour intervals for the graupel mixing ratio are 0.1 g kg^{-1} (effect of topography)

Chapter 5

9 December 1991

On 9 December 1991 a solitary supercell storm developed in the BPRP and caused severe hail damage to a farming community to the east of Bethlehem. In this chapter this case day and the results obtained from the numerical simulation will be discussed in detail.

In sections 5.1 and 5.2 the weather patterns leading up to the severe hailstorm on the afternoon of the 9 December 1991 are discussed. In section 5.2.2 the mesoscale conditions within which this hailstorm developed are discussed.

Sections 5.3 and 5.4 deals with the numerical simulation of the hailstorm. Section 5.3 deals with the set-ups and initialization of the model, while in section 5.4 the results obtained during the model runs are discussed. Section 5.5 contains the conclusions of this case study.

5.1   Weather patterns for 8 December 1991

Isolated showers fell over the Northern and Eastern Cape on this day due to a cold front that passed over these regions. The cold front moved to over the Free State, with the Atlantic high ridging along the Cape south-west coast. This ridging is also reflected in the 850 hPa contour field over the western interior behind the cold front (figure 5.1). The position of the cold front can clearly be seen on the map depicting maximum temperatures for the day (figure 5.2). From this figure, it can be seen that the cold front has already passed over Bloemfontein and was on its way to the Bethlehem area. Both the upper and surface troughs were situated over the central

101

interior, resulting in fairly general rainfalls with occasionally heavy showers in places, over Northern and Eastern Transvaal, Northwest, Gauteng, KwaZulu/Natal and the Free State.

From the 12:00 SAST Bethlehem sounding (figure 5.3), it can be seen that the lower layers of the atmosphere were very moist and unstable. The upper layers of the atmosphere were drier, especially at 300 hPa.

5.2 Weather patterns for 9 December 1991

5.2.1 Synoptic circulation

The cold front continued its eastwards movement and was now situated north-east of the Free State (figure 5.4). A surface trough was situated over the Free State and the Atlantic high was ridging in strongly along the south coast. The movement of the cold front can be seen clearly on the maximum temperature chart for the day (figure 5.5). On this map it can be seen that temperatures in the area behind the cold front were recovering. The only remaining evidence of the passage of the cold front was the cool pool of air to the east of Bethlehem in the Aberfeldy area. (Incidently it is in this area that the severe hailstorm of that day developed). Scattered rain and showers occurred in the moist air to the east of the interior surface trough, while fine conditions prevailed in the dry air over the western regions. Figure 5.6, shows the Meteosat image for 11:55 UT, 9 December 1991. In this image the cloud band to the north of the country, which is associated with the cold front, is clearly visible. Small patches of cloud development can also be seen on the east coast. This image highlights the fact that dry, cloudless conditions prevailed over the interior of the country.

The 12:00 UT Bethlehem sounding of the day (figure 5.7) become more stable and the surface temperature has increased to 21.6°C. Drying out has occurred on the lower layers of the atmosphere and there was an inversion present above 600 hPa. The dry air in the upper layers descended and was now situated between 500 and

102

600 hPa. The Showalter Index for the day was 3.3 and no severe weather was expected or predicted for the day.

5.2.2 Mesoscale conditions

During the afternoon of 9 December 1991, a solitary supercell storm developed to the east of Bethlehem in the Aberfeldy/Kestell area. This storm developed at approximately 14:30 SAST and lived until 17:30 SAST. During its lifetime it caused approximately one million Rands damage to maize and wheat crops in the Aberfeldy and Warden areas. It was estimated that 1300 ha of wheat and 500 ha of maize were destroyed (Star newspaper, 11/12/91).

The development and movement of the storm are depicted in the series of radar-rain-rate plots for the day (figures 5.8a to 5.8d). Note that these plots, as was the case for figures 4.5a to 4.5f, were plotted on a coordinate system where the y-axis represents magnetic north. As before a secondary coordinate system, indicating true north, has been overlaid on all the plots. The path followed by this supercell is depicted in the storm track plot (figure 5.9) - again take note of the direction of true north.

This day was unique in the sense that apart from the supercell responsible for the extensive hail damage to the east of Bethlehem, no other convective activity occurred over the entire BPRP area.

5.3 The model set-up and initialization

In order to simulate this hailstorm, the non-hydrostatic, anelastic, three-dimensional Clark model was again used. The domain within which the simulation was performed was a 360 x 360 km window over the Bethlehem area, with -28°N and 28.5°E as the centre point (figure 5.10). The domain for this simulation was chosen differently to the one used in Chapter 4 to simulate the hailstorm of 24 November 1992. The

103

reason for this was to ensure that the area where the supercell developed and propagated in would remain well inside the model domain. A three-dimensional plot of the domain, as viewed from the north-east, is displayed in figure 5.11.

The model's horizontal grid resolution was set to 4 km, which gave 92 grid points in both the x (east) and y (north) directions. The model's vertical dimension (z) consisted of 62 grid points. Vertical stretching was again applied in the z-direction and this resulted in a resolution which varied from about 0.2 km between grid points in the lower layers, to about 1 km between grid points in the upper layers. This gave a vertical extent of approximately 23 km. The upper 18 grid points were used as a buffer zone to prevent gravity waves from propagating from the upper lid of the model domain into the research area and thereby affecting the results.

The basic model run was initialized with the 12:00 UT Bethlehem sounding for 9 December 1991 (figure 5.7). The other model runs were initialized with composite soundings made up from the soundings of Bloemfontein, Bethlehem and Durban.

5.4   Results

The results obtained during the numerical simulation of the severe supercell storm of 9 December 1991 will now be discussed in detail. Section 5.4.1 contains the results from the basic model run. Since the basic model run failed to simulate the development of the supercell, attempts were made to improve the model results. The results from these model runs are discussed in section 5.4.2.

5.4.1 Basic model run

Figures 5.12a to 5.12d are a series of three-dimensional model predicted rain water mixing ratio field plots for a total of 45 minutes. All the values on these plots are of rain water mixing ratios greater or equal to 0.1 g kg^{-1}. The first signs of development took place after 105 minutes of simulation (local time 15:45 SAST). Initial

104

development started in the south-east of the model domain. This development was very small and insignificant and it dissipated fast. After 150 minutes of simulation (local time 16:30 SAST) no rain cells were visible in this area anymore. Around 120 minutes of simulation (local time 16:00 SAST) new rain cell development was noted in the north-west of the model domain. At first this development strengthened slightly, then it started to spread-out over the northern part of the domain and dissipated. By 16:45 SAST (165 minutes of simulation) all development throughout the model domain has dissipated (this graph is not shown).

Figures 5.13a to 5.13d are a series of three-dimensional model predicted graupel mixing ratio field plots for a total of 45 minutes. Again all the values are of graupel mixing ratios greater or equal to 0.1 g kg^{-1}. As for the rain, the graupel first developed in the south-east of the model domain. Approximately 15 minutes later, development started in the north-west. Again the development in the south-east dissipated fast, while the development in the north-west first strengthened slightly, before spreading out over the northern part of the domain and dissipated. The first signs of graupel development were noticed shortly after 90 minutes of simulation (not shown). In comparison, the first rain development only appeared approximately 15 minutes later. After 150 minutes of simulation, the graupel development had all but dissipated. At that stage there were still patches of rain development visible to the north.

The model was run for a considerable time after all development dissipated, but no new development was noted. All the development that took place throughout the model simulation was small, shallow and insignificant. Not only was the development that took place insignificant, but it was also very far removed from the area where the supercell developed. Even so, the model did not fail completely. The general mesoscale conditions for this day were clear skies with little convective activity. The model succeeded in predicting these general mesoscale conditions, it only failed in predicting the development of the severe supercell to the east of Bethlehem.

Keeping in mind the synoptic conditions that occurred that day, it is possible that the supercell developed in a convergence zone (with dry air to the west and moist, cooler air to the east due to the ridging of the Atlantic High pressure system) which was set up between Bethlehem and Harrismith. If this was the case, the trigger mechanism responsible for the development of the supercell might only have been visible in the airmass in the immediate vicinity of where the storm developed. The numerical simulation of this storm was done by initializing the model with only Bethlehem's sounding. Thus, if the trigger mechanism was not evident in the airmass over Bethlehem, the model would not have been able to simulate it.

It is interesting to note that although the topographical contours in the model domain are very steep, no significant development was predicted over the mountainous areas during this case study. This is in direct contrast to what was noted during the 24 November 1992 case study. Observations over the BPRP area have shown that when the surface wind over the project area has a north-western component, development over and close to the mountains are favoured, as was the case for 24 November 1992, (Terblanche, 1996). On 9 December 1991 the surface wind had a south-eastern component. The fact that the model did not predict development over the mountains in this case is thus very significant. It proved that the model is capable of simulating local characteristics.

5.4.2 Possible improvements

Although the model succeeded in predicting the general mesoscale conditions experienced over the BPRP area for this case study day, it was disappointing that the model failed in simulating the severe supercell storm that developed that day. There are two possible routes that can be taken in order to improve this situation. The first, and ultimate, is to initialize the model with large scale data. This area of research falls outside the scope of this dissertation, but it is a future area of research that needs to be investigated. The second possibility is to initialize the model with a

106

composite sounding. Apart from the Bethlehem sounding, the soundings of interest are those of Bloemfontein and Durban.

Comparing the three soundings, one notices that the layer of dry air between 600 and 500 hPa that is visible in the Bethlehem sounding (figure 5.7) is also visible in the Bloemfontein and Durban soundings (not shown). Consequently, this part of the sounding was left unchanged during all the model runs. Above 500 hPa all three soundings were very similar and this part was also left unchanged.

With the passage of the cold front all three stations' surface temperature decreased on 8 December. On 9 December, Bloemfontein started to warm up again, while the surface temperatures at Bethlehem and Durban remained almost unchanged. All three the stations' surface moisture values were around 12 g kg^{-1} on 8 December. Bloemfontein and Bethlehem's surface moisture decreased to 7 and 8 g kg^{-1}, respectively on 9 December, while Durban's surface moisture remained at 12 g kg^{-1}.

Observations showed that when the upper-air winds have a southern component, gravity waves form to the north of the mountains (Terblanche, 1996). This can, even in unfavourable conditions, lead to the development of convective activity over the area where the supercell developed on the case day. On 9 December 1991 the upper-air wind over Bethlehem and Durban had a south-western component, while over Bloemfontein it had a due westerly component.

From the above analysis, a variety of composite soundings were compiled. These soundings were compiled through a combination of the following:
-       Smoothing the upper air inversion of the Bethlehem sounding.
-       Increased the moisture in the lower layers of the initializing sounding. This process produced a series of soundings all with their surface moisture 1 g kg^{-1} higher than the previous one, with the lowest value equal to 8 and the highest value equal to 11 g kg^{-1}.

- Durban's surface temperature was 2°C higher than Bethlehem's. The surface temperature of the initializing sounding was therefore increased by 1°C.
- Changing the direction of the wind to try to create gravity waves to the north of the mountains.

This process produced a vast number of soundings that could be used to initialize the model with (these soundings are not shown). Unfortunately, regardless with which sounding the model was initialized with, the final results did not change dramatically. The only clear difference noted during these runs, was that a higher surface moisture value resulted in slightly deeper cloud development. This difference was not significant and the clouds still did not develop over the right area nor did they develop into bigger longer-living clouds (these results are not shown).

The above process was a long and slow one. When running a detailed mesoscale model operationally, this process will be to time consuming and there will also be no way of predicting which composite sounding is going to produce the correct results. Even if this process could somehow be used operationally, it has been proven conclusively that the model results will more than likely not improve, even if a well-compiled composite sounding is used. The only alternative to improving the model results is to initialize the model with large scale data.

5.5 Summary

The Clark model was used to predict the development of a severe hail producing supercell that developed to the east of Bethlehem on 9 December 1991. Apart from this supercell, there was no significant convective activity that developed over the BPRP area that day.

The model predicted the general convective conditions of this day very accurately, but failed to predict the development of the severe supercell. It was argued that if the trigger mechanism responsible for the development of this supercell was only visible

108

in the airmass in the immediate vicinity of this storm, the model would not have been able to predict its development since it was initialize with a sounding taken at Bethlehem.

In order to try to improve the model results, the model was initialized with a series of composite soundings compiled from the soundings taken at Bloemfontein, Bethlehem and Durban. This made no difference to the model results and the model still failed to predict the development of the severe supercell. Due to the time involved in compiling composite soundings and running the model, this route cannot be followed in an operational programme. Even if this was possible, this study proved that improved results cannot be guaranteed. This leads to the conclusion that the only possible route to improved model predictions would be to initialize the model with large scale data.

Fig. 5.1   Synoptic weather map for 12:00 UT, 8 December 1991
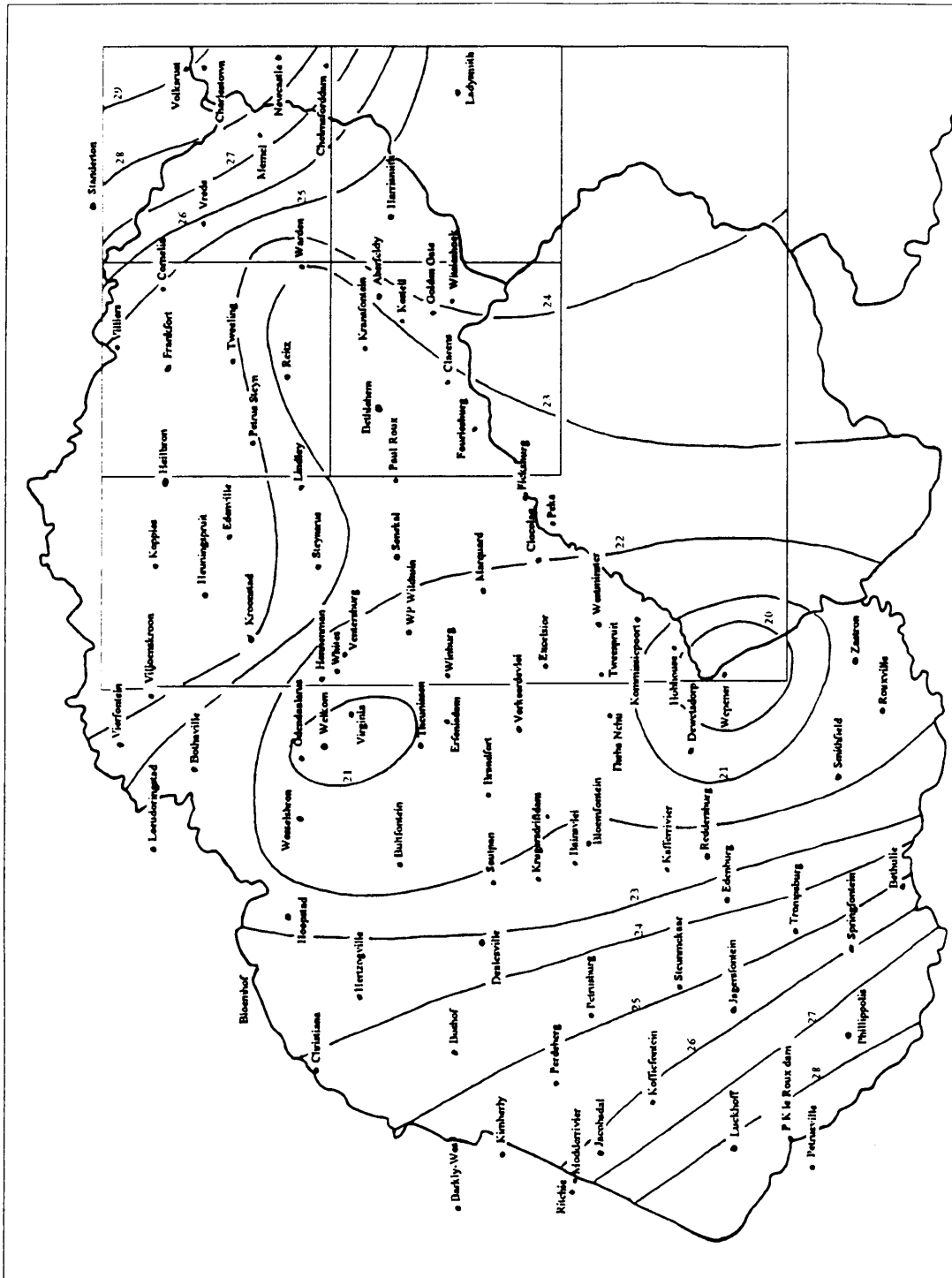
Fig. 5.2 Maximum temperature map for the Free State, 8 December 1991

111
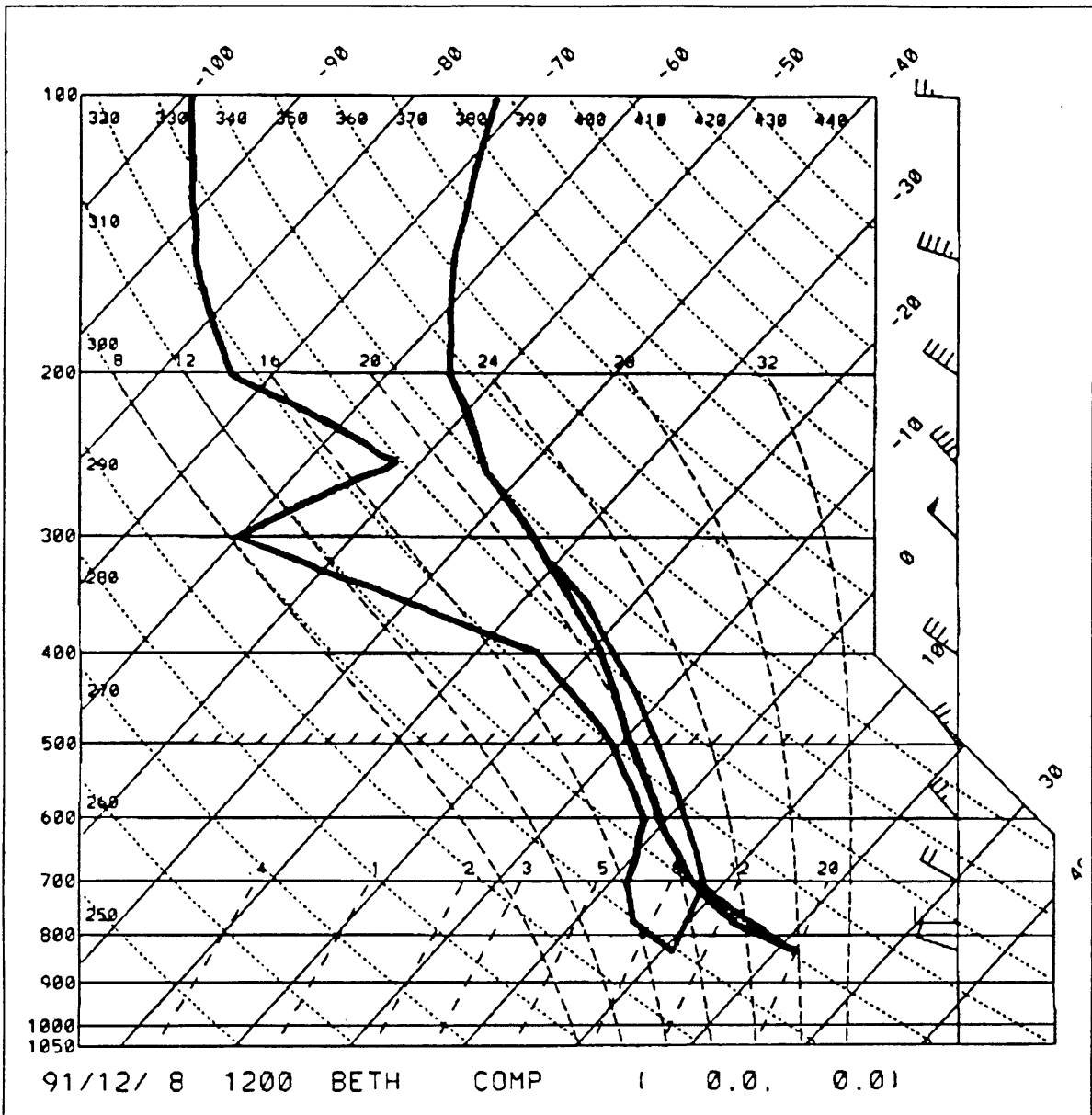
Fig. 5.3   Bethlehem sounding for 12:00 UT, 8 Decmber 1991

113

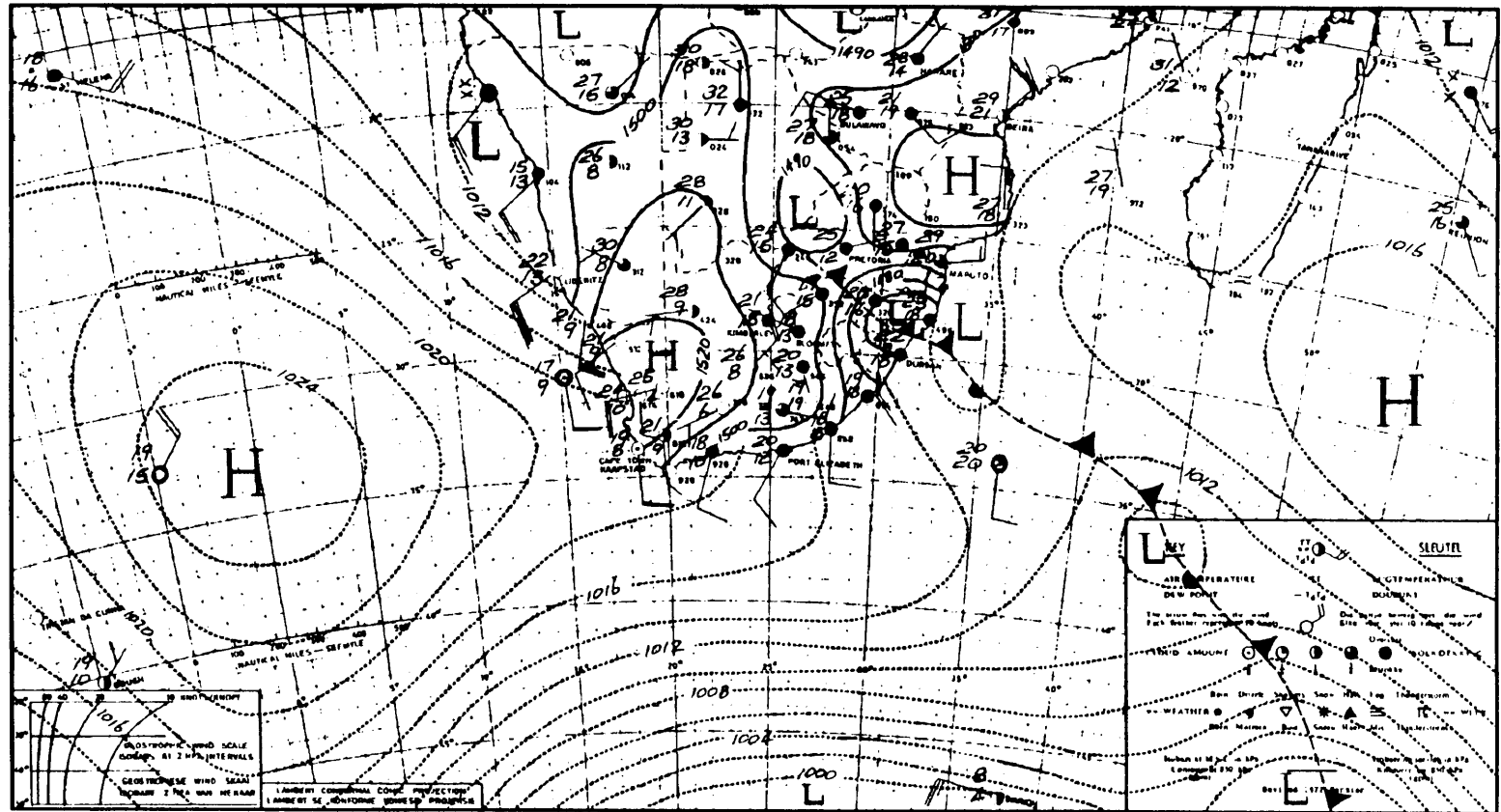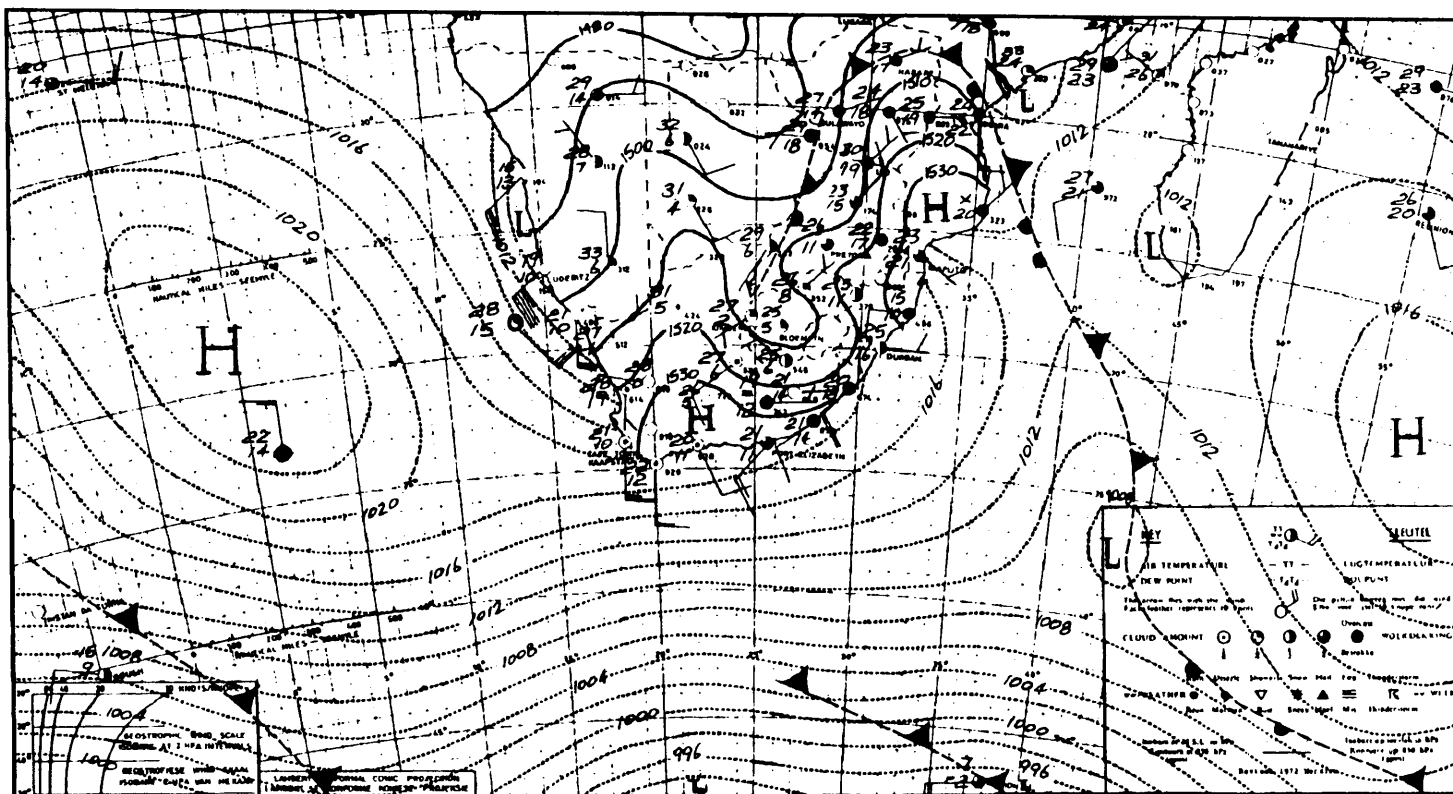
Fig. 5.4   Synoptic weather map for 12:00 UT, 9 December 1991
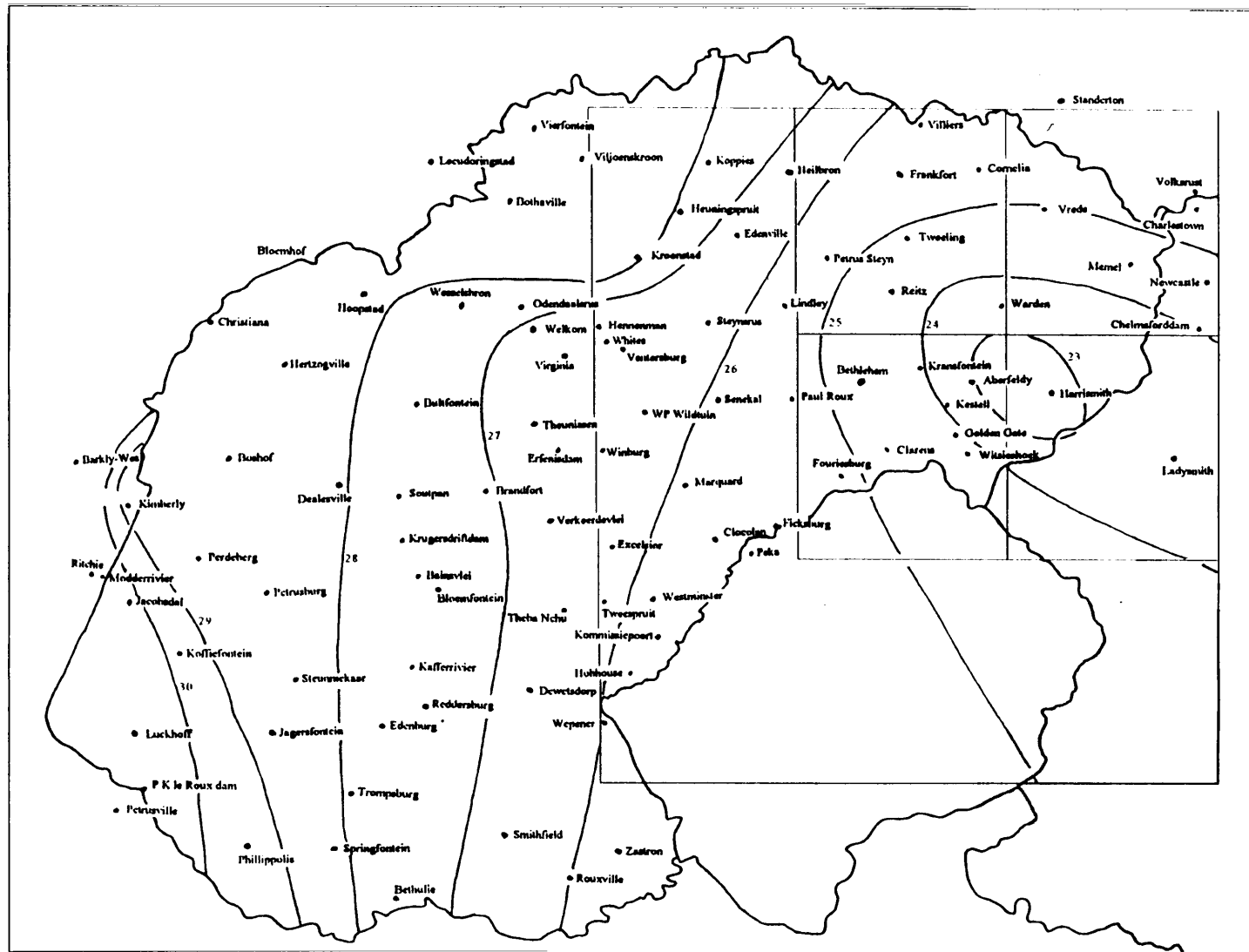
Fig. 5.5   Maximum temperature map for the Free State, 9 December 1991
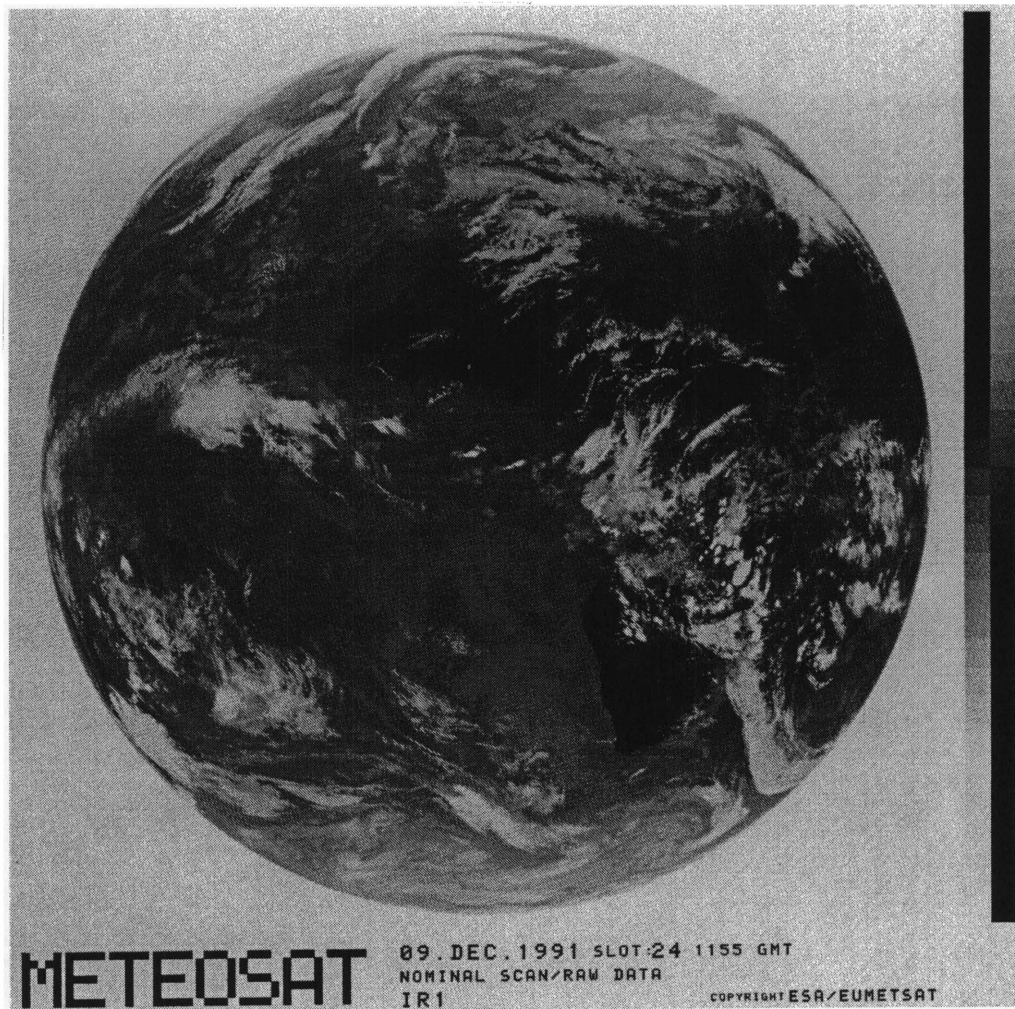
Fig. 5.6   Meteosat image for 11:55 UT, 9 December 1991

115
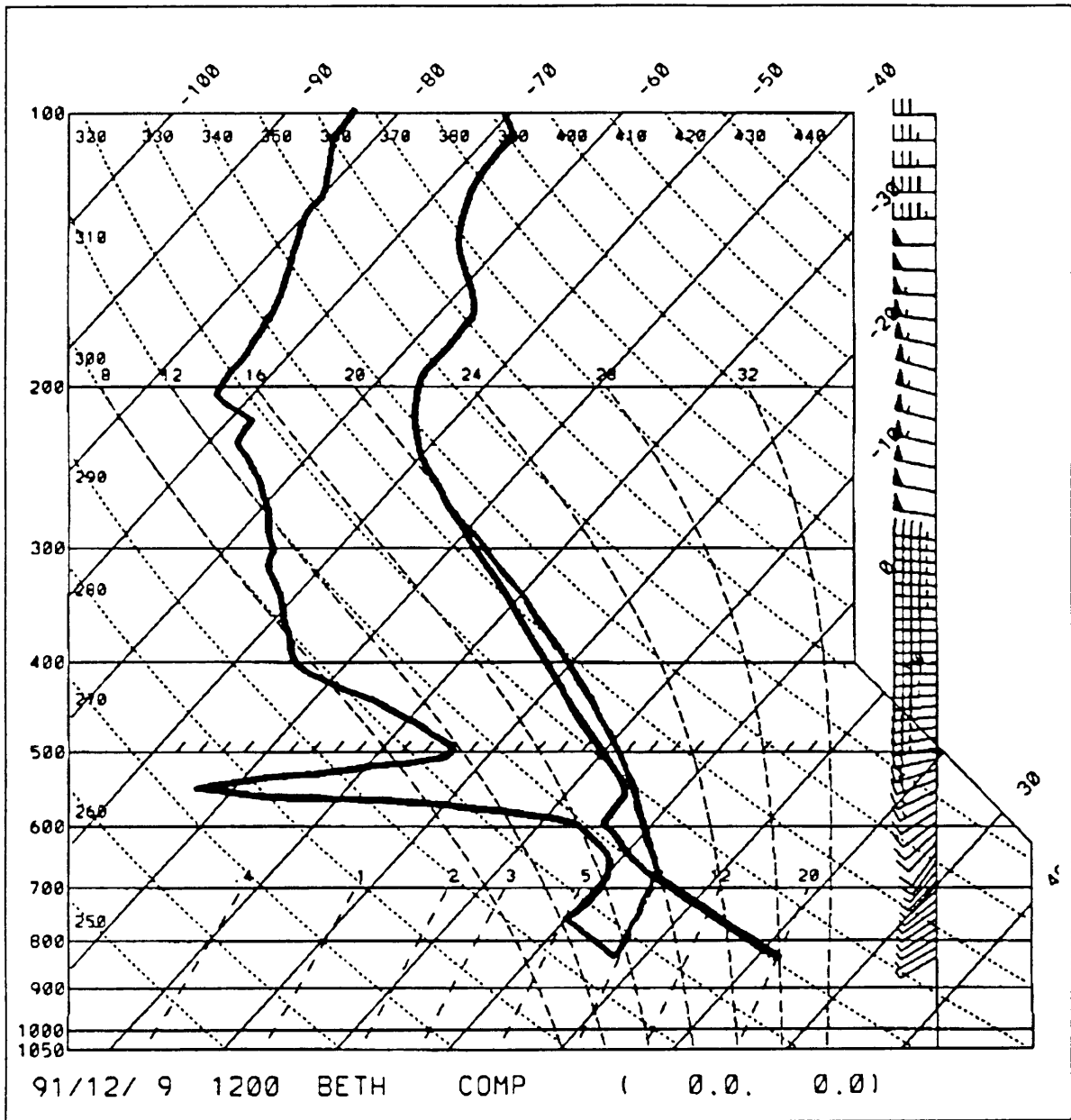
Fig. 5.7　　　Bethlehem sounding for 12:00 UT, 9 December 1991

116

117

BETHLEHEM RADAR — RAIN RATE (MM/H)

Kilometers S-N

1-3
3-6
6-9

12-15
15 <

9-DEC- 91 15:22

Kilometers W-E

BETHLEHEM RADAR — RAIN RATE (MM/H)

Kilometers S-N

1-3
3-6
6-9

12-15
15 <

9-DEC- 91 15:47

Kilometers W-E
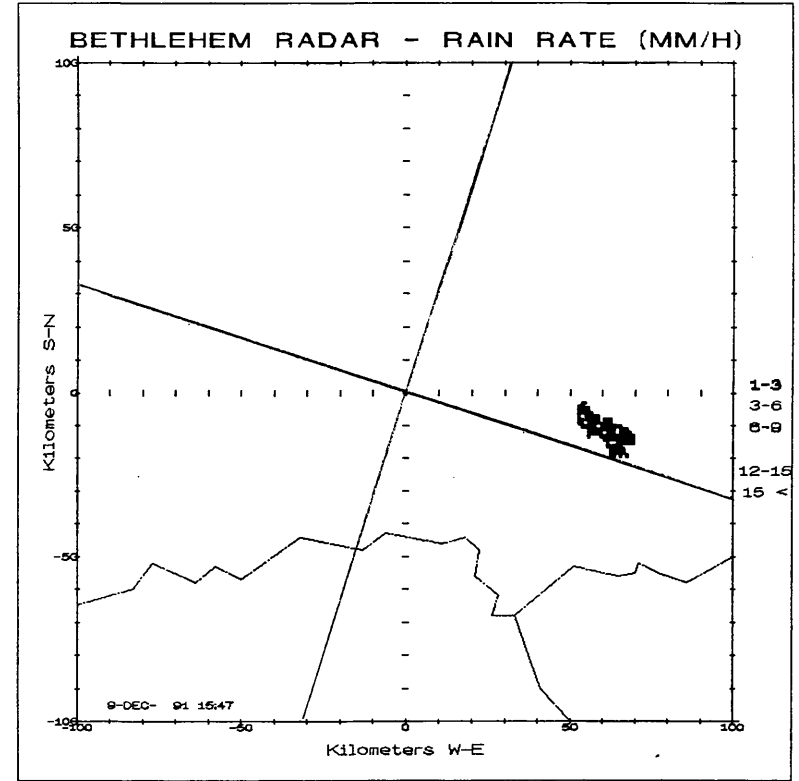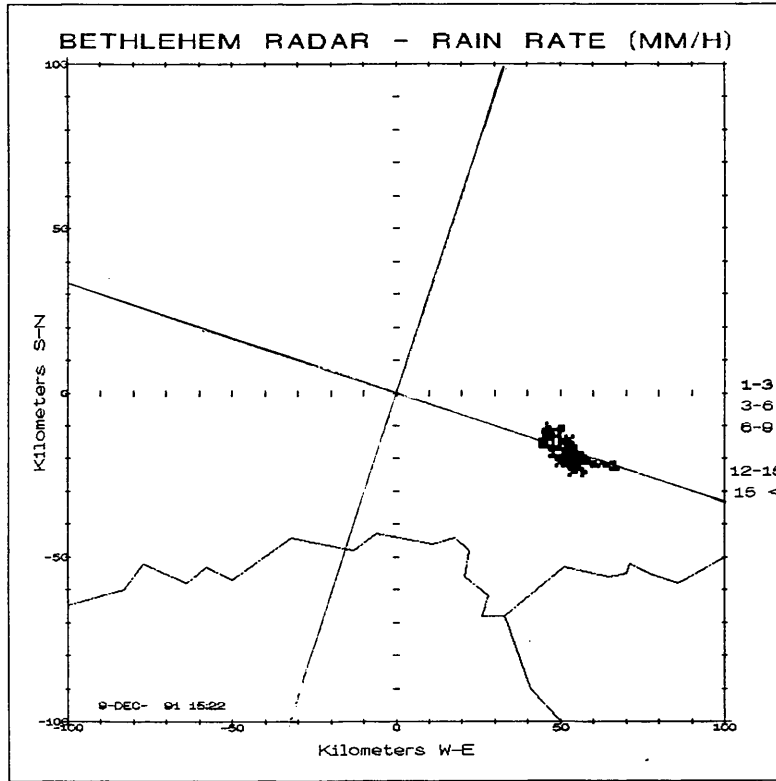
Fig. 5.8a,b   Radar-rain-rate over the Bethlehem area for 9 December 1991 (15:22 and 15:47 SAST)

BETHLEHEM RADAR – RAIN RATE (MM/H)

BETHLEHEM RADAR – RAIN RATE (MM/H)
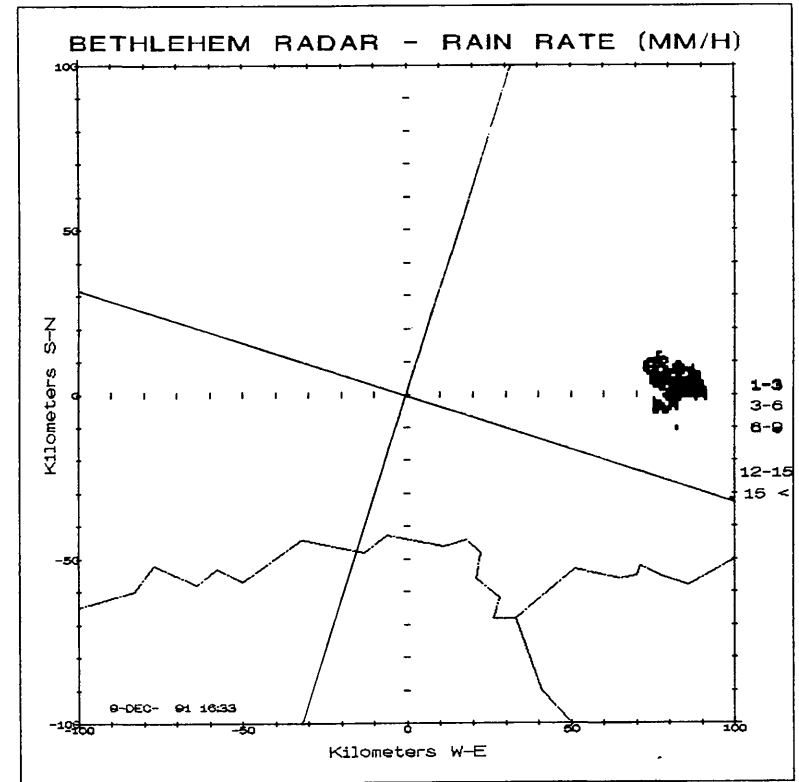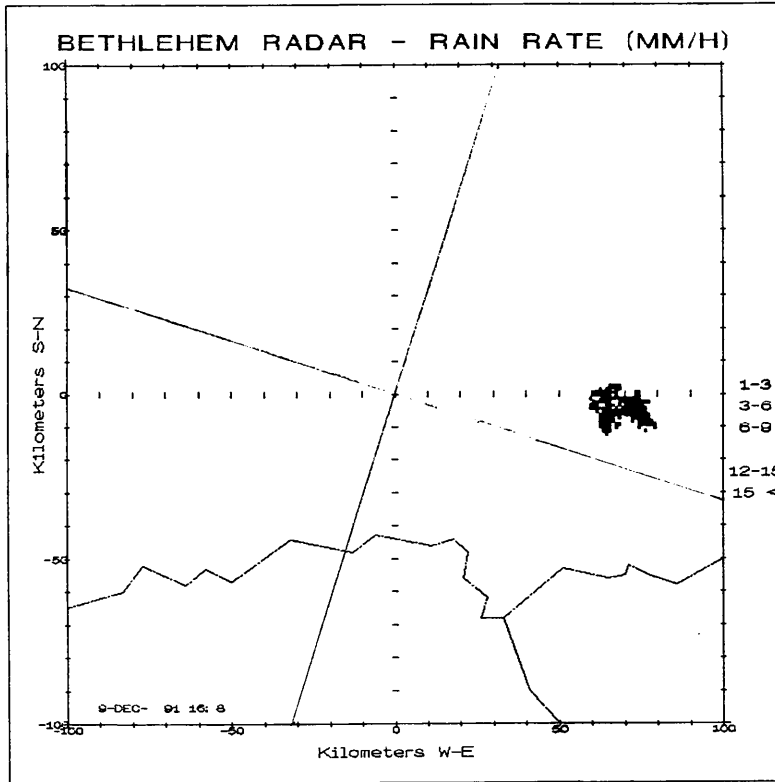
Fig. 5.8c,d   Radar-rain-rate over the Bethlehem area for 9 December 1991 (16:06 and 16:33 SAST)

STORM TRACKS.

DATE   911209
SEQUENCE #   33
PERSISTENCE :   5
MAX SPEED   :   90
MAX TIME INT :   30
DBZ THRESHOLD :   30

Kilometers S-N

Kilometers W-E
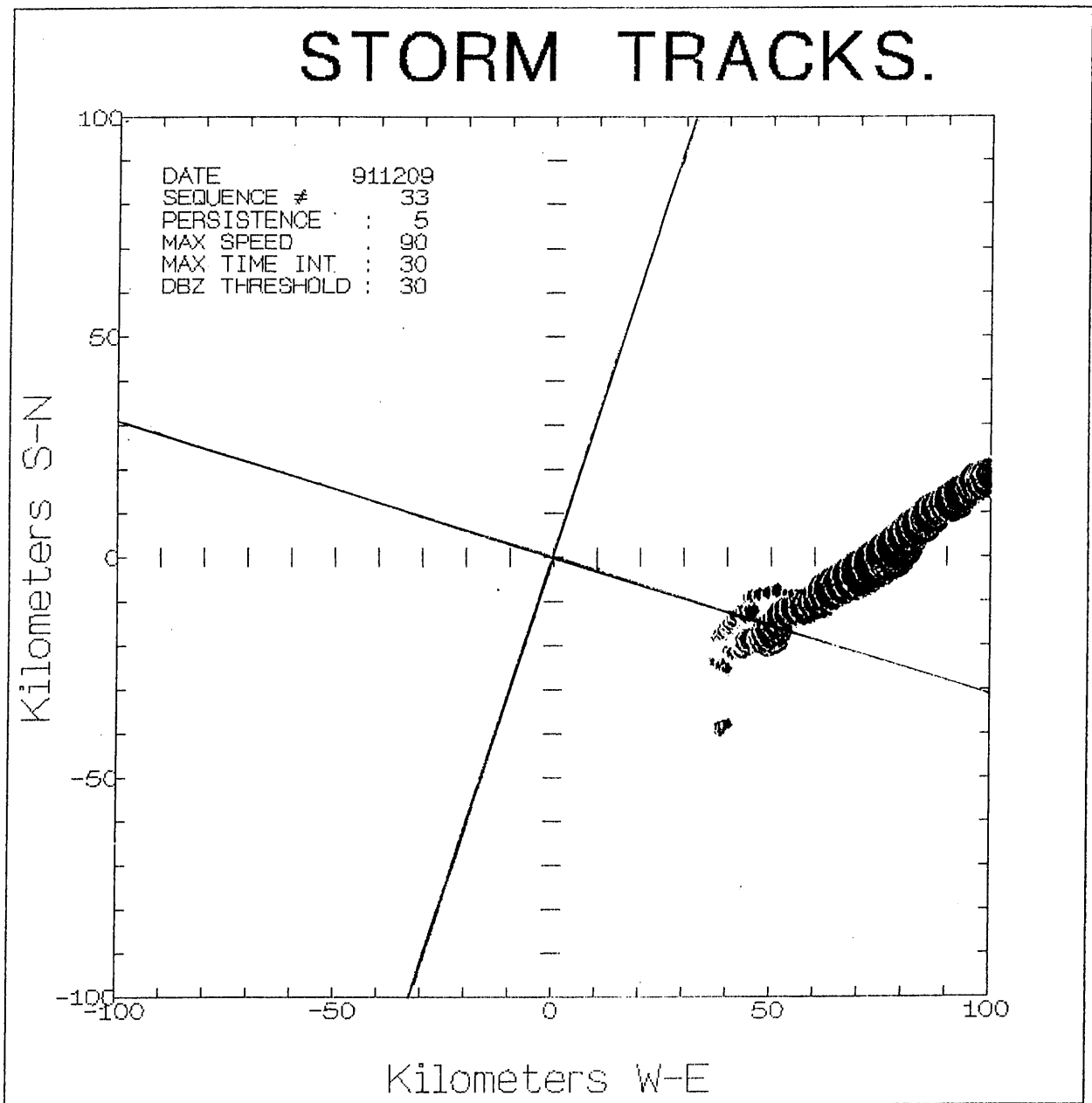
Fig. 5.9   Radar storm track of the supercell storm of 9 December 1991

119
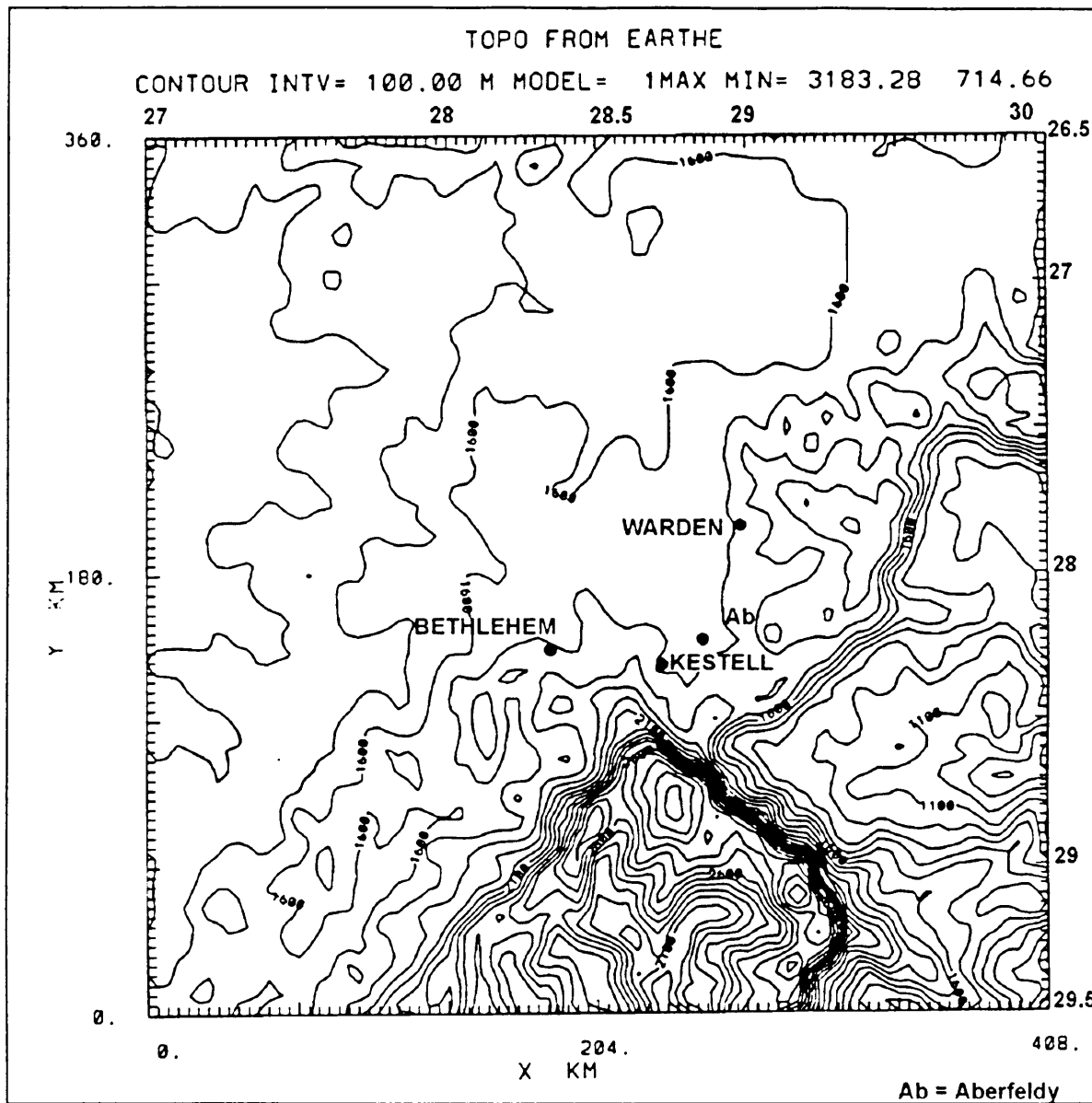
Fig. 5.10 A 360 x 360 km, two-dimensional topography plot of the model domain over the Bethlehem area.

120
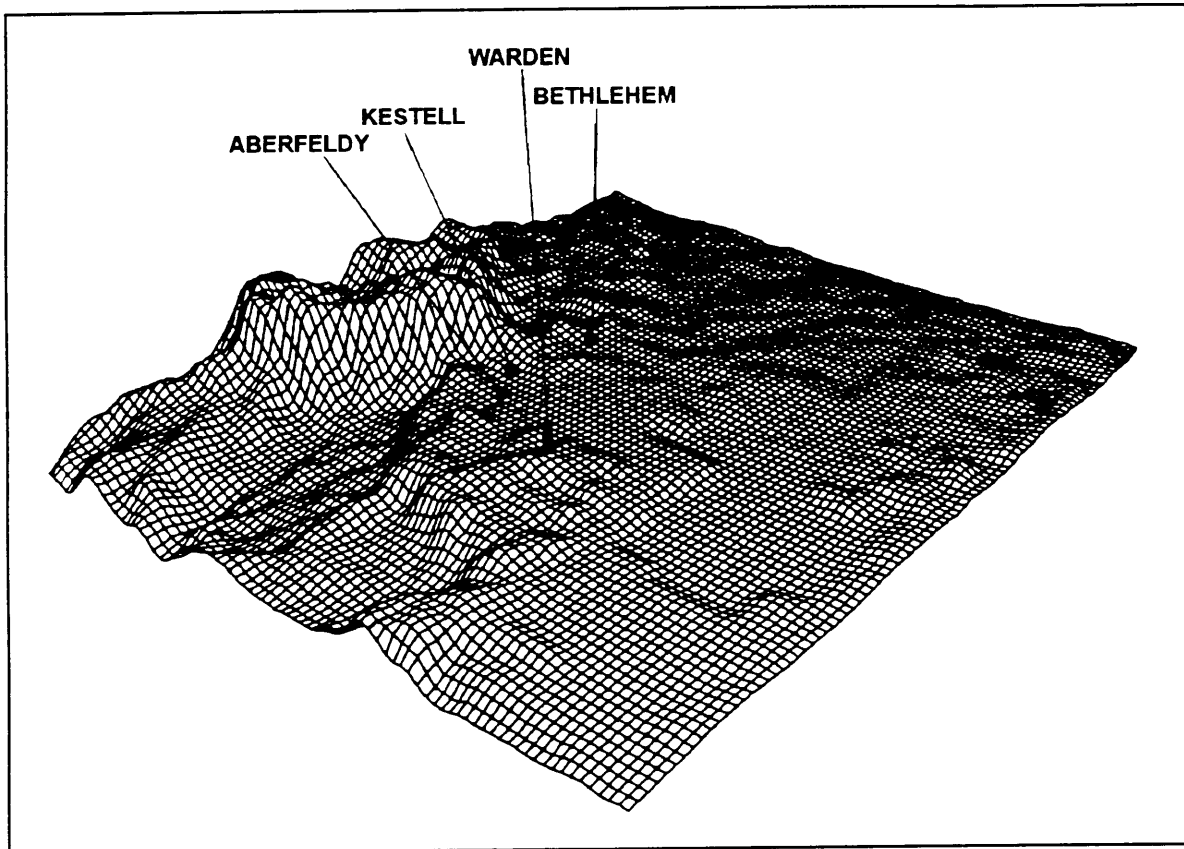
Fig. 5.11   A 360 x 360 km, three-dimensional topography plot of the model
domain over the Bethlehem area.

121

VALUES.GE. 0.1000E+00 AT TIME= 105.00MIN
QR FIELD (GR/KG)

VALUES.GE. 0.1000E+00 AT TIME= 120.00MIN
QR FIELD (GR/KG)

N◄

N◄

Fig. 5.12a,b Three-dimensional model generated rain water mixing ratio fields, as viewed from the north-east, after 105 and
120 minutes of simulation (15:45 and 16:00 SAST). Values shown are for rain water mixing ratios greater or equal
to 0.1 g kg^{-1} (basic model run)

VALUES.GE. 0.1000E+00 AT TIME= 135.00MIN
QR FIELD (GR/KG)

VALUES.GE. 0.1000E+00 AT TIME= 150.00MIN
QR FIELD (GR/KG)

N◄

N◄

Fig. 5.12c,d   Three-dimensional model generated rain water mixing ratio fields, as viewed from the north-east, after 135 and 150 minutes of simulation (16:15 and 16:30 SAST). Values shown are for rain water mixing ratios greater or equal to 0.1 g kg⁻¹ (basic model run)

124

VALUES.GE. 0.1000E+0⦁ AT TIME= 105.00MIN
CLOUD ICE -B- MIX|NG RATIO (G/KG)

VALUES.GE. 0.1000E+0⦁ AT TIME= 120.00MIN
CLOUD ICE -B- MIX|NG RATIO (G/KG)

N◀

N◀
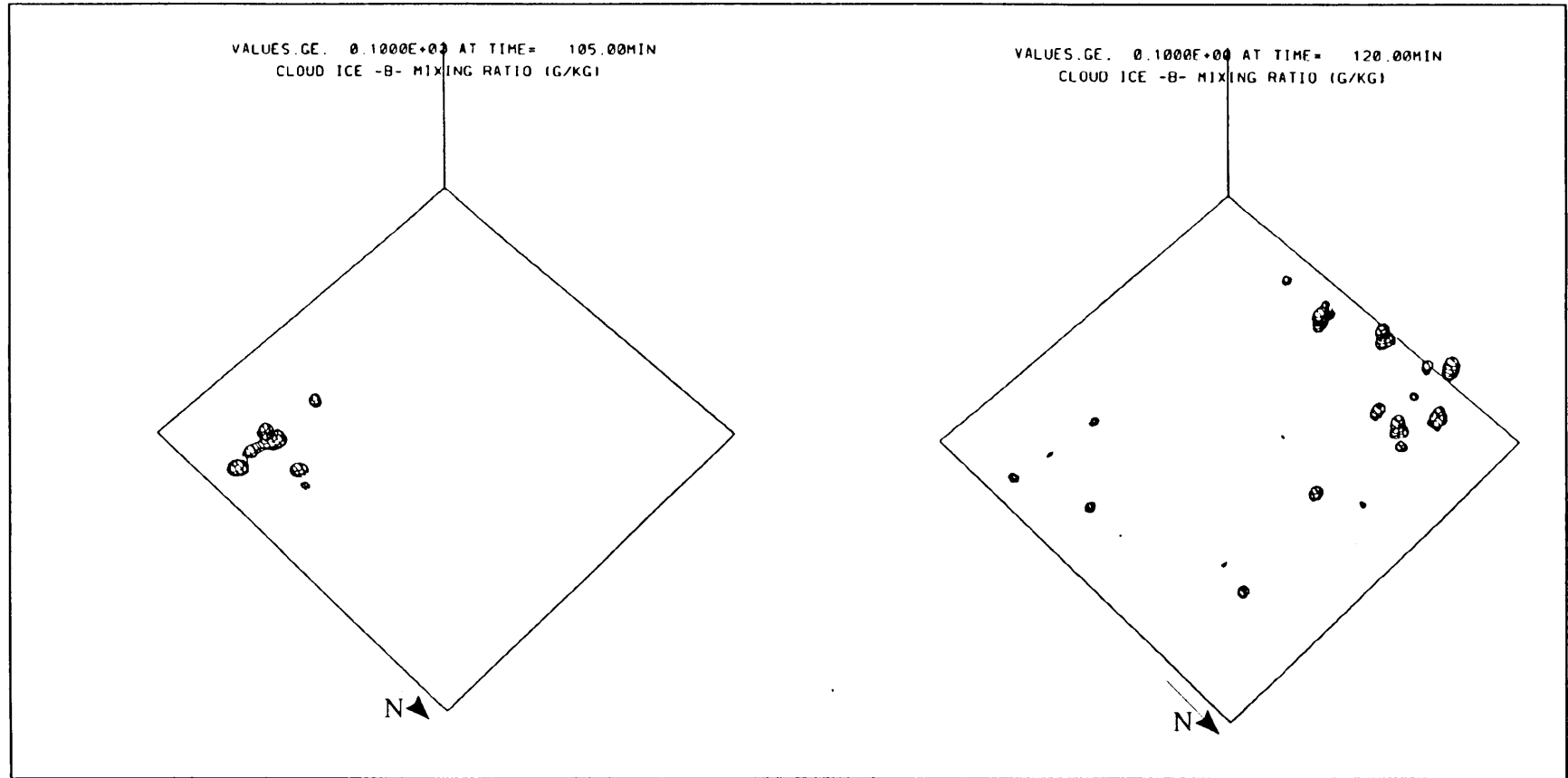
Fig. 5.13a,b   Three-dimensional model generated graupel mixing ratio fields, as viewed from the north-east, after 105 and 120 minutes of simulation (15:45 and 16:00 SAST). Values shown are for graupel mixing ratios greater or equal to 0.1 g kg⁻¹ (basic model run)

VALUES.GE. 0.1000E+00 AT TIME= 135.00MIN
CLOUD ICE -B- MIXING RATIO (G/KG)

VALUES.GE. 0.1000E+00 AT TIME= 150.00MIN
CLOUD ICE -B- MIXING RATIO (G/KG)

N◀

N◀
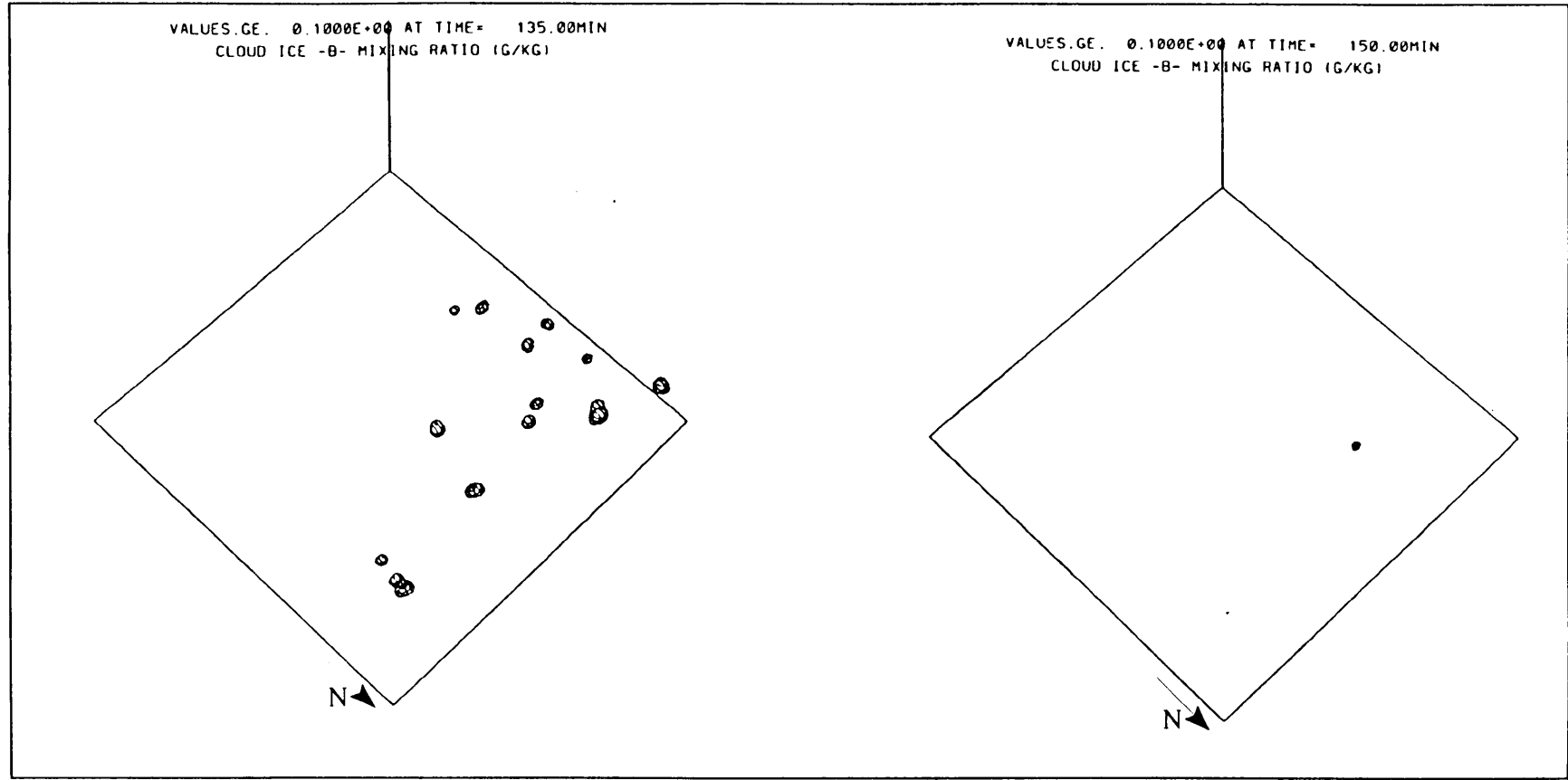
Fig. 5.13c,d   Three-dimensional model generated graupel mixing ratio fields, as viewed from the north-east, after 135 and 150 minutes of simulation (16:15 and 16:30 SAST). Values shown are for graupel mixing ratios greater or equal to 0.1 g kg⁻¹ (basic model run)

Chapter 6

Conclusions and Recommended Future Research

The purpose of this dissertation was twofold: 1) To study the possible usage of a mesoscale model as a tool in the South African precipitation research programme and thereby increasing the mesoscale modelling expertise in South Africa and 2) To study the dynamical and physical aspects of severe hail producing thunderstorms over the Free State.
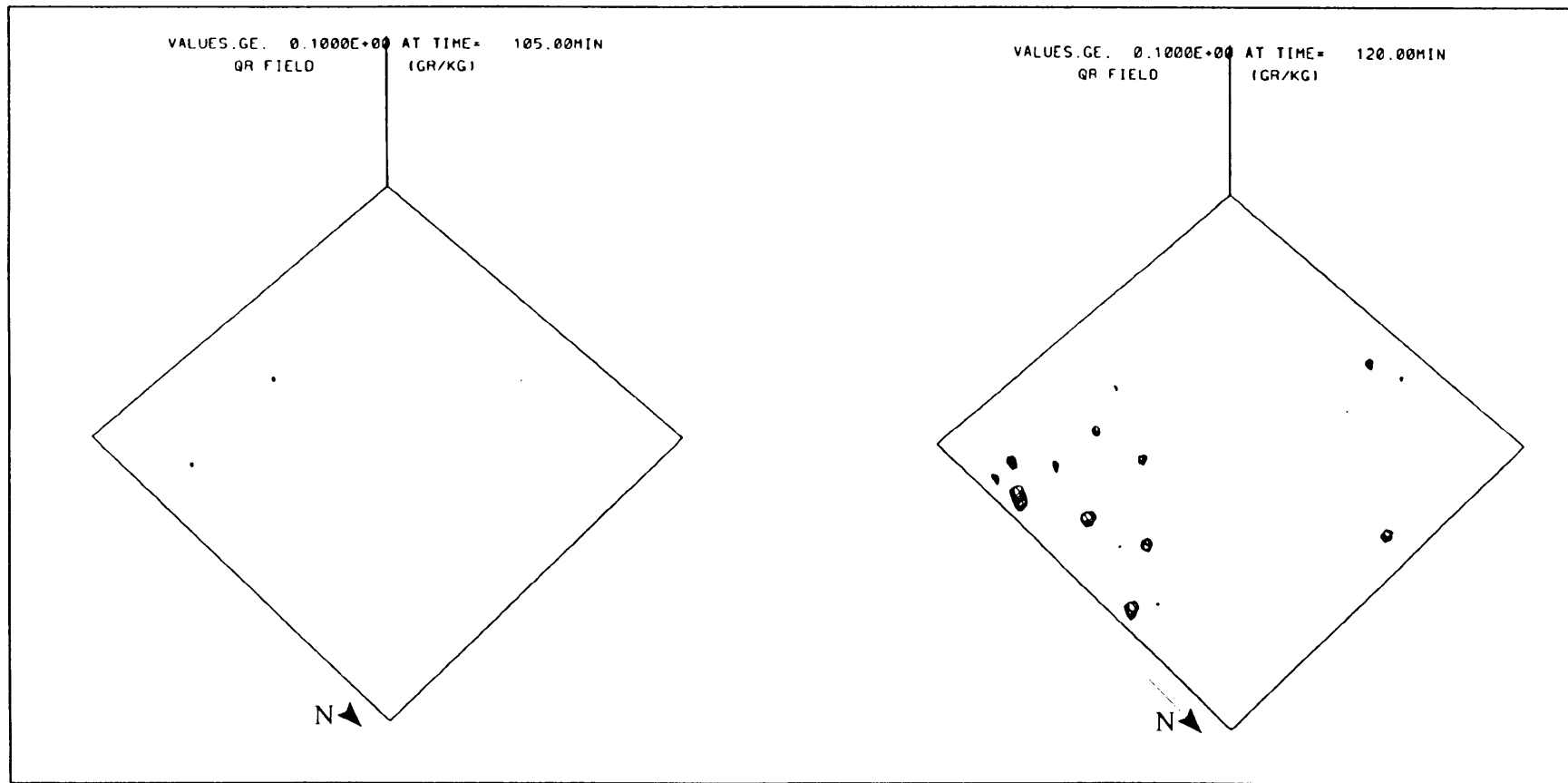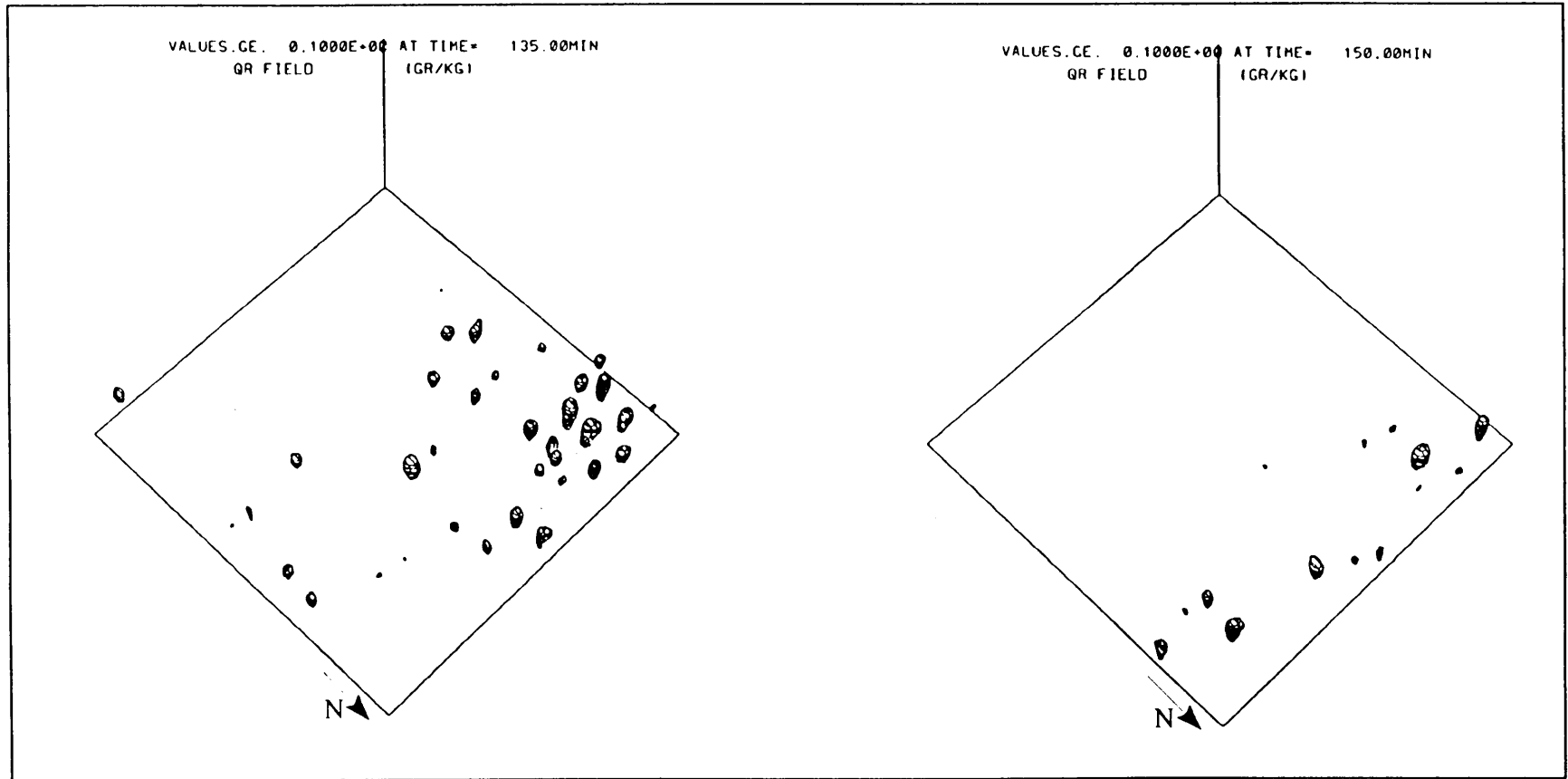
1. Precipitation research, with a view to rainfall augmentation, especially in a drought stricken country like South Africa is an attractive option as a source of good quality water. Numerical models can be useful tools in these programmes to help investigate the complicated interactions between the dynamical, microphysical and thermodynamical processes in clouds. They can also be of great benefit to better understand the outcome of cloud seeding activities. Since detailed mesoscale models can depict both the seeded and unseeded outcomes of any particular case, they can play a valuable role in the formation of a seeding hypothesis.

2. Annually hail causes millions of Rand of damage to livestock, crops and property in South Africa. It is therefore essential that studies into this phenomena be conducted, especially in an area like the Free State, where major farming activities and a high incidence of hail occurrences coincide.

126

6.1 Conclusions of this dissertation

The Clark mesoscale cloud model was chosen in an attempt to find answers to both the above objectives. Since the Clark model has only been used once in a study over South Africa, this dissertation serves as a first step to try to establish the usefulness of this model over the project area for the chosen purposes.

In this study the modelling results were evaluated by making use of actual radar data. This is not a common route followed by modellers, but radar data combined with mesoscale modelling results are crucial to a better understanding of cloud fields and the effect seeding has on them.

The study was successful in that it not only proved that the model has the potential to be used over this area, but it also pointed out areas where further research will be needed. Areas where caution is needed when using the model in its current status, are also addressed.

The model predicted the severe multicell storm of the 24 November 1992 over the Bethlehem area timeously and accurately. It succeeded in capturing the majority of the dynamical and physical aspects associated with this particular storm. A shortcoming experienced during this case study was that the model failed to precipitate the graupel that developed. This is a recognized problem that is going to require more research in order to establish a workable ice parameterization scheme able to simulate the ice phase in South African storms more accurately.

For this case study two major sensitivity studies were also done and it was established that:

- The surface heating played a major role in controlling the initial time of development as well as the lifetime of these storms. It also, to some extent, controls the detail development.

127

-       The topography controls the area of preferred development and the movement of the storms, while the steepness of the topographical gradients controls the intensity and the definition of the developed storm.

The model failed to predict the severe supercell that developed over the BPRP area on 9 December 1991. This day was unique in the sense that, except for the solitary supercell that brought hail to the farming community to the east of Bethlehem, no other convective activity took place over the area that day. The model simulation for that day predicted no major convective activity. From this point of view the model did not fail, since it did manage to predict the general convective conditions, or lack there of, which were characteristic of that day. It only failed as far as not developing the solitary supercell to the east of Bethlehem.

It was reasoned that the air mass responsible for the development of the supercell might never have moved over the Bethlehem area. It would therefore be impossible for the model to simulate this storm, if the trigger mechanism responsible for the development of the storm was not visible in the sounding used to initialize the model. Consequently, a series of composite soundings compiled from soundings taken at Bloemfontein, Bethlehem and Durban, were used to initialize the model. This is not the route that will be taken in an operational programme, but it had to be followed in order to prove, either way, the merit of this process. During this study it was proven conclusively that this is not the approach to take. This leaves only one alternative - to initialize the model with large scale data. During large scale initialization, the model will be initialized with a number of soundings throughout the model domain. Thus, greatly improving the probability that local trigger mechanisms responsible for the development of severe storms will be detected by the model. This is outside the scope of the dissertation, but is a definite future research area.

If the Clark model is to be used in the South African rainfall stimulation research programme, it must be able to accurately simulate a wide range of mesoscale conditions over the project area. The purpose of this dissertation was to attempt to

establish if the Clark model could do this. The model accurately simulated the severe multicell storm of 24 November 1992. In doing so it proved that it is capable of simulating extreme cases. This also suggested that it might be capable of simulating more general, everyday mesoscale conditions. The model also accurately simulated the general mesoscale conditions of 9 December 1991. This proved the assumption, that if the model could predict severe conditions, it would also be able to predict more general conditions. The model failed to predict the severe supercell storm that developed on 9 December 1991. Pointing out, that if a severe storm's trigger mechanism is not visible in the initializing sounding, the model will not be able to simulate the development of such a storm.

In summary - the model, in its current status, is capable of accurately simulating general mesoscale conditions over the project area. The ice parameterization scheme and large scale initialization are areas identified where future improvements can be made to the model. Once this is done, more accurate and usable results will surely be obtained. This would be very valuable to the rainfall stimulation programme. It would also provide a tool that can be used to conduct research into severe weather activities any where in South Africa.

6.2   Recommended future research

After the model processes concerning better ice-phase parameterization and model initialization have been addressed the following studies are recommended for future research:

a.   Severe weather simulations

With the aid of a mesoscale model we can add to our understanding of the development and movement of storms. By doing numerical simulations of cumulus complexes the complicated interactions between microphysical and dynamical processes in clouds can be studied. In turn, this expertise can be utilized to study,

129

and ultimately predict, the development and movement of severe storms over any location in South Africa.

b.   The design of precipitation research experiments

Mesoscale models can be used to help with the development of a seeding hypothesis. The model can also be utilized to assist in the developing of methods for rainfall stimulation and to try to find the conditions that will optimize the treatment. In other words, the model can be used to find answers to questions concerning seeding location, seeding time, seeding amount, etc.

Decision making in the rainfall stimulation project is an involved process and it is not possible for an individual to take all the factors into account. Models have the potential to predict the factors needed to make decisions, since they are able to predict where and when convective activity will take place.

In South Africa precipitation research is not restricted to one area. The model can therefore be used to evaluate the "seedability" of a given cloud or cloud type or even a collection of clouds in any geographical region.

Precipitation research in South Africa is moving towards an area experiment. In such a case it is important to study the effect seeding will have on an entire cloud field - i.e., to study the effect cloud seeding will have on the distribution of precipitation over an area. To find out if the seeding of individual clouds can establish a more favourable environment to facilitate the development of successive generations of clouds or result in the suppression/enhancement of neighbouring clouds.

It is also desirable to seed clouds as soon as possible. Thus, especially in an area experiment it is becoming more and more important to be able to predict the area of initial development since this will ensure that the biggest possible effect will be achieved.

130

c. The evaluation of precipitation research experiments

Mesoscale models are capable of accurately predicting effects like enhanced cloud growth, time of first echo development, lifetime of echoes, etc. These parameters can in turn be used in the statistical analysis of the field experiments. With the aid of a mesoscale model, days can be categorised according to their predicted reaction to modification, thus helping to stratify the data for analysis purposes.

In the current precipitation research project seeding takes place at cloud base. Measurements at -10°C level are then made to establish the effect of seeding. By preforming tracer experiments with the Clark model, it would be possible to study how the seeding material is advected into the cloud and to determine the size and position of the area effected by the seeding.

References

Abstract of Agricultural Statistics, 1996:. Department of Agricultural Economics and Marketing, Directorate of Agricultural Economic Trends, Pretoria, Republic of South Africa.

Atlas, D., R.C. Srivastava, and R.S. Sekhon, 1973: Doppler radar characteristics of precipitation at vertical incidence. *Rev. Geophys. Space Phys.*, **11**, 1 - 35.

Arakawa, A., 1966: Computational design for long-term numerical integration of the equations of fluid motion: Two-dimensional incompressible flow. Part I. *J. Comput. Phys.,* **1**, 119 - 143.

Balaji, V., and T.L. Clark, 1988: Scale selection in locally forced convective fields and the initiation of deep cumulus. *J. Atmos. Sci.*, **45**, 3188 - 3211.

Browning, K.A., 1962: Cellular structure of convective storms. *Met. Mag.*, **91**, 341-350.

Browning, K.A., and G.B. Foote, 1976: Airflow and hail growth in supercell storms and some implications for hail suppression. *Quarterly Journal of the Royal Meteorological Society*, **102**, 499 - 534.

Bruintjes, R.T., 1992: Observational and numerical studies of cloud and precipitation development with a view to rainfall enhancement, Ph.D dissertation, Univ. of South Africa, 181 pp.

Bruintjes, R.T., T.L. Clark, and W.D. Hall, 1994: Interactions between topographic airflow and cloud/precipitation development during the passage of a winter storm in Arizona. *J. Atmos. Sci.*, **51**, 48 - 67.

Bruintjes, R.T., T.L. Clark, and W.D. Hall, 1995: The dispersion of tracer plumes in mountainous regions in central Arizona: Comparisons between observations and modelling results. *J. Appl. Meteor*, **34**, 971 - 988.

132

Carte, A.E., 1965: Hailstorms in South Africa. *South African Weather Bureau Newsletter*, 1965, 58 - 61.

Carte, A.E., 1966a: Hail Studies in South Africa 1962 - 1966. *South African Weather Bureau Newsletter*, 1966, 151 - 155.

Carte, A.E., 1966b: Features of Transvaal hailstorms. *Quarterly Journal of the Royal Meteorological Society*, **92**, 290 - 296.

Carte, A.E., 1979: Sustained storms on the Transvaal Highveld. *South African Geographical Journal*, **61**, 39 - 56.

Carte, A.E., 1980: Some comparisons between hailstorms on the Transvaal Highveld and those elsewhere. *Proceedings of the 8th International Conference on Cloud Physics*, Clermont Ferrand, France, 473 - 476.

Carte, A.E., 1981: Morphology of persistent storms in the Transvaal on 16/17 October, 1978. *Beitrage zur Physik der Atmosphare*, **54**, 86 - 100.

Carte, A.E., and I.L. Basson, 1970: Hail in the Pretoria-Witwatersrand area 1962-1969. *CSIR Research Report 293*, CSIR, Pretoria, 28 pp.

Carte, A.E., and G. Held, 1972: Hailstorms in 1970/71. *CSIR Research Report 312*, CSIR, Pretoria, 1 - 45.

Carte, A.E., and G. Held, 1978: Variability of hailstorms on the South African Plateau. *J. Appl. Meteor.*, **17**, 365 - 373.

Carte, A.E., and G.N. Mader, 1977: Hailstorms in the Transvaal on 29 November 1972. *Quarterly Journal of the Royal Meteorological Society*, **103**, 731 - 749.

Chisholm, A.J., and J.H. Renick, 1972: Supercell and multicell Alberta hailstorms. *International Cloud Physics Conference*, London, August 1972.

Clark, T.L., 1977: A small-scale dynamic model using a terrain-following coordinate transformation. *J. Comput. Phys.*, **24**, 186 - 215.

Clark, T.L., 1979: Numerical simulations with a three-dimensional cloud model: Lateral boundary condition experiments and multicellular severe storm simulations. *J. Atmos. Sci.,* **36**, 2191 - 2215.

Clark, T.L., and R.D. Farley, 1984: Severe downslope windstorm calculations in two and three spatial dimensions using anelastic interactive grid nesting: A possible mechanism for gustiness. *J. Atmos. Sci.,* **41**, 329 - 350.

Clark, T.L., and R. Gall, 1982: Three-dimensional numerical model simulations of airflow over mountainous terrain: A comparison with observations. *Mon. Wea. Rev.,* **110**, 766 - 791.

Clark, T.L., and W.D. Hall, 1991: Multi-domain simulations of the time dependent Navier Stokes equations: Benchmark Error analyses of nesting procedures. *J. Comput. Phys.,* **92**, 456 - 481.

Clark, T.L., W.D. Hall, and R.M. Banta, 1994: Two- and three-dimensional simulations of the 9 January 1989 severe Boulder windstorm: Comparison with observations. *J. Atmos. Sci.,* **51**, 2317 - 2343.

Clark, T.L., T. Hauf, and J.J. Kuettner, 1986: Convectively forced internal gravity waves: Results from two-dimensional experiments. *Quart. J. Roy. Meteor. Soc..* **112**, 899 - 925.

Cosgrove, C., 1986: Climatology of the North-eastern Orange Free State. *Bethlehem Weather Modification Experiment,* Progress Report No 28, South African Weather Bureau, Pretoria.

Court, A.P., 1979a: The contribution of General Rain, Scattered Rain and Isolated Rain in the Bethlehem area. *Bethlehem Weather Modification Experiment,* Progress Report No 5, South African Weather Bureau, Pretoria.

Court, A.P., 1979b: Hail observations in the BEWMEX area. *Bethlehem Weather Modification Experiment,* Progress Report No 13, South African Weather Bureau, Pretoria.

Farley, R.D., and H.D. Orville, 1986: Numerical modeling of hailstorms and hailstone growth. Part I: Preliminary model verification and sensitivity tests., *J. Climate and Appl. Meteo.,* **25**, 2014 - 2035.

Gall, R.L., R.T. Williams, and T.L. Clark, 1987: On the minimum scale of fronts. *J. Atmos. Sci.*, **44**, 2562 - 2574.

Gall, R.L., R.T. Williams, and T.L. Clark, 1988: Gravity waves generated during frontogenesis. *J. Atmos. Sci.*, **45**, 2204 - 2219.

Garbowski, W.W., and T.L. Clark, 1991: Cloud-environment interface instability: Rising thermal calculations in two spatial dimensions. *J. Atmos. Sci.*, **48**, 527 - 546.

Garbowski, W.W., and T.L. Clark, 1993a: Cloud-environment interface instability. Part II: Extension to three spatial dimensions. *J. Atmos. Sci.*, **50**, 555 - 573.

Garbowski, W.W., and T.L. Clark, 1993b: Cloud-environment interface instability. Part III: Direct influence of environmental shear. *J. Atmos. Sci.*, **50**, 3821 - 3828.

Garstang, M., B.E. Kelbe, G.D. Emmitt, and W.B. London, 1987: Generation of convective storms over the Escarpment of Northeastern South Africa. *Monthly Weather Review*, **115**, 429 - 443.

Greenacre, M., and M. Pearce, 1979: Patterns of "General Rain" and "Scattered Rain" in the BEWMEX area 1961-1975. *Bethlehem Weather Modification Experiment*, Progress Report No 9, South African Weather Bureau, Pretoria.

Grosh, R.C., *et al*, 1990: , Programme for Atmospheric Water Supply. Phase 2 1987 - 1989. Volume 3: Radar data interpretation, cloud modelling and statistical considerations. Report to the Water Research Commission, Pretoria, March 1990.

Harrison, M.S.J., 1983: Rain day frequency and mean daily rainfall intensity as determinants of total rainfall over the Eastern Orange Free State. *Journal of Climatology*, **3**, 35 - 45.

Harrison, M.S.J., *et al*, 1978: Cloud physics section planning report 1977. *Bethlehem Weather Modification Experiment,* Progress Report No 6, South African Weather Bureau, Pretoria.

135

Hauf, T., and T.L. Clark, 1989: Three dimensional numerical experiments on convectively forced internal gravity waves. *Q.J. Roy. Meteor. Soc.*, **115**, 309 - 333.

Held, G., 1973: Ten years of hail observations in the Pretoria-Witwatersrand area. *Journal de Recherches Atmospheriques*, **7**, 185 - 197.

Held, G., 1974: Hail frequency in the Pretoria-Witwatersrand area during 1962 to 1972. *Pure and Applied Geophysics*, **112**, 765 - 776.

Held, G., 1977: 'n Somer waartydens min hael in the Pretoria-Witwatersrand gebied voorgekom het. *South African Weather Bureau Newsletter*, no 334, Weather Bureau, Pretoria.

Held, G., 1978: The probability of hail in relation to radar echo heights on the South African Highveld. *J. Appl. Meteor.*, **17**, 755 - 762.

Held, G., and A.E. Carte, 1973: Thunderstorms in 1971/72. *CSIR Research Report 322*, CSIR, Pretoria.

Held, G., and A.E. Carte, 1979: Hailstorms in the Transvaal during January 1975. *South African Geographical Journal*, **61**, 128 - 142.

Heymsfield, A.J., and L.M. Miloshevich, 1993: Homogeneous ice nucleation and supercooled liquid water in orographic wave clouds. *J. Atmos. Sci.,* **50**, 2335 - 2353.

Hudak, D., 1988: Summertime weather and its predictability in the eastern Orange Free State. *S A Journal of Science*, **84**, 39 - 44.

Hudak, D., and D. Smith, 1980: Climate statistics of the BEWMEX area: A review with emphasis on the 1977/78 season. *Bethlehem Weather Modification Experiment,* Progress Report No 18, South African Weather Bureau, Pretoria.

Hudak, D., and P.C.L. Steyn, 1980: Forecasting in the BEWMEX area. *Bethlehem Weather Modification Experiment,* Progress Report No 19, South African Weather Bureau, Pretoria.

Hughes, P., and R. Wood, 1993: Hail: The white plague, *Weatherwise*, **46**, 16 - 21.

Kelbe, B.E., 1984: Cumulus cloud characteristics of the Eastern Transvaal Lowveld. *Water SA*, **10**, 81 - 90.

Kelbe, B.E., and J.M. De Jager, 1986: Analysis of the synoptic and mesoscale factors influencing convection in the Orange Free State. Document 7.4, University of the Orange Free State, Bloemfontein, 93 pp.

Kessler, E., 1969: On the distribution and continuity of water substance in atmospheric circulations. *Meteor. Monogr., 32,* Amer. Meteor. Soc., 84 pp.

Koenig, L.R., 1972: Parameterization of ice growth for numerical calculations of cloud dynamics. *Mon. Wea. Rev.,* **100**, 417 - 423.

Koenig, L.R., and F.W. Murray, 1976: Ice-bearing cumulus clouds evolution: Numerical simulation and general comparison against observations. *J. Appl. Meteor.,* **15**, 747 - 762.

Lilly, D.K., 1962: On the numerical simulation of buoyant convection. *Tellus*, **14**, 148 - 172.

Mader, G.N., 1979: Numerical studies of storms in the Transvaal. *South African Geographical Journal*, **61**, 86 - 98.

Mader, G.N., H. Neishlos, M.M. Saunders, and A.E. Carte, 1986: Some characteristics of storms on the Transvaal Highveld. *Journal of Climatology*, **6**, 173 - 182.

Mather, G.K., 1977: An analysis of a possible crop response to hail suppression seeding: The Nelspruit Hail Suppression Project. *J. Appl. Meteor.*, **16**, 959 - 970.

Mather, G.K., E.K. Bigg, and S. Renton, 1990: Apparent persistence effects in the Nelspruit area from silver iodide seeding for hail suppression. *J. Appl. Meteor.*, **24**, 806 - 811.

Mather, G.K., and D.E. Terblanche, 1993: The National Precipitation Research Programme, Final report 1990 - 1992, Report to the Water Research Commission, Pretoria, March 1993.

Mather, G.K., D. Treddenick, and R. Parsons, 1976: An observed relationship between the height of the 45 dBZ contours in storm profiles and surface hail reports. *J. Appl. Meteor.*, **15**, 1336 - 1340.

Obasi, G.O.P., 1995: Water resources management in Southern Africa - A vision for the future. *Conference of SADC (SOUTH AFRICA Development Community) Ministers Responsible for Water Resource Management:* Pretoria 23 & 24 November 1995.

Olivier, J., 1988: The relationship between altitude and hail frequency in the Transvaal. *South African Journal of Science*, **84**, 587 - 588.

Olivier, J., 1989: Some temporal aspects of Transvaal hail. *South African Geographer*, **16**, 39 - 53.

Olivier, J., 1990: Hail in the Transvaal. Some geographical and climatological aspects. D.Sc Thesis, Randse Afrikaanse Universiteit.

Orville, H.D., 1990: The uses of cloud models in weather modification, *J. Weather Modification*, **22**, 137 - 142.

Peltier, W.R., and T.L. Clark, 1979: The evolution and stability of finite-amplitude mountain waves. Part II: Surface wave drag and severe downslope windstorms. *J. Atmos. Sci.*, **36**, 1499 - 1529.

Poolman, E.R., 1992: Die voorspelling van haelkorrelgroei in Suid-Africa. M.Sc Thesis. Universiteit van Pretoria.

Rakovec, J., 1989: Thunderstorms and hail. *Theoretical and Applied Climatology*, **40**, 179 - 187.

Reader's Digest atlas of Southern Africa, 1982: Farming the land, 62 - 63.

Schulze, B.R., 1965: Climate of South Africa - Part 8: General survey. *Weather Bureau, Department of Environment Affairs*, WB28, 330 pp.

Smagorinsky, J., 1963: General circulation experiments with the primitive equations. Part I. The basic experiment. *Mon. Wea. Rev. ,* **91**, 99 - 164.

Smolarkiewicz, P.K., 1984: A fully multidimensional positive definite advection transport algorithm with small implicit diffusion. *J. Comput. Phys.,* **54**, 325 - 362.

Smolarkiewicz, P.K., and T.L. Clark, 1985: Numerical simulation of the evolution of a three-dimensional field of cumulus clouds: Part I. Model description, comparison with observations and sensitivity studies. *J. Atmos. Sci,* **42**, 502 - 522.

Star Newspaper, 11 December 1991.

Steyn, P.C.L., 1984: The relationship between the 300 hPa circulation pattern and rainfall classification in the Bethlehem region. *Bethlehem Weather Modification Experiment,* Progress Report No 24, South African Weather Bureau, Pretoria.

Steyn, P.C.L., 1988: Classification and analysis of mesoscale weather systems in the Bethlehem area. *Bethlehem Weather Modification Experiment,* Progress Report No 34, South African Weather Bureau, Pretoria.

Steyn, P.C.L., and R.T. Bruintjes, 1990: Convective cloud characteristics for the Bethlehem area. *Water SA,* **16**, 115 - 118.

Terblanche, D.E., 1985: Die Pretoria-haelstorm van 1 November 1985. *South African Weather Bureau Newsletter,* November 1985, 1 - 6.

Terblanche, D.E., 1996: Personal communication.

Terblanche, D.E., F.O. Hiscutt, and D.J. Dicks, 1994: The upgrading and performance testing of the Bethlehem weather radar. *S A J Sci.,* **90**, 588 - 595.

Tyson, P.D., 1984: The atmospheric modulation of extended wet and dry spells over SA, 1958-1978. *J Climatology,* **4**, 621-635.

Van Heerden, J., D.E. Terblanche, and G.C. Schulze, 1988: The Southern Oscillation and South African summer rainfall. *J. Climatology*, **8**, 577 - 597.

Van Niekerk, L., 1996: Laat elke druppel tel. *Conserva*, **11**, 15.

WMO, 1981: The dynamic of hailstorms and related uncertainties of hail suppression. Weather Modification Programme, Hail Suppression Research, Report no 3, Geneva, February 1981.

Weisman, M.L., and J.B. Klemp, 1986: Mesoscale Meteorology and Forecasting. Editor Peter S. Ray, 331 - 358.